ESTIMATING DIFFUSE RADIATION ON HORIZONTAL SURFACES AND TOTAL RADIATION ON TILTED SURFACES

by

DOUGLAS T. REINDL

A thesis submitted in partial fulfillment of the

requirements for the degree of

MASTER OF SCIENCE

(Mechanical Engineering)

at the

UNIVERSITY OF WISCONSIN - MADISON

1988

Acknowledgments

I would like to thank my advisors, Professor Bill Beckman and Professor Jack Duffie for their support and providing many of the ideas related to this research. Bill thank you for pushing me to take those extra steps. I seriously doubt that the Solar Energy Lab would be around today had it not been for the leadership and care of Jack Duffie; thanks Jack. A special thanks to Professor Sandy Klein for sparing 5 minutes in his 25 hour days to discuss my research. I have enjoyed the fellowship of the students in the lab. Tim, thanks for breaking up the monotony and exchanging ideas.

Thanks Dad and Mom for your support, guidance, and encouragement in all of my work. Thanks to my brothers and sisters, you have really helped me grow. To my good friend and colleague Jerry, your advice has been indispensable.

To my wife Reneé, in appreciation for the patience, understanding, and love you have given me.

Financial assistance for this work has been provided by the United States Department of Energy.

Abstract

The objectives of this research concern two main topics: methods of estimating hourly diffuse radiation on a horizontal surface and evaluation of hourly tilted surface radiation models.

The influence of climatic and geometric variables on the hourly diffuse fraction is studied based on a data set with 22,000 hourly measurements from five North American and European locations. The goal is to determine if other predictor variables, in addition to the clearness index, will significantly reduce the standard error of correlations which are based solely on the clearness index (referred to as Liu and Jordan type correlations).

Stepwise regression is used to reduce a set of 28 predictor variables down to four significant predictors: the clearness index, solar altitude, ambient temperature, and relative humidity. A correlation which is a function of these four predictor variables is developed to predict the hourly diffuse fraction. In cases when ambient temperature and or relative humidity data are not available, a second "reduced" correlation which expresses the diffuse fraction as a function of clearness index and solar altitude is developed. A third correlation of the Liu and Jordan type ($I_d/I = f(k_t)$) is derived from the same data set to provide a direct measure of the value of the added predictor variables.

The full diffuse fraction correlation reduced the residual sum squares by 14% when compared to the correlation that is a function of the clearness index only. The reduced correlation diminished the residual sum squares by 9%.

The performance of tilted surface models is investigated using monthly average hourly utilizable energy as a metric. Differences between the utilizable energy measured and the utilizable energy predicted are observed for various surface slope/azimuth orientations and critical radiation levels. Normalized root mean square

difference (NRMSD) and normalized mean bias difference (NMBD) statistics are formed to quantify each model's ability to estimate the utilizable energy on a tilted surface.

Three existing tilted surface radiation models are evaluated: isotropic, Hay, and Perez. In addition, a new tilted surface algorithm based on the Hay model is developed and evaluated. The tilted surface radiation models in this investigation share the same techniques for calculating the beam and ground reflected radiation on a tilted surface; they only differ in the treatment of calculating diffuse radiation on a tilted surface.

Estimating the hourly radiation on a tilted surface requires knowing the division of global radiation into its beam and diffuse components. A database composed of four years of hourly radiation data from Albany, New York and one year of hourly radiation data from San Antonio, Texas provide the basis for model comparisons. Measured values of global horizontal and diffuse radiation on a horizontal surface were available for input to the tilted surface models. The influence of horizontal diffuse on tilted surface model performance is examined by comparing the predicted utilizable energy on a tilted surface using measured horizontal diffuse and predicted horizontal diffuse radiation (using various diffuse fraction correlations). The database also contained tilted surface radiation measurements for five different surface slope/azimuth orientations (43°s, 90°n, 90°s, 90°e, 90°w).

The difference in the utilizable energy measured and the utilizable energy predicted are observed, via the NRMSD and NMBD statistics, for the five surface slope/azimuth orientations and a wide range of critical radiation levels. On an overall basis, the isotropic sky model showed the poorest performance and is not recommended for estimating the hourly radiation on a tilted surface. The anisotropic models (Hay, Perez, and new model) all have comparable performance. The Hay and

new model are much simpler to use when compared to the Perez model. Within each model's limitations, any of the anisotropic models should yield acceptable performance for estimating the radiation on a tilted surface.

The tilted surface models showed little sensitivity to the input of horizontal diffuse radiation. There was no significant degradation of tilted surface model performance when a diffuse fraction correlation is used to estimate the horizontal diffuse radiation for tilted surface model input.

Table of Contents

List of Figures

List of Tables

Nomenclature

AI	anisotropy index
a/c	weighted circumsolar solid angle
CRSS	Composite residual sum squares
d.f.	degrees of freedom
F	F - statistic
F_1'	reduced brightness coefficient (circumsolar)
F_2'	reduced brightness coefficient (horizon brightening)
f	modulating function
G_{sc}	solar constant (a value of 1353 W/m^2 was used)
H_o	null hypothesis
I	hourly total radiation on a horizontal surface, (kJ/m^2)
I_b	hourly beam radiation on a horizontal surface, (kJ/m^2)
I_{bn}	hourly beam radiation at normal incidence, (kJ/m^2)
$I_{b,T}$	hourly beam radiation on a tilted surface, (kJ/m^2)
I_d	hourly diffuse radiation on a horizontal surface, (kJ/m^2)
$I_{d,T}$	hourly diffuse radiation on a tilted surface, (kJ/m^2)
$I_{g,T}$	hourly ground reflected radiation on a tilted surface, (kJ/m^2)
I_o	hourly extraterrestrial radiation on a horizontal surface, (kJ/m^2)
I_{on}	hourly extraterrestrial radiation at normal incidence, (kJ/m^2)
I_T	hourly total radiation on a tilted surface, (kJ/m^2)
$I_{T,c}$	hourly critical radiation level on a tilted surface, (kJ/m^2)
k	hourly diffuse fraction
k_t	hourly clearness index

l	length of atmosphere
LST	Local standard time
m	optical air mass
MBD	Mean bias difference
n	day of the year, number of observations
NMBD	Normalized mean bias difference
MSreg	Mean square due to regression
MSresid	Mean square due to residual
NRMSD	Normalized root mean square difference
p	number of parameters
r_{xy}	Correlation coefficient
R_b	geometric factor for beam radiation
R^2	Multiple correlation coefficient
RH	Relative humidity, (fraction)
RMSD	Root mean square difference
SS	Sum of squares
t	t - stastic
T_a	ambient temperature, (C)
T_{dp}	dew point temperature, (C)
T_{wb}	wet bulb temperature, (C)
TST	True solar time
UE	Monthly average hourly utilizable energy
$\hat{x}$	predicted value of x
$\overline{x}$	average value of x
$\underline{x}$	x matrix

Greek Symbols

α	solar altitude angle, circumsolar half angle
β	surface slope
β_i	true model parameter
γ	surface azimuth angle
Δ	sky brightness parameter
δ	declination
ε	sky clearness parameter, model error, residual
κ	mass extinction coefficient, (L^2/m)
λ	wave length
ρ	density, (m/L^3)
ρ_g	ground reflectance
θ	angle of incidence
θ_z	zenith angle
τ	vertical optical depth
ϕ	latitude, relative humidity (fraction)
ω	hour angle, humidity ratio

Subscripts

b	beam radiation
d	diffuse radiation
cir	circumsolar diffuse
D	dust
g	ground reflected
hor	horizon diffuse
i	datum

iso	isotropic diffuse
n	normal incidence radiation
o	extraterrestrial
oz	ozone
R	Rayleigh
T	tilted surface radiation
w	water vapor

Chapter 1 INTRODUCTION

This chapter is intended to identify areas that show potential for improving existing diffuse fraction correlations and models used to estimate terrestrial solar radiation on inclined surfaces from measured horizontal solar radiation. Research objectives are established and the thesis organization presented.

1.1 Problem Definition

It is of great value to study solar energy systems using computer simulation programs such as TRNSYS [1]. Computer simulation provides a medium for both research and design of systems. The modular architecture of TRNSYS allows detailed models to be formulated for transient analysis on a system or subsystem level. The transient nature of real systems is mimicked by TRNSYS using hourly (or smaller) time steps. In a research regime, computer simulation offers a controlled environment to study a system's performance and response to variations in parameters, properties, inputs, etc. This leads to a better understanding of the systems and their sensitivities. Computer-aided simulation is also a cost effective tool that can be used to evaluate a wide variety of complex system configurations and design alternatives such as collector sizes, orientations, storage volumes, etc. in a relatively short period of time.

A crucial input required in transient simulation of solar energy systems is hourly radiation incident on the collecting surface. Because radiation (in the solar spectrum) is the driving force for solar systems, accurate hourly radiation values

are essential for meaningful simulation results. Incorrect or unrealistic solar radiation data can abrogate proposed solar system designs which result from the simulations.

A problem that arises when attempting to design or predict actual solar system performance is the lack of measured radiation data for simulation input. Actual measurements of hourly solar radiation data would be desirable for input but probably are not available for the site and collector orientation under consideration. Hourly radiation and weather data are available for various locations in the United States through the National Oceanic and Atmospheric Administration (NOAA), SOLMET [2]. In the case of SOLMET data, global horizontal radiation is the only true measured radiation value. Typically, collecting devices are not oriented horizontally but sloped at some angle, β, with respect to the horizontal. Thus, the total radiation on a tilted surface is required for simulation input and must be calculated from horizontal radiation data.

The total radiation incident on a tilted surface is composed of three distinct elements: beam, diffuse, and ground reflected. Beam radiation is the component from the sun that reaches the earth's surface without change in its direction of propagation. Diffuse radiation is the portion of radiation whose direction has been changed (possibly several times) as it passes through the earth's atmosphere. Diffuse radiation can be further divided into three sub-components: circumsolar, horizon brightening, and sky diffuse. Circumsolar diffuse radiation results from particles in the atmosphere (commonly referred to as aerosols) scattering the incident radiation. Circumsolar scattering is predominantly forward directed and

limited to the region in the neighborhood of the sun. The magnitude of circumsolar diffuse is dependent on the scattering particle's composition, size, and distribution in the atmosphere. Additional information on circumsolar radiation can be found from Watt [3]. Horizon brightening is the increase in diffuse radiation near the horizon due to a larger portion (with respect to the sky dome) of the incident radiation scattering as it passes through the longer pathlength of atmosphere near the horizon and by multiple internal reflections of radiation within the earth's atmosphere. Clear sky measurements made by Temps and Coulson [4] confirm an increased intensity of radiation near the horizon; this increase is horizon brightening. The sky component is the remaining diffuse energy which is assumed to be isotropically distributed over the sky dome. Ground reflected radiation results from both beam and diffuse striking the earth's surface in the collector's field of view and reflecting with an effective albedo, ρ_g, to the collector surface.

The investigation undertaken in this research deals with broadband solar radiation models, i.e. the models are not spectrally dependent. The wavelength band of interest for solar energy applications is in the range from $0.3-3.0\,\mu m$ according to Duffie and Beckman [5]. Radiation at wavelengths less than $0.3\,\mu m$ will not reach the earth's surface due to the strong absorption of ozone in the atmosphere [6]. Much of the radiation above $2.5\,\mu m$ is absorbed in the atmosphere by H_2O and CO_2. At wavelengths larger than $3.0\,\mu m$, there is no appreciable energy from a thermal systems utilization standpoint. The broadband assumption

greatly simplifies models which predict both diffuse radiation on a horizontal surface and total radiation on a tilted surface by eliminating the need to integrate over all radiation wavelengths.

Because of the importance of hourly tilted surface radiation as an input variable for simulations and its potential complexity due to the large number of components, it seems fitting to measure the tilted surface radiation directly for input. In reality, the use of hourly tilted surface radiation data as an input for system simulation is not practical due to the prohibitive costs associated with measuring radiation on all the possible collector surface slope/azimuth orientations for a proposed system and site location over a long period of time. However, hourly global radiation on a **horizontal** surface is one of the most widely available measurements in addition other climatic variables (ambient temperature, dew point, etc.). Extensive databases exist for a variety of locations including SOLMET [2], McKay [7]. Hay and McKay [8] indicate that monitoring global horizontal radiation produces: measurements that are spatially representative, measurements that are free from horizon obstructions, and measurements that minimize the influence of local conditions such as ground albedo.

If only global horizontal radiation is measured, two problems exist: first, to determine the fraction of the global which is diffuse (or beam); second, to estimate the respective beam, diffuse, and ground reflected components on a tilted surface of any orientation. Several correlations have been developed to determine the diffuse fraction given measured global horizontal. Orgill and Hollands [9] and Erbs, et al. [10] correlate the diffuse fraction with the hourly clearness index, $k_t(=I_d$

/I). Stauter and Klein [5] use a clearness index, k_c , relative to a "clear sky" radiation, I_c , as a predictor of the diffuse fraction. Iqbal [11] built on the work of Bugler [12] to develop a correlation which predicts hourly diffuse radiation (in the form I_d/I_o) as a function of k_t and solar altitude. The models based on k_t (commonly referred to as Liu and Jordan type models) are desirable because the only required input is hourly global horizontal radiation, I. Extraterrestrial radiation is also required but can easily be calculated from equations given in Appendix A. Davies, et al. [13] concluded that the Liu and Jordan type models (Orgill and Hollands, Erbs, etc.) provided the best estimates of hourly diffuse radiation when compared to other cloud based models. If the diffuse radiation is estimated, the beam radiation can be calculated from the following relationship:

$$I_b = I - I_d \tag{1.1}$$

The drawback of diffuse fraction correlations based on k_t is the large standard error associated with hourly estimates of the diffuse fraction. It is important that the diffuse radiation be determined as accurately as possible to ensure minimum error when calculating radiation on a tilted surface. Error in prediction of diffuse radiation also introduces error into the estimate of beam radiation (by equation 1.1) and its projection to tilted surface.

Subsequent to determining the magnitude of the beam and diffuse radiation on a horizontal surface, a method for projecting each radiation component onto a tilted surface of any orientation must be employed. The beam radiation can be projected to the tilted surface by a simple geometric calculation as given in [5].

$$R_b = \frac{\cos(\theta)}{\cos(\theta_z)} = \frac{I_{b,T}}{I_b} \tag{1.2}$$

Projecting diffuse radiation onto tilted surfaces is more difficult because each diffuse component must be treated separately. The diffuse components: circumsolar, sky, and horizon brightening each have different magnitudes and angular relationships with respect to the collector; thus each component must be treated individually. One method of simplifying the calculation of tilted surface diffuse is to assume that all the diffuse radiation is isotropic (uniformly distributed over the complete sky dome) as done by TRNSYS [1] and Duffie and Beckman [5] (originating from Hottel and Woertz [14]). Several authors have investigated the validity of the isotropic sky model [8,15,16,17]. All studies conclude that the isotropic model underpredicts radiation on south facing surfaces. By underpredicting incident radiation, the isotropic model leads to conservative estimates (probably representing a lower bound) of system performance.

Several models which account for the anisotropic behavior of diffuse radiation have been proposed and tested in large scale model evaluation studies [18,19]. Two models that consistently appear as good performers in the studies are the Perez, et al. [20] model and the Hay and Davies [21] model. By accounting for

the circumsolar, horizon brightening, and sky diffuse, the Perez model provides hourly estimates of the tilted surface diffuse radiation. The Hay model only considers circumsolar and sky diffuse radiation to provide hourly diffuse radiation on a tilted surface. Both models have the same required inputs but the simplified Perez model is cumbersome and difficult to use while the Hay model simple and quite elegant. Hay and McKay [19] use a large database composed of tilted surface data to compare model predictions with measured data ranking all models from best to worst. In addition to comparing measured and predicted values of tilted surface radiation, van den Brink [18] uses various reference systems (dwellings with and without active solar, swimming pools, etc.) to explore model effects on the auxiliary energy required when using measured and predicted values of radiation. This method lacks the generality to extend the results to other types of solar systems. From a thermal system point of view, it is of interest to compare the model's ability to estimate the utilizable energy on a tilted surface at varying critical radiation levels. The critical radiation level is defined as the minimum quantity of radiation required to overcome losses and produce useful output. Utilizable energy (as used in this research) is a statistic that represents the monthly average hourly amount that the critical radiation level was exceeded (for further discussion of utilizable energy concepts see Appendix A). Since every solar energy system has an associated critical level, the utilizable energy for that system's critical level can be calculated. Utilizable energy provides a means of comparing model predictions independent of a particular system; thus is a more general method for comparing the performance of tilted surface radiation models.

In summary, it is important to provide precise estimates of hourly diffuse radiation on a horizontal surface when only the hourly global horizontal radiation is known and to properly "project" that diffuse irradiance onto a tilted surface of any orientation. Meaningful simulations of solar energy system performance will not be realistic without accurate inputs of the system's driving force, solar radiation on the collecting device.

1.2 Research Objectives

The objectives of this research concerns two main topics: methods of estimating the hourly diffuse fraction on a horizontal surface; and evaluation of tilted surface radiation models.

In each case there is a significant question that needs to be answered. First, additional climatic information (ambient temperature, dew point, etc.) is usually measured along with global horizontal radiation at the monitoring sites; can this information be used to reduce the standard error associated with estimating the diffuse fraction via correlations which use k_t only? Error in determining the diffuse fraction on a horizontal surface effects both projected diffuse radiation and beam radiation (beam radiation is calculated given total and estimated diffuse) to the tilted surface. Second, what is the best model for determining hourly radiation on a surface of any orientation using utilizable energy as a metric?

1.3 Thesis Organization

This thesis is organized into four main chapters. Chapter 2 will discuss the data sets used in the diffuse fraction correlation research and the tilted surface model investigation.

In Chapter 3, theoretical models using the radiative transfer equation will be introduced and contrasted with the current broadband empirical correlations typically used to estimate hourly diffuse radiation. An hourly diffuse fraction correlation that utilizes additional climatic information is developed and its relative improvement over current diffuse fraction correlations is quantified.

Chapter 4 compares three existing tilted surface models on a utilizable energy basis. A fourth model, based on the Hay anisotropic model, is proposed and its performance evaluated along with the other three models.

Chapter 5 discusses the overall conclusions of the research. Model recommendations are made as well as suggestions for future areas of research.

Chapter 2 Solar Radiation Data

Accurate knowledge of solar radiation provides valuable information for studies among a number of diverse disciplines including: biology, climatology, hydrology, daylighting, building load analysis, solar system design, etc. The research described in this thesis deals with the evaluation of both diffuse fraction radiation models and tilted surface radiation models in the context of solar system applications.

Good quality solar radiation measurements are an absolute necessity for diffuse fraction radiation model studies and tilted surface radiation model evaluation. This chapter is intended to provide a brief overview of the instruments associated with radiation measurements, databases used in the course of this research, and the quality control procedures applied to all datasets.

2.1 Instrumentation

As indicated in section 1.1, the single most widely available radiation measurements is the total or global radiation on a horizontal surface. The total radiation on a horizontal surface is the sum of beam and diffuse radiation components. By measuring any two of these three quantities, the remaining can be calculated by equation (1.1). The two basic instrument types used to measure these radiation components are discussed below.

One commonly used instrument for measuring radiation is a pyranometer. Pyranometers can be configured to measure the total radiation (on a horizontal or tilted surface), the diffuse radiation, and the ground reflected radiation. Pyranometers measure radiation indirectly by comparing the surface temperatures between a black detector and a white detector exposed to incident radiation. The black detector has a high absorptance in the solar spectrum while the white detector has a high reflectance in the solar spectrum. Thermopiles monitor the detector temperatures and produce a voltage proportional to the detector's temperature. The temperature difference between the black detector and the white detector is a measure of the absorbed radiation. Both detectors are covered by a hemispherical glass dome to help eliminate environmental effects (wind, dust, etc.). When the unit is calibrated, the thermopiles produce an output voltage proportional to the incident radiation flux nearly independent of ambient temperature. Mohr, et.al. [22] and Nast [23] stress the importance of re-calibrating instruments prior to site installation to assure that the common sources of instrument error will be eliminated or minimized.

An unshaded pyranometer oriented horizontally is exposed to beam and diffuse radiation from the complete sky dome; thus, the total (or hemispherical) radiation on a horizontal surface will be measured. When tilted at some slope, β, the pyranometer will measure the total radiation on a tilted surface which includes that part of the beam, diffuse, and ground reflected radiation that is in the instrument's field of view. The pyranometer can also be configured to measure the diffuse by "blocking" out that portion of the sky containing beam radiation. This is usually accomplished by means of a shade ring or disk positioned between

the sun and the instrument's detector to block the beam radiation from the sun. Unfortunately, the shading device blocks a portion of the diffuse radiation that normally would reach the detector; thus correction factors that account for this diffuse shading must be applied to the instrument observations. Similarly, ground reflected radiation can be measured by orienting the instrument vertically and shading its view to the sky as discussed in Hay and McKay [8].

When using pyranometer data, it is beneficial to understand factors that influence the instruments performance. This knowledge may help in decisions regarding the rejection of spurious data that arise during quality control tests, as well as providing a level confidence (or doubt) in the quantities the pyranometer was used to measure (i.e. some pyranometers are sensitive to tilt and should not be used for tilted surface measurements). Factors that influence the performance of pyranometers include: detector nonlinearity, incidence angle dependence, slope orientation, and climatic effects i.e. wind speed, temperature, etc. A basic instrument requirement for accurate radiation measurements is assuring linearity between the incident radiation and the instrument's electrical output. The absorptance of solar radiation for a given surface is dependent on the incidence angle of radiation impinging upon that surface. As the incidence angle of radiation increases, the absorptance of the surface decreases. The accuracy of most pyranometers deteriorates rapidly as the incidence angle of radiation becomes greater than 80°. Because of convective flow changes in the hemispherical dome housing the detector, some pyranometers are sensitive to being tilted. Climatic conditions can also influence the performance of some pyranometers. For example, high wind conditions can increase the convective losses of the instru-

ment's detectors causing inaccurate radiation measurements. Proper instrument calibration and compensation can counter the majority of the above mentioned performance degrading effects [22,23].

Another commonly used instrument for measuring solar radiation is the pyrheliometer. A pyrheliometer is used to monitor the beam irradiance at normal incidence. A tube shields the detector from diffuse radiation while providing a direct field of view (typically 5.7°) of the sun and a small region around it. With proper calibration, the voltage output from a thermopile located at the detector's base will be proportional to the incident radiation. An important component associated with the pyrheliometer is a drive tracking mechanism which keeps the tube pointed directly at the sun. Improper tracking can cause large errors in the measured direct normal; thus, both instrument calibration and drive accuracy are vital to the reliability of pyrheliometer data.

For further information related to instruments and their use, see Duffie and Beckman [5] and WMO [24].

2.2 Radiation Database

In this investigation, radiation data are required for two purposes: developing an improved diffuse fraction correlation and evaluating the performance of tilted surface models. The specific data needs for each task overlap but differ slightly. Hourly measurements of global horizontal, diffuse (or direct normal), ambient temperature, and dew point (or wet bulb) are required to study their influence on

the diffuse fraction. Evaluating the performance of tilted surface models requires hourly values of global horizontal, diffuse (or direct normal), and total radiation on tilted surfaces of various slope and azimuth orientations. The primary dataset used to accomplish the above objectives represents six locations with a minimum of one year of data from each location.

A recurring question related to the development of empirical correlations is "how much data is needed to develop a reliable model ?" Erbs [10] suggests that the exact number is somewhat arbitrary but he recommends 10 years per location for the data to be representative. This recommendation is based on monthly average daily values of radiation which by its nature will require longer time spans when compared to hourly data values. Balaras [25] suggests that 15 years of solar radiation data are required for representative annual averages. For hourly models, the number of years of data to represent a location will be much less than the 10-15 year intervals recommended for monthly and annual averages. The author believes that the total time duration along with the number of locations represented in the primary dataset provide sufficient data for developing an hourly diffuse fraction correlation.

A full description of the data (on a location by location basis) used in this research is provided below.

2.2.1 Albany, New York

The data from Albany, New York were taken under the Solar Energy Meteorological Research and Training Sites (SERMTS) [26] program at the State University of New York, Albany. The data was reported in the Research Cooperator Format [27]. Table 2.1 lists a summary of the Albany site location and data duration and Table 2.2 lists the measurements available during the span of the four year data period at Albany.

Table 2.1: Albany Site Information

Location:	Albany, New York	Latitude:	42.7° north
Data Period:	1/1/79 - 12/31/82	Longitude:	73.8° west
Interval:	Integrated hourly (LST)	Standard Meridian:	75.0° west

Table 2.2: Albany Site Measurements

Instrument	Description	Inst. Type	Interval	Units
1000 *	Global, horizontal	Eppley PSP	60 min. integ.	kJ/m^2-hr
1460	Global, 33°s **	(280-2800 nm)	"	"
1560	Global, 43°s **	"	"	"
1660	Global, 53°s **	"	"	"
1920	Global, 90°n **	LiCor Pyranometer	"	"
1940	Global, 90°e **	(400-1200 nm)	"	"
1960	Global, 90°s **	"	"	"
1980	Global, 90°w **	"	"	"
2010	Direct normal	Eppley NIP	"	"
3000	Diffuse, horizontal	Eppley PSP w/disc	"	"
3001	Diffuse, horizontal	Eppley PSP w/band	"	"
9300	Ambient Temp.	1	60 min. Ave.	°C
9320	Dew point	2	"	"

* Consistent with the Research Cooperator Format.
** Artificial horizons affixed to sensors eliminate ground reflected radiation.
1 - Climatronics motor aspirated temperature sensor.
2 - Climatronics with LiCl dew cell sensor.

2.2.2 San Antonio, Texas

Data were also taken under the SERMTS program at Trinity University, San Antonio, Texas. The Trinity data are reported in the Research Cooperator Format [27]. Table 2.3 provides site information for the Trinity location and Table 2.4 lists the measurements made at the Trinity site during the data period.

Table 2.3: Trinity Site Information

Location:	San Antonio, Texas	Latitude:	29.5° north
Data Period:	1/1/80 - 12/31/80	Longitude:	98.5° west
Interval:	Integrated hourly (TST)	Standard Meridian:	90° west

Table 2.4: Trinity Site Measurements

Instrument	Description	Inst. Type	Interval	Units
1000 *	Global, horizontal	Eppley PSP	60 min. integ.	kJ/m²-hr
1260	Global, 20°s **	(295-2800 nm)	"	"
1360	Global, 30°s **	"	"	"
1460	Global, 40°s **	"	"	"
1920	Global, 90°n **	"	"	"
1940	Global, 90°e **	"	"	"
1960	Global, 90°s **	"	"	"
1980	Global, 90°w **	"	"	"
2010	Direct normal	Eppley NIP	"	"
3000	Diffuse, horizontal	Eppley PSP w/disc	"	"
3001	Diffuse, horizontal	Eppley PSP w/band	"	"

* Consistent with the Research Cooperator Format.
** Artificial horizons affixed to sensors.

2.2.3 Cape Canaveral, Florida

Data from Cape Canaveral, Florida were provided by the Florida Solar Energy Center (FSEC). This data set will be referred to as the Cape data in the remainder of this thesis. The Cape site does not include as extensive measure-

ments as the Albany and Trinity sites but the data are applicable for the development of an hourly diffuse fraction correlation. Cape site summary is given in Table 2.5 and Table 2.6 lists the available measurements made at the Cape site.

Table 2.5: Cape Site Information

Location:	Cape Canaveral, Florida	Latitude:	28.42° north
Data Period:	1/1/80 - 12/31/80	Longitude:	80.61° west
Interval:	Integrated hourly (LST)	Standard Meridian:	75° west

Table 2.6: Cape Site Measurements

Instrument	Description	Inst. Type	Interval	Units
1 *	Ambient Temp.	a	60 min. ave.	°C
2	Dew Point	b	of 5 min.	"
3	Relative Humidity	c	readings	%
4	Global, horizontal	Eppley PSP	60 min. ave. of	W/m^2
5	Direct normal	Eppley NIP	10 sec reads	"

* Data is in FSEC Format.
a - platinum resistance thermometer, ± 0.1 °C.
b - bifular heating element wound over LiCl treated fiberglass cloth encasing a three thermistor network, ± 0.5 °C.
c - thin film capacitor, ± 2%, 0-80% RH; ± 3%, 80-100% RH.

2.2.4 Europe

Three sites with one year of data from each location comprise the European dataset. The European datasets are not in the Research Cooperator Format and detailed information on specific sites is not available. Table 2.7 indicates the locations and site information available and Table 2.8 details the radiation and climatic information monitored at the European sites. All the data measurement information is common to the three sites.

Table 2.7: European Site Information

Location:	Copenhagen, Denmark	Latitude:	55.68° north
Data Period:	1/1 - 12/31; year n/a	Longitude:	12.57° east
Interval:	Integrated hourly (TST)	Standard Meridian:	15.0° east
Location:	Hamburg, Germany	Latitude:	53.5° north
Data Period:	1/1 - 12/31; year n/a	Longitude:	10.0° east
Interval:	Integrated hourly (TST)	Standard Meridian:	15.0° east
Location:	Valentia, Ireland	Latitude:	51.95° north
Data Period:	1/1 - 12/31; year n/a	Longitude:	10.22° west
Interval:	Integrated hourly (TST)	Standard Meridian:	0.0°

Table 2.8: European Site Measurements

Instrument	Description	Inst. Type	Interval	Units
1	Ambient Temp.	unknown	spot obs.	°C
2	Wet bulb	unknown	"	"
3	Global, horizontal	*	*	W/m^2
4	Diffuse, horizontal	"	"	"
5	Direct normal	"	"	"

* - Radiation measurements were performed by logging irradiance from Kipp solarimeters every minute and forming a mean over the hour. Diffuse measurements used Kipp instruments with a shade ring. Beam measurements were taken with pyrheliometers.

2.3 Data Quality Control

The integrity and validity of any empirically derived correlation relies on the volume and quality of data used in the model development. It is assumed that a sufficient volume of data exists but the quality of the data need to be examined.

Prior to the development of an hourly diffuse fraction correlation or testing tilted surface models, it was necessary to screen the datasets to assure that erroneous data points were eliminated. Since complete equipment and data logs for each location were not available to identify and eliminate data points associated with known sources of error, various methods were employed to determine if the hourly measurements were reasonable. Three types of data checks were performed to identify missing data, data which clearly violate physical limits, and extreme data.

When the data were known to be "bad" or "missing", the data fields were filled with a key sequence of numbers to clearly indicate the erroneous observation. Data fields filled with 9s for the SERMTS and European data and 32767 for Cape data indicated missing or bad data. Any hour with data flagged as bad or missing was omitted. Night hours were also excluded from the datasets. Thus as a first pass for data checking, daytime hours with presumed good values were used and subjected to further quality tests.

The next step is to identify data points which violate physical limits. Any hour with an observation that violated a physical limit or conservation principle was eliminated from the dataset. For example, reported hours with negative values of radiation were deleted from the dataset. By conservation principles (equation 1.1), the fraction of the total radiation which is diffuse cannot be greater than 1. If the measured values of total and diffuse radiation produced a diffuse fraction greater than 1, the hour was not used. Hours that beam radiation exceeded the extraterrestrial beam radiation were also eliminated. From thermodynamic principles, the dew point temperature cannot be greater than the dry bulb ambient temperature. If the measured dew point temperature was larger than the measured dry bulb ambient temperature, the hour was removed from the dataset.

In other circumstances, reported data values did not exceed physical limits but were categorized as "extreme" or outliers and had to be edited manually. Anscombe [28] discusses conditions for rejecting outliers indicating that if the outlier was caused by a large measurement or instrumentation error, discarding the data is justified. If the outlier appears to be the result of some non-normality and

its exact cause cannot be identified, the data point can be discarded from a statistical analysis based the least squares method but the observation should not be forgotten i.e. there may be important information in a collection of outlying points.

There are various combinations of the diffuse fraction and clearness index values which would produce questionable data points. The limits below were used to identify such particular cases. (Similar limits were used by Erbs [10].) Under cloudy overcast sky conditions (low values of k_t), it is reasonable to expect that a large portion of the incoming radiation will be scattered by the clouds in the atmosphere resulting in a large diffuse fraction. Case 1 places a limit on the diffuse fraction under the cloudy overcast sky conditions. If an hour had measured diffuse fraction that was less than 0.90 for a clearness index less than 0.20, it was eliminated from the dataset. For clear sky conditions (high values of k_t), a smaller portion of the total radiation received on a horizontal surface will be diffuse. Case 2 places a limit on the diffuse fraction under clear sky conditions. If the measured diffuse fraction was greater than 0.80 for a clearness index greater than 0.60, the hour was not used in the final dataset.

Case 1 $\qquad I_d/I < 0.90 \text{ and } k_t < 0.20$

Case 2 $\qquad I_d/I > 0.80 \text{ and } k_t > 0.60$

Even though less than 1% of the data points fell into the above category, the points were omitted due to suspected pyrheliometer tracking and instrument calibration errors.

Another condition checked was hours with $k_t > 1.0$. It is possible for the total radiation on a horizontal surface to exceed the extraterrestrial radiation on a horizontal surface for short intervals under partly cloudy sky conditions due to reflected radiation off of clouds in addition to the direct and diffuse radiation impinging upon the pyranometer. It is less likely for an integrated hourly global value to exceed the integrated hourly extraterrestrial value. A limit of $k_t \leq 1.1$ was imposed on the data.

The quality tests discussed will help eliminate spurious data and minimize any impact that suspect data would have on a derived correlation. The final dataset was constructed from the measured data that passed all of the quality control checks discussed above.

Chapter 3 Determination of Horizontal Diffuse Radiation

In general solar radiation measurements are made on a horizontal surface; but values of solar radiation on a tilted surface are needed for input to solar system simulations. The methods for calculating the radiation on a tilted surface require that the magnitude of the beam and diffuse components on a horizontal surface be known. The most common hourly radiation measurement is the global or total radiation on a horizontal surface. In cases when the diffuse (or beam) radiation on a horizontal surface is not measured, alternative methods must be employed to estimate the magnitude of the diffuse (or beam) component. By measuring the total radiation on a horizontal surface and estimating the diffuse radiation, the beam radiation component can be calculated by equation (1.1).

Fundamentally there are two methods for estimating the diffuse (or beam) radiation on a horizontal surface: solving the radiative transfer equation or empirical correlations. The two methods differ greatly in the computational effort and information required to estimate the diffuse (or beam) radiation. Both methods will be discussed in this chapter. First, the radiative transfer equation will be introduced (in its beam form for simplicity) to illustrate the difficulties associated with its solution on an hourly basis. Second, empirical diffuse fraction correlations will be presented along with the development of a new hourly diffuse fraction correlation. In both cases, it is assumed that the global radiation on a horizontal surface is measured.

3.1 Theoretical Model

On a monochromatic basis, the radiation on a horizontal surface is expressed as a sum of the monochromatic beam and diffuse components.

$$I_\lambda = I_{b,\lambda} + I_{d,\lambda} \tag{3.1}$$

The attenuation of monochromatic beam radiation as is passes through the earth's atmosphere, Figure 3.1, is commonly described by using Lambert's law given in equation (3.2). The atmosphere is assumed to be horizontal parallel-plane and cloudless.

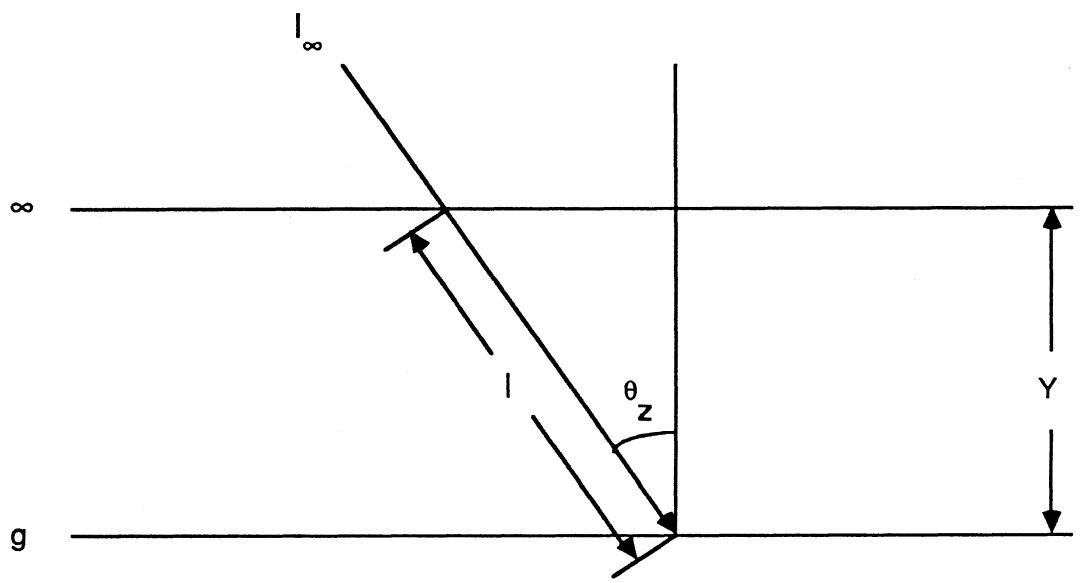

Figure 3.1: Atmospheric Radiation Geometry

$$dI_\lambda = -I_\lambda \kappa_\lambda \rho \, dl \tag{3.2}$$

where:

κ_λ = mass extinction coefficient, L^2/m

ρ = density, m/L^3

dl = differential path length, L

dI_λ = differential radiation intensity, E/L^2

but from Figure 3.1,

$$l = \frac{Y}{\cos(\theta_z)}$$

$$dl = \frac{dY}{\cos(\theta_z)}$$

substituting dl into (3.2),

$$dI_\lambda = -I_\lambda \kappa_\lambda \rho \, dY \, / \cos(\theta_z) \tag{3.3}$$

integrating (3.3) from outer atmosphere to ground level,

$$\int_\infty^g dI_\lambda / I_\lambda = -\int_\infty^g \kappa_\lambda \rho \, / \cos(\theta_z) \, dY \tag{3.4}$$

$$I_\lambda = I_{\infty,\lambda} \exp\left[-\int_\infty^g \kappa_\lambda \rho \, / \cos(\theta_z) \, dY \right] \tag{3.5}$$

Paltridge and Platt [30] define optical depth as the wavelength dependent quantity given by equation (3.6).

$$\tau_\lambda = \int_{\infty}^{g} \kappa_\lambda \rho \, dY \tag{3.6}$$

thus, equation (3.5) reduces to the following;

$$I_\lambda = I_{\infty,\lambda} \exp - [\tau_\lambda m] \tag{3.7}$$

where:

I_λ = beam normal radiation at the earth's surface, E/m^2

$I_{\infty,\lambda}$ = beam normal radiation above the earth's atmosphere, E/m^2

τ_λ = vertical optical depth, (dimensionless)

$m = 1/\cos(\theta_z)$, relative air mass, (dimensionless)

In equation (3.7), the vertical optical depth (VOD) consists of both absorption and scattering coefficients. Paltridge and Platt [30] indicate that the main difficulty in solving the transfer equation centers around determining the absorption and scattering coefficients as a function of wavelength for all atmospheric constituents as well as the coefficient's dependence on pressure and temperature. In the clear sky case, the vertical optical depth will be the sum of extinction due to both scatter and absorption.

$$\tau_\lambda = \tau_{R,\lambda} + \tau_{oz,\lambda} + \tau_{w,\lambda} + \tau_{D,\lambda} \tag{3.8}$$

The respective components in equation (3.8) represent Rayleigh scatter, ozone absorption, combined scatter and absorption by water vapor and dust,

respectively. Paltridge and Platt [30] list both functional forms and approximations to all of the vertical optical depth coefficients. The Rayleigh scatter component can be approximated as a simple function of wavelength only. The ozone absorption becomes more complicated requiring knowledge of the amounts of ozone at various levels in the atmosphere. Water vapor absorption and scattering is even more complex. Water vapor absorption is highly dependent on wavelength, pressure, and temperature; the relationships to accurately determine the necessary coefficients are not available. The final component is dust absorption and scattering. Characterizing dust scatter and absorption is similar to characterizing clouds. Both have complex particle shapes, sizes, atmospheric distributions, and radiative properties; consequently, significant simplifications are necessary to determine the vertical optical depth.

Although not presented, vertical optical depths can be approximated by methods given in Paltridge and Platt [30]. When each of the vertical optical depths are computed, the transfer equation must be integrated over all wavelengths. Typically, this is accomplished by integrating over small wavelength bands because the mass extinction coefficients are highly wavelength dependent.

It can be seen that a significant amount of computation is needed to employ the radiative transfer equation for calculating the beam radiation reaching the earth's surface under the assumed cloudless sky conditions. Numerous simplifications and approximations are required to obtain the vertical optical depths for the various atmospheric absorbing and scattering constituents. Goody [29] points out that although the equation of transfer is the primary building block in atmospheric

radiative transfer problems, its physical content is slight due to the approximations necessary to determine the VOD coefficients. Under partly cloudy sky conditions, determining the VOD coefficients become nearly impossible due to the complex nature of the clouds. Detailed knowledge of the cloud distributions within the atmosphere and cloud microphysics are required to attempt to approximate some type of VOD. Therefore, the radiative transfer equation has little practical use in estimating the beam radiation reaching the earth's surface for all sky conditions. Although the radiative transfer equation was presented in its beam radiation form, it can be formulated (with more difficulty) to estimate diffuse radiation.

3.2 Diffuse Fraction Correlations

An alternative to solving the radiative transfer equation is to use empirical models or correlations derived from extensive databases of radiation measurements. The empirical correlations presented in this thesis will estimate the diffuse fraction of the global horizontal radiation. The primary advantage of empirical correlations is computational simplicity which becomes very important in computer-aided simulations of solar energy systems. For a yearly solar system simulation, hourly radiation values must be calculated upward of 4000 times. In this application, simple empirical models are attractive to ease the computational burden that would result from using the full transfer equation. The disadvantages of empirical correlations are the high standard error of predicting the diffuse fraction and the correlation's potential for being location dependent.

Early work by Liu and Jordan [31] showed a relationship between daily diffuse and daily total radiation on a horizontal surface. Although their original correlation was developed for daily values, it has been used for computing the hourly diffuse fraction as a function of the hourly clearness index, k_t [1]. Other authors have developed diffuse fraction correlations as a function of the clearness index, k_t [9,10] specifically for hourly intervals. Fundamentally these models are similar and will be referred to as Liu and Jordan type models.

A drawback with using the Liu and Jordan type models is the high standard error associated with estimating the hourly diffuse fraction. The scatter plot shown in Figure 3.2a graphically illustrates the problem of estimating the hourly diffuse fraction as a function of k_t. For example, at $k_t = 0.5$, the measured diffuse fraction ranges from $0.25 < I_d/I < 1.0$. It is clear that the hourly diffuse fraction is not a function of k_t only. Models such as Orgill and Hollands [9] and Erbs [10] provide a single deterministic value of the hourly diffuse fraction for a given k_t. In an effort to mimic the variation of the diffuse fraction at a particular value of k_t, Hollands and Chra [32] developed a probability density function which allows the diffuse fraction, k, to vary about its mean value, $\bar{k}$, at a given k_t. Other authors suggest that the variation of the diffuse fraction for a particular value of k_t is due to other unidentified variables [9,11,12,33,34].

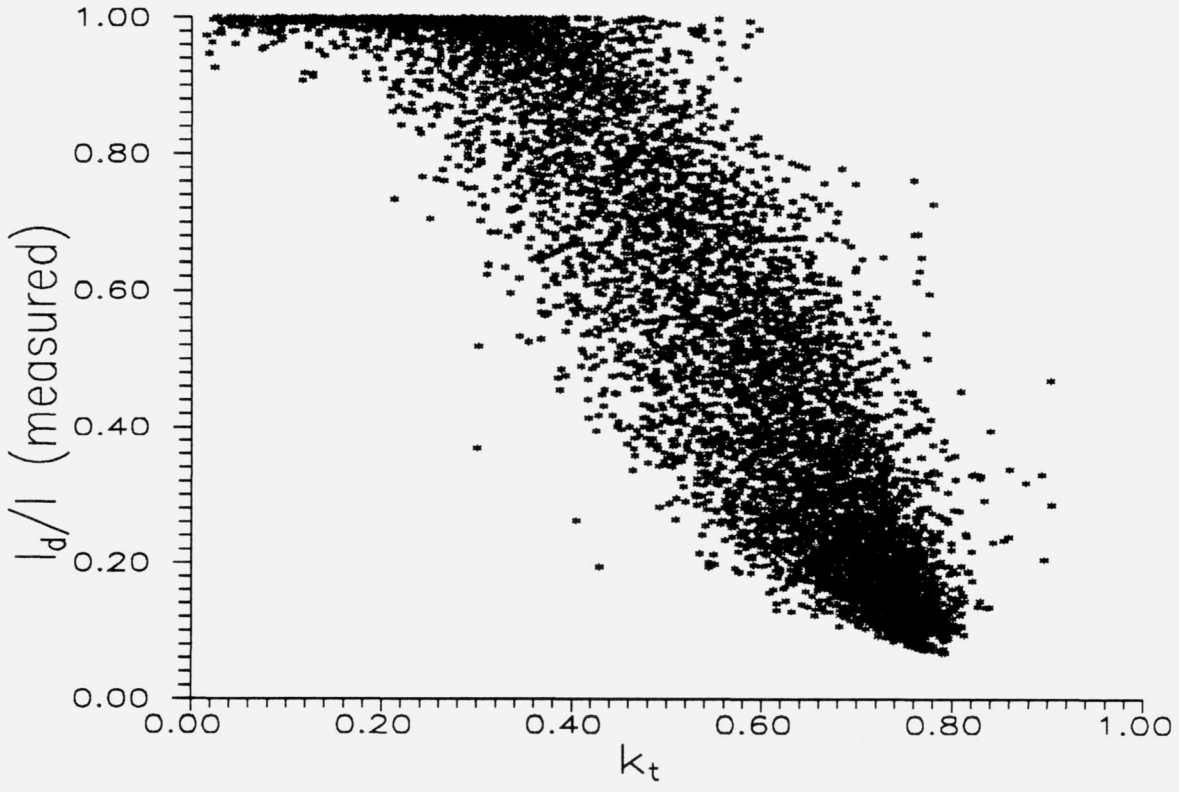

Figure 3.2a: Diffuse fraction vs. clearness index for Albany 1979-1982

Histogram of kt distribution for Albany Data 1979; N = 2178
Each * represents 10 obs.

Midpoint	Count	
0.00	5	*
0.05	35	****
0.10	35	****
0.15	17	**
0.20	36	****
0.25	51	******
0.30	120	**********
0.35	106	**********
0.40	111	**********
0.45	160	**********
0.50	159	**********
0.55	155	**********
0.60	217	**********
0.65	256	**********
0.70	321	**********
0.75	307	**********
0.80	86	*********
0.85	1	*

Histogram of kt distribution for Albany Data 1980; N = 2214
Each * represents 10 obs.

Midpoint	Count	
0.10	4	*
0.15	12	**
0.20	26	***
0.25	57	******
0.30	99	**********
0.35	164	**********
0.40	152	**********
0.45	161	**********
0.50	180	**********
0.55	203	**********
0.60	226	**********
0.65	264	**********
0.70	336	**********
0.75	279	**********
0.80	47	*****
0.85	2	*
0.90	2	*

Figure 3.2: (b) Clearness index distribution, Albany 1979
(c) Clearness index distribution, Albany 1980

Histogram of kt distribution for Albany Data 1981; N = 2126
Each * represents 10 obs.

Midpoint	Count	
0.05	5	*
0.10	12	**
0.15	24	***
0.20	48	*****
0.25	89	*********
0.30	118	**********
0.35	141	**********
0.40	172	**********
0.45	134	**********
0.50	160	**********
0.55	151	**********
0.60	203	**********
0.65	227	**********
0.70	302	**********
0.75	285	**********
0.80	52	******
0.85	1	*
0.90	2	*

Histogram of kt distribution for Albany Data 1982; N = 1994
Each * represents 10 obs.

Midpoint	Count	
0.05	5	*
0.10	25	***
0.15	25	***
0.20	41	*****
0.25	85	*********
0.30	86	*********
0.35	120	**********
0.40	98	**********
0.45	126	**********
0.50	156	**********
0.55	175	**********
0.60	223	**********
0.65	226	**********
0.70	294	**********
0.75	246	**********
0.80	55	******
0.85	8	*

Figure 3.2: (d) Clearness index distribution, Albany 1981
(e) Clearness index distribution, Albany 1982

Garrison [33] uses post - 1976 SOLMET data from 33 U.S. sites to graphically illustrate the diffuse fraction's dependence on surface albedo, atmospheric precipitable moisture, atmospheric turbidity, solar elevation, and global horizontal radiation. Without further statistical analysis, the relative significance of the variables suggested by Garrison [33] remains unknown. Skartveit and Olseth [34] and Iqbal [11] suggest that the second most important variable after k_t is solar elevation.

The research described in this thesis focused on assessing the influence of commonly measured climatic variables on the diffuse fraction and correlating the significant variables to reduce the standard error of Liu and Jordan type models. First, examples of existing hourly diffuse fraction correlations are introduced. Second, the influence of commonly measured climatic variables on the diffuse fraction are investigated. Third, a new hourly diffuse fraction correlation is presented. Fourth, the relative improvement of the new correlation over current Liu and Jordan type models is quantified.

3.2.1 Existing Correlations

Several authors, already mentioned, have proposed models for calculating the hourly diffuse fraction given the hourly clearness index. Three models commonly used to calculate the hourly diffuse fraction are given below.

3.2.1.1 Liu and Jordan Model

A relationship between the daily diffuse and daily total radiation was developed based on 10 years of data (1947-1956) from Blue Hill, Massachusetts (latitude = 42° N). On an hourly basis, the correlation is given by [1]:

$$\hat{I}_d/I = 1.0045 + 0.04349\, k_t - 3.5227\, k_t^2 + 2.6313\, k_t^3 \qquad k_t \le 0.75 \qquad (3.9)$$

$$\hat{I}_d/I = 0.166 \qquad k_t > 0.75 \qquad (3.10)$$

Erbs [10] points out that the Liu and Jordan hourly correlation underpredicts the diffuse fraction due to possible instrumentation errors or the fact that the correlation is a daily rather than an hourly model (although it has been applied to hourly data by many authors).

3.2.1.2 Orgill and Hollands

Orgill and Hollands [9] use four years of data (September, 1967 - August, 1971) from Toronto, Canada to develop an hourly diffuse fraction correlation as a function of the clearness index. The four years of data yielded 12,704 valid hourly periods to base the three piece curve fit of $I_d/I = f(k_t)$.

$$\hat{I}_d/I = 1.0 - 0.249\, k_t \qquad 0 \le k_t < 0.35 \qquad (3.11)$$

$$\hat{I}_d/I = 1.557 - 1.84\, k_t \qquad 0.35 \le k_t \le 0.75 \qquad (3.12)$$

$$\hat{I}_d/I = 0.177 \qquad k_t > 0.75 \qquad (3.13)$$

3.2.1.3 Erbs

Erbs [10] used a database composed of four U.S. locations to develop an hourly diffuse fraction correlation as a function of the hourly clearness index. The correlation is very similar to that of Orgill and Hollands. Erbs also uses a three piece curve to fit the diffuse fraction. The primary difference between the Erbs correlation and the Orgill and Hollands correlation, with the exception of the individual data sets, is that Erbs chose to use a fourth order polynomial in the center portion of the curve fit. The two models yield essentially the same result.

$$\hat{I}_d/I = 1.0 - 0.09\, k_t \qquad k_t \le 0.22 \qquad (3.14)$$

$$\hat{I}_d/I = 0.9511 - 0.1604\, k_t + 4.388\, k_t^2 - 16.638\, k_t^3 + 12.336\, k_t^4 \qquad 0.22 < k_t \le 0.8 \qquad (3.15)$$

$$\hat{I}_d/I = 0.165 \qquad k_t > 0.8 \qquad (3.16)$$

The three correlations are shown graphically in Figure 3.3. The similarity of the Orgill and Hollands and Erbs correlation is obvious. Also, the underpredicting nature of the Liu and Jordan model is evident. It is important to remember that the curves shown in Figure 3.3 actually represent average values of the diffuse fraction at a given value of k_t. In contrast, Figure 3.1 illustrates an example of actual measured diffuse fraction data plotted against k_t.

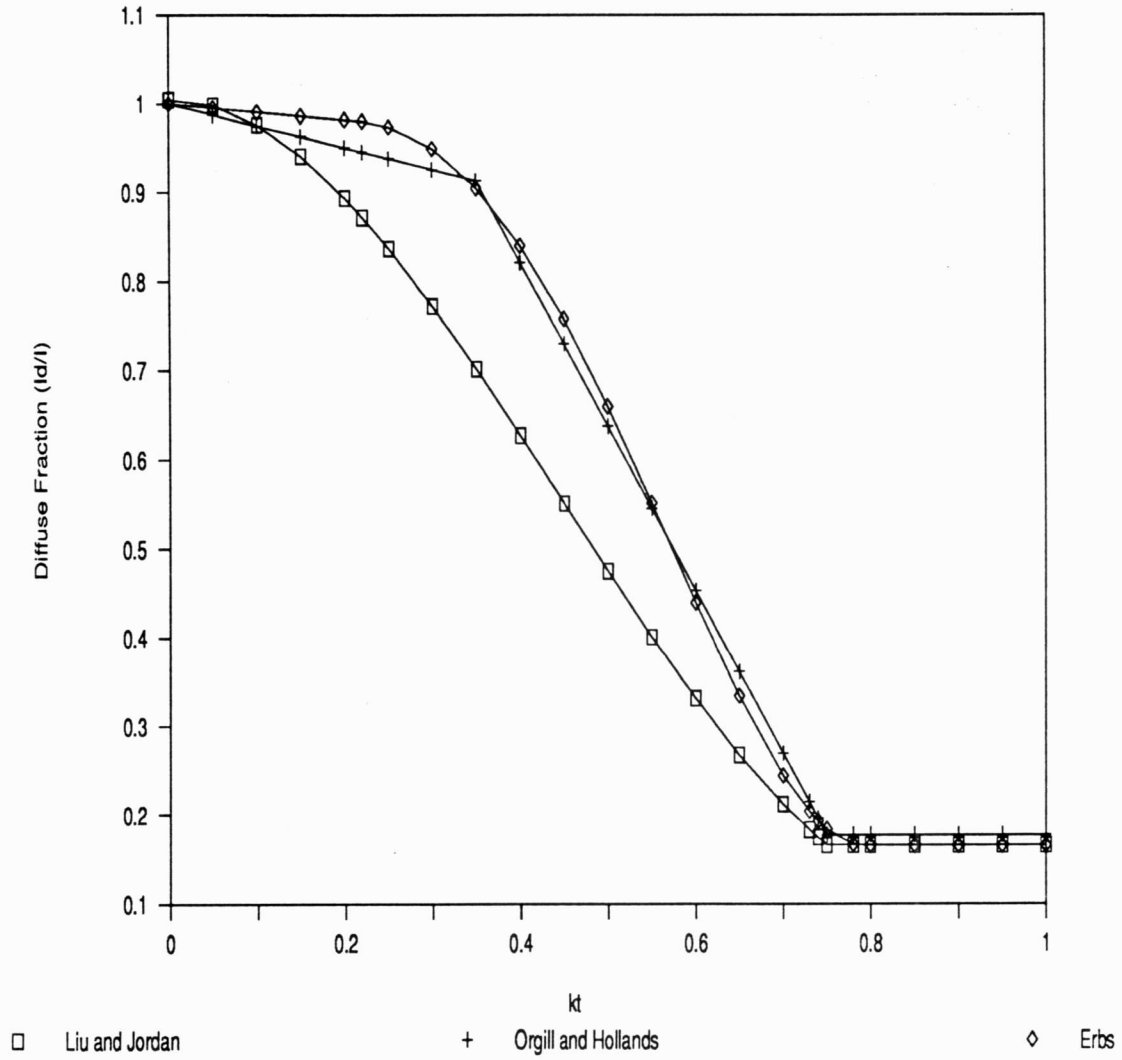

Figure 3.3: Existing hourly diffuse fraction correlations

3.2.2 Development of A New Hourly Diffuse Fraction Correlation

The motivation behind investigating hourly diffuse fraction correlations is to determine if incorporating additional predictor variables will significantly reduce the standard error of the current Liu and Jordan type models. The goal is to find an hourly diffuse fraction model which is more accurate than current Liu and Jordan type models but computationally simple for use in hourly simulation programs such as TRNSYS [1]. Also, the correlation's inputs should be limited to commonly observed climatic variables or quantities that can be calculated from commonly observed climatic variables e.g. ambient temperature, wet bulb temperature, dew point temperature, relative humidity, etc.

3.2.2.1 Datasets Used

Hourly radiation and climatic data from five locations (Albany, Cape, Hamburg, Valentia, and Copenhagen) provided the basis for the investigation into improving the current diffuse fraction correlations. The necessary hourly measurements for this study included global horizontal radiation, diffuse (or direct normal beam) radiation, ambient temperature, and wet bulb (or dew point) temperature. Complete site information for each location is provided in section 2.2.

Two methods, direct and indirect, are used to determine the hourly diffuse radiation on a horizontal surface. The direct method is to simply use the value of diffuse radiation observed from a shaded pyranometer (with the appropriate shade ring correction factors applied). The European locations measured diffuse radia-

tion with a ring shaded pyranometer while the Albany location measured diffuse radiation with both ring shaded and disk shaded pyranometers. The indirect method for determining the hourly diffuse radiation is by subtraction of pyrheliometer measured direct normal beam radiation from the observed global horizontal radiation given by:

$$I_d = I - I_{dn}\cos(\theta_z) \tag{3.17}$$

where I_d is the hourly diffuse radiation on a horizontal surface, I is the hourly global radiation on a horizontal surface, I_{dn} is the hourly measured direct normal beam radiation, and θ_z is the solar zenith angle calculated at the midpoint of the hour.

The accuracy of both methods is debatable. Hogan and Loxsom [36] show that corrected ring shaded pyranometer diffuse radiation measurements are more accurate than diffuse radiation calculated indirectly from measured global horizontal and direct normal beam radiation. On the other hand, Huang [37] maintains that calculated diffuse radiation from global and direct normal beam radiation is more accurate. The indirect method for calculating diffuse radiation has two potential sources of error: measured global radiation and measured direct normal beam radiation. The two sources of error can compound resulting in inaccurate estimates of the diffuse radiation. For the purposes of this study, directly measured diffuse radiation by shaded pyranometers will be used in lieu of

calculating the diffuse radiation from global and direct normal beam radiation. However, the indirect method will be used to estimate the diffuse radiation when the pyranometer measurements are bad or missing.

A complete dataset was formed with the measurements that met the quality control criteria discussed here and in section 2.3. The available hourly data for each location on a monthly basis is given in Table 3.1.

Table 3.1 Distribution of Valid Hourly Data

Month	Albany *	Cape	Hamburg	Valentia	Copenhagen
J	402	272	140	153	106
F	493	239	190	200	176
M	382	325	265	287	278
A	887	304	316	343	333
M	694	362	366	407	395
J	1074	343	405	416	375
J	1231	350	429	416	428
A	933	330	362	326	358
S	944	274	298	306	295
O	720	305	232	242	210
N	432	222	152	168	136
D	320	270	124	122	60
Total	8512	3596	3279	3386	3150

* - Albany: 1979 - 1982
Total data points all locations = 21923

Prior to performing any type of statistical analysis, it is useful to view overall plots of the diffuse fraction vs. the clearness index on a location by location basis.

The plots help reveal obvious errors and unusual characteristics of the measured diffuse fraction and clearness index values; included with the plots are histograms of the distribution of clearness index values.

U.S. Data: The diffuse fraction plotted against the clearness index for the Albany, New York data was presented in Figure 3.2. As noted in section 3.2, a large range of diffuse fraction values may exist for a given clearness index. The Cape Canaveral, Florida data shown in Figure 3.4 is very similar to the Albany data.

European Data: The European data exhibits several peculiarities. First, the Valentia dataset in Figure 3.5 has several hours with a diffuse fraction around 0.94 at very low values of k_t. This behavior is not as salient in the other data sets. The Hamburg data in Figure 3.6 has a solid line of unity diffuse fraction values for a large range of the clearness index ($0 \leq k_t \leq 0.5$). The Copenhagen data in Figure 3.7 has "bands" of diffuse fraction values (near $I/I_d = 1.0$) that occur over wide ranges of k_t. Also, lower diffuse fractions are observed at middle values of k_t making the data in center portion of the plot appear to be more widely spread. The k_t distributions indicate that the average k_t value for the European data is lower than the average k_t of the U.S. data. It is clear that location differences in the data sets exist.

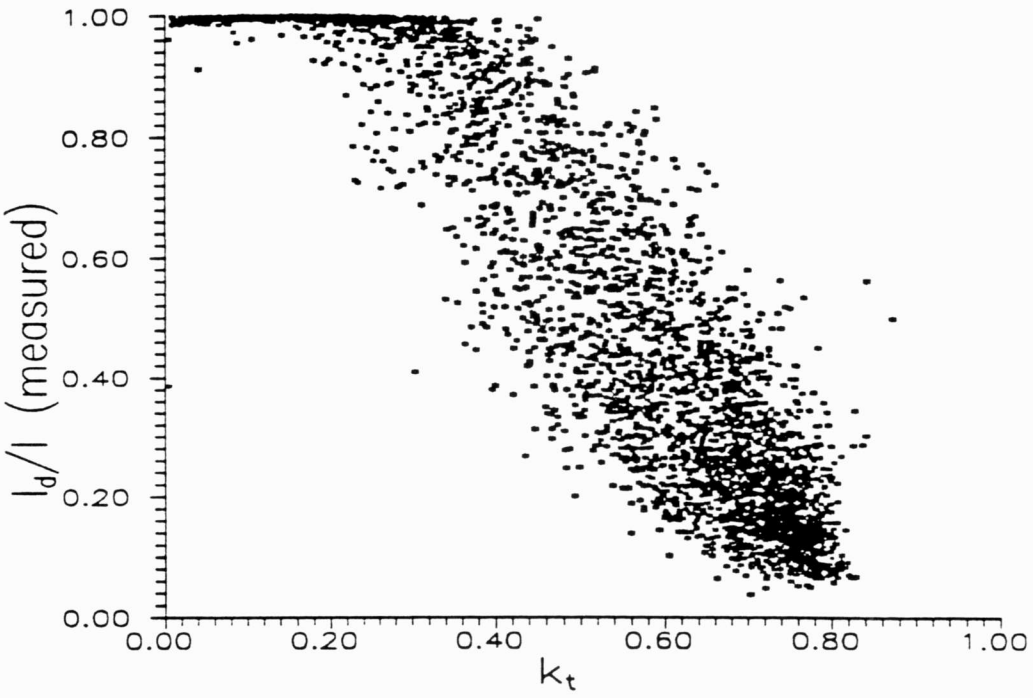

Histogram of kt distribution for Florida data. N = 3596
Each * represents 15 obs.

Midpoint	Count	
0.00	14	*
0.05	48	****
0.10	73	*****
0.15	85	******
0.20	105	*******
0.25	124	*********
0.30	112	********
0.35	146	**********
0.40	165	**********
0.45	204	**************
0.50	212	**************
0.55	288	********************
0.60	312	*********************
0.65	379	**************************
0.70	538	**************************************
0.75	600	**
0.80	185	*************
0.85	6	*

Figure 3.4: Measured Diffuse fraction vs. clearness index and clearness distribution for Cape Canaveral, Florida

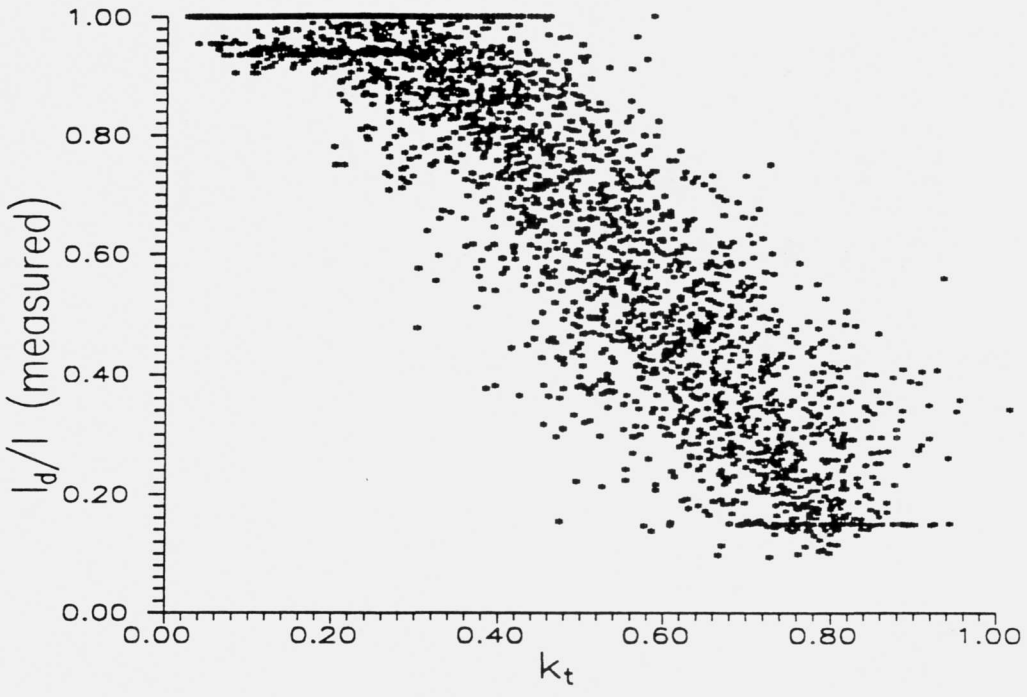

Valentia data

Histogram of kt distribution for Valentia data. N = 3386
Each * represents 15 obs.

Midpoint	Count	
0.0	31	***
0.1	388	*************************
0.2	501	**********************************
0.3	508	**********************************
0.4	442	*****************************
0.5	390	*************************
0.6	415	*****************************
0.7	386	*************************
0.8	275	******************
0.9	47	****
1.0	3	*

Figure 3.5: Measured diffuse fraction vs. clearness index and clearness index distribution for Valentia

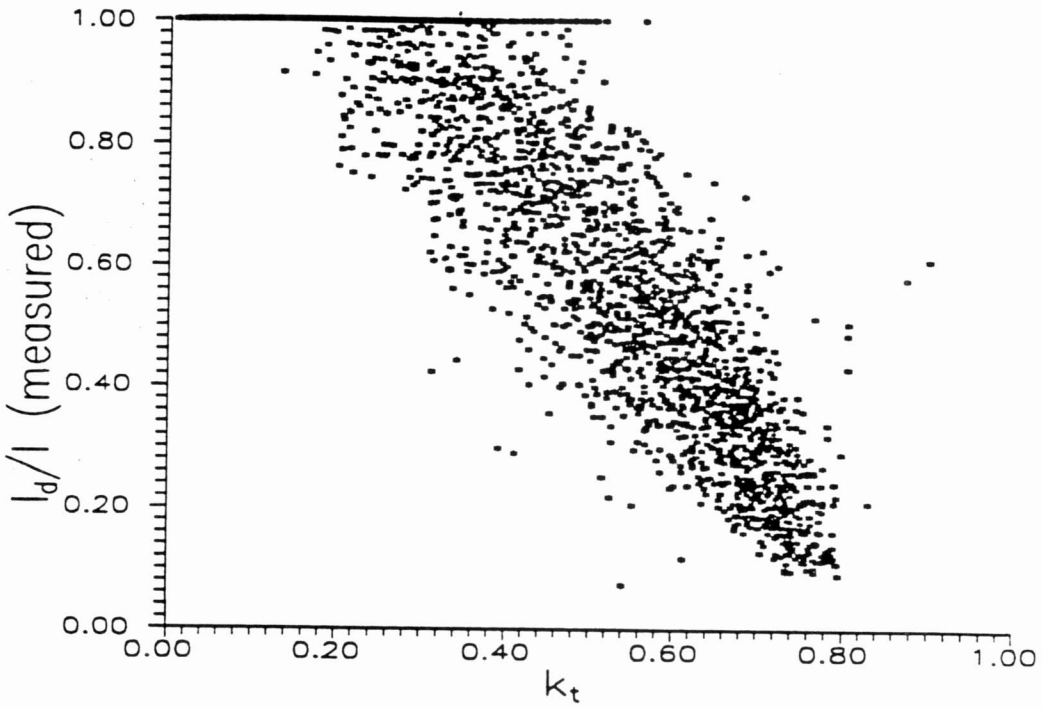

Histogram of kt distribution for Hamburg data. N = 3279
Each * represents 10 obs.

Midpoint	Count	
0.00	14	**
0.05	223	**********
0.10	259	**********
0.15	208	**********
0.20	209	**********
0.25	199	**********
0.30	200	**********
0.35	198	**********
0.40	187	**********
0.45	216	**********
0.50	203	**********
0.55	225	**********
0.60	238	**********
0.65	237	**********
0.70	270	**********
0.75	158	**********
0.80	32	****
0.85	2	*
0.90	1	*

Figure 3.6: Measured Diffuse fraction vs. clearness index and clearness distribution for Hamburg

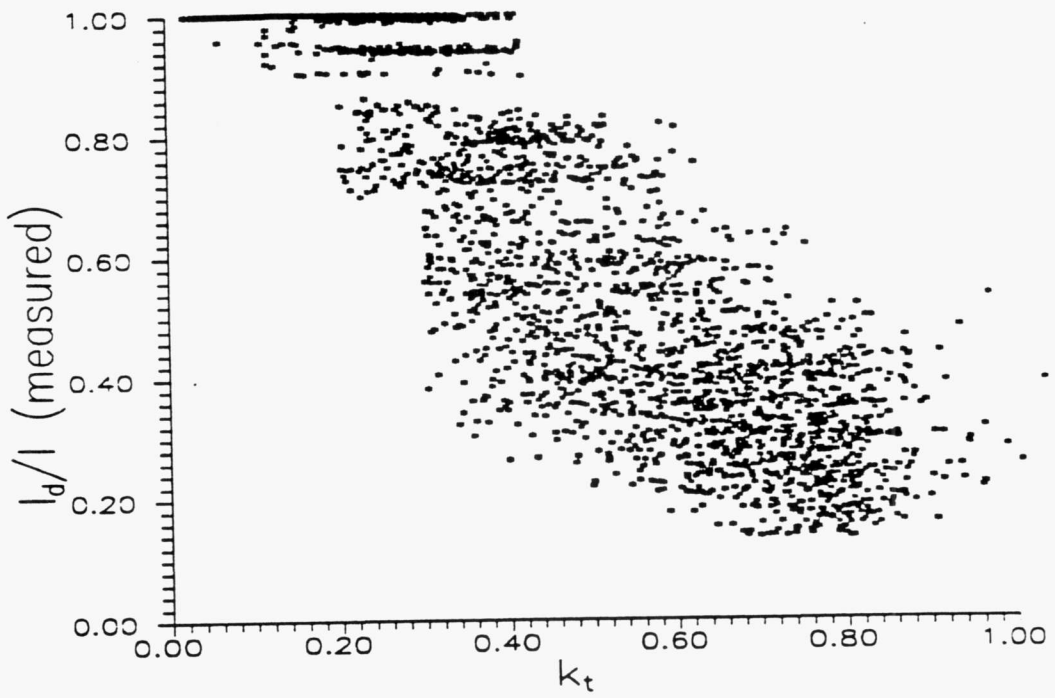

Histogram of kt distribution for Copenhagen N = 3150
Each * represents 10 obs.

Midpoint	Count	
0.0	46	*****
0.1	427	**********
0.2	403	**********
0.3	382	*********
0.4	416	**********
0.5	343	********
0.6	348	********
0.7	378	*********
0.8	349	********
0.9	54	******
1.0	4	*

Figure 3.7: Measured Diffuse fraction vs. clearness index and clearness distribution for Copenhagen

3.2.2.2 Model Development

Several steps are necessary to develop an empirical model which improves the prediction capabilities of the current Liu and Jordan type models. The approach used in this study included the following four basic steps: assemble a set of predictor variables, identify a potential model form, adopt a predictor selection procedure, and fit the model.

Predictor variables are independent variables that may affect the response. It is clear that the response, the diffuse fraction, is affected by the predictor, k_t. Garrison [33] suggests that the diffuse fraction also depends on ground reflectance, atmospheric precipitable water, atmospheric turbidity, and solar elevation. The set of predictors used in this study was limited to k_t and other commonly measured climatic data. Factors such as atmospheric turbidity and ground reflectance were not included because they are not commonly measured. Other subjective quantities such as cloud type, visibility, etc. were avoided as potential predictors because they lack repeatability. The full set of predictor variables used in this investigation is given in Table 3.2.

Table 3.2: Diffuse Fraction Predictor Variables

$T_a(hr)$	$T_{wb}(hr)$
$\overline{T_a}(hr)$	$\overline{T_{wb}}(hr)$
$T_a(hr)/\overline{T_a}(hr)$	$T_{wb}(hr)/\overline{T_{wb}}(hr)$
$T_{dp}(hr)$	$k_t(hr)$
$\overline{T_{dp}}(hr)$	$\overline{k_t}(hr)$
$T_{dp}(hr)/\overline{T_{dp}}(hr)$	$k_t(hr)/\overline{k_t}(hr)$
$\omega(hr)$	$\phi(hr)$
$\overline{\omega}(hr)$	$\overline{\phi}(hr)$
$\omega(hr)/\overline{\omega}(hr)$	$\phi(hr)/\overline{\phi}(hr)$
$\sin(\alpha)$	$T_a(hr) \cdot \phi(hr)$
$m = 1 / \cos(\theta_z)$	$\phi(hr) / [T_a + 273]$
$k_t(hr) \cdot m$	$\phi(hr)/\overline{\phi}(hr) \cdot T_a(hr)$
$\exp[\sin(\alpha)]$	$\exp[\phi(hr)/(T_a(hr))]$
$\exp[k_t \cdot m]$	$\exp[\phi(hr)/(\overline{\phi}(hr) \cdot T_a(hr))]$

where:

$T_a(hr)$ = hourly ambient temperature, C.

$T_{wb}(hr)$ = hourly wet bulb temperature, C.

$T_{dp}(hr)$ = hourly dew point temperature, C.

$\phi(hr)$ = hourly relative humidity, %.

$\omega(hr)$ = hourly humidity ratio, dimensionless.

$k_t(hr)$ = clearness index, dimensionless.

$\overline{X}(hr)$ = indicates monthly average hourly quantity.

α = solar altitude.

m = optical air mass.

The TRNSYS Type 33 psychrometrics subroutine was used to calculate the relative humidity, humidity ratio, and dew point temperature given the hourly ambient temperature and hourly wet bulb temperature at an assumed total pressure of 1 atmosphere.

Water vapor is one of the atmospheric constituents that absorbs and scatters solar radiation as it passes through the earth's atmosphere. The humidity ratio is defined as the ratio of the mass of water vapor to the mass of dry air. Thus, it would seem that the humidity ratio would provide some indication of the moisture content in the atmosphere and lead to a measure of the amount of solar radiation scattered as it passes through the atmosphere. Similarly, the relative humidity along with the ambient temperature may provide an indication of the water vapor content in the atmosphere leading to a measure of the amount of solar radiation scattered.

Monthly average hourly quantities and ratios of the hourly to monthly average hourly values of the climatic predictors and k_t were included in an attempt to account for possible predictor location dependence. For example, the range of ambient temperature over a year at Albany, New York will be much larger than the range of ambient temperature for Cape Canaveral, Florida but each location experiences a similar range of measured diffuse fractions over the year. However, the ratio of hourly ambient temperature to monthly average hourly ambient for both locations may be approximately the same magnitude. This form of scaling the predictors may help their correlation with the response.

Other predictors such as the sine of the solar altitude or air mass have been suggested as significant predictors of the diffuse fraction [11,12,33,34]. These predictor variables provide a measure of the path length required for radiation to reach the earth's surface. With a longer path length, more air molecules and other

atmospheric constituents are available to absorb and scatter the incoming solar radiation. The exponential forms used in the predictor set are an attempt to mimic the extinction effects as given in the transfer equation.

With the set of predictors identified, a model form must be established e.g. linear, nonlinear, first order, second order, etc. The Liu and Jordan type models presented in section 3.2.1 are all linear models. Liu and Jordan [1] and Orgill and Hollands [9] use first order piecewise fitted models. In other words, the data is fit in two or three intervals of k_t rather than fitting data over the entire range of k_t. The piecewise procedure allows lower order models (straight line) to be fit in each interval rather than a more complicated higher order model to fit the diffuse fraction over the entire range of k_t. For this study, a linear model of the following form will be used to fit the data:

$$y = \beta_0 + \beta_1 x_1 + \beta_2 x_2 + \ldots + \beta_j x_j + \varepsilon \qquad (3.18)$$

where: y is true the response, β_j is the j^{th} model parameter, and x_j is the j^{th} predictor, ε represents the model error.

The Liu and Jordan type models rely on multiple piece curve fitting to accurately predict the diffuse fraction as a function of the clearness index. Based on the overall plots of diffuse fraction vs. clearness index shown in Figures 3.2a and 3.4 - 3.7, it is clear that a piecewise model in k_t will fit the data better than a single piece model. The question here is: should a multiple piece curve be used in a higher *dimensional* model ? In other words, if the final model was a function of

three variables, x_1, x_2, and x_3, is it acceptable to fit the response in multiple pieces based on one variable, say x_1 ? This procedure would be acceptable if the variable x_1 is highly correlated with the response and x_2 and x_3 were somewhat less correlated with the response.

To further investigate the possibility of using a piecewise approach, correlation coefficients for each predictor variable were calculated. The correlation coefficient, r_{xy}, is a measure of the linear association of the variable, x, with the variable, y. Minitab [39] was used to calculate the correlation coefficients for each predictor variable; a subset of the correlation coefficient results are given below.

Table 3.3: Variable Correlation Coefficients, r_{xy}

	I_d/I (hr)	k_t (hr)	$\sin(\alpha)$	T_a (hr)	ϕ(hr)
k_t (hr)	-0.894				
$\sin(\alpha)$	-0.239	0.342			
T_a (hr)	-0.194	0.195	0.503		
ϕ(hr)	-0.439	-0.460	-0.233	-0.065	
ω(hr)	0.004	-0.003	0.312	-0.755	0.467

It is clear that k_t has a substantially higher correlation with the diffuse fraction when compared to the other variables. Therefore, fitting the diffuse fraction piecewise in k_t is acceptable. Based on the scatter plots given in Figures 3.2a and 3.4-3.7, three intervals of k_t seems appropriate. The intervals of k_t are initially approximated by the intervals used by Orgill and Hollands: lower interval $k_t \leq 0.35$, middle interval $0.35 < k_t < 0.75$, and high interval $k_t \geq 0.75$.

At this point, the question of fitting other predictor variables in a piecewise fashion arises. Predictor variables other than k_t will not be fit piecewise for several reasons. First, the statistical analysis and predictor selection for a set of approximately thirty variables would become too complex if each predictor were allowed variable intervals. Second, the goal of maintaining a simple model would be in jeopardy if several variables had to be fit piecewise. Fitting each variable piecewise would require a separate equation for all possible intervals of the selected variables. For example, if three variables were deemed significant and each variable required three intervals, 27 unique equations would have to be provided to estimate the hourly diffuse fraction for all possible variable intervals. Therefore, other predictor variables are not fit in a piecewise manner.

With the set of potential predictor variables assembled (Table 3.2) and a tentative model form defined (equation 3.18), a predictor variable selection procedure must be established. One selection procedure is the method of all possible regressions. With this method, all possible combinations of predictor variables are fit and the best regression equation is selected. The best equation will have a minimum overall standard error with a reasonable number of variables in the equation. Given the large number of predictor variables in this investigation (28), the computational effort required to carry out all possible regressions is prohibitive. For three intervals of k_t, the number of regressions to complete all possible combinations would be $3 \cdot 2^{27} = 402{,}653{,}184$.

An alternative to all possible regressions is the stepwise regression procedure (stepwise and other selection procedures are discussed in Appendix B). The goal in applying the stepwise procedure is to minimize the standard error and the number of variables in the final correlation.

In an effort to gain understanding of the diffuse fraction's association with the predictor variables, analysis was performed on the center interval of k_t ($0.35 < k_t < 0.75$). Stepwise regressions were performed on a monthly basis for each location to determine if location or seasonal bias existed in the selection of the best set of predictors. The complete set of predictor variables listed in Table 3.2 was used in the stepwise procedure. On a monthly basis, there was not a great deal of consistency in the variable selection due to the relatively short time interval; therefore, stepwise regression was performed on a yearly basis for each location. The results of the stepwise regression for the first 5 variables selected are listed in Tables 3.4 - 3.13. The tables include parameter estimates, t-ratios, and the overall standard errors of the correlation at each step. In this case, the t-ratio is related to the F-statistic and is a measure of the variable's "strength." A high t-ratio indicates that the variable is important in explaining deviations in the response, diffuse fraction. For further information on stepwise regression, F-statistics or t-ratios, consult Appendix B.

Table 3.4: Stepwise Regression Results, Albany (1979)

Variable	Step 1	2	3	4	5
k_t t-ratio	-1.916 -61.13	-1.854 -62.98	-1.731 -58.35	-1.667 -55.67	-1.685 -56.37
$k_t \cdot m$ t-ratio		-0.095 -15.69	-0.086 -14.83	-0.112 -17.47	-0.122 -18.38
$\phi/(\bar{\phi}T_a)$ t-ratio			0.661 12.72	0.675 13.29	0.633 12.41
$\overline{k_t}$ t-ratio				-0.312 -8.70	-0.226 -5.76
$\overline{T_{wb}}$ t-ratio					-0.002 -5.25
std. error	0.141	0.131	0.125	0.122	0.121

Table 3.5: Stepwise Regression Results, Albany (1980)

Variable	Step 1	2	3	4	5
k_t t-ratio	-1.920 -67.81	-1.844 -67.53	-1.734 -60.22	-1.681 -55.60	-1.675 -55.74
$k_t \cdot m$ t-ratio		-0.084 -14.16	-0.082 -14.55	-0.097 -15.53	-0.114 -16.03
$\phi/(\bar{\phi}T_a)$ t-ratio			0.488 9.93	0.528 10.71	0.491 9.90
$\overline{k_t}$ t-ratio				-0.214 -5.37	-0.227 -5.73
$\overline{T_{wb}}$ t-ratio					-0.002 -4.97
std. error	0.138	0.131	0.127	0.126	0.126

Table 3.6: Stepwise Regression Results, Albany (1981)

Variable	Step 1	2	3	4	5
k_t t-ratio	-1.938 -68.71	-1.822 -67.95	-1.787 -68.60	-1.708 -63.26	-1.675 -61.37
$k_t \cdot m$ t-ratio		-0.095 -17.10	-0.128 -20.86	-0.112 -19.81	-0.192 -13.74
$\overline{T_{wb}}$ t-ratio			-0.004 -11.03	-0.004 -11.11	-0.005 -12.06
$\phi/\overline{\phi}$ t-ratio				0.145 8.79	0.135 8.24
$\exp(k_t \cdot m)$ t-ratio					0.012 5.74
std. error	0.134	0.123	0.119	0.116	0.115

Table 3.7: Stepwise Regression Results, Albany (1982)

Variable	Step 1	2	3	4	5
k_t t-ratio	-1.773 -58.71	-1.967 -67.94	-1.989 -70.64	-1.909 -64.80	-1.898 -64.96
$\sin(\alpha)$ t-ratio		0.288 19.06	0.362 22.00	0.352 21.77	0.351 21.95
T_a t-ratio			-0.004 -9.86	-0.008 -12.52	-0.007 -10.35
ω t-ratio				0.108 7.81	0.137 9.38
$\overline{\omega}$ t-ratio					-0.099 -5.62
std. error	0.130	0.116	0.113	0.110	0.109

Table 3.8: Stepwise Regression Results, Cape

Variable	Step 1	2	3	4	5
k_t t-ratio	-1.694 -69.18	-1.937 -82.42	-1.946 -86.13	-1.910 -82.97	-1.889 -80.14
sin(α) t-ratio		0.320 26.45	0.409 31.06	0.411 31.47	0.414 31.75
$\overline{T_a}$ t-ratio			-0.009 -14.38	-0.012 -15.49	-0.009 -8.74
$\overline{T_a}\phi$ t-ratio				0.005 6.76	0.017 5.10
ω t-ratio					-0.143 -3.80
std. error	0.136	0.120	0.116	0.115	0.114

Table 3.9: Stepwise Regression Results, Hamburg

Variable	Step 1	2	3	4	5
k_t t-ratio	-1.687 -65.26	-1.747 -67.41	-1.715 -67.98	-1.684 -64.64	-1.669 -62.55
sin(α) t-ratio		0.142 9.80	0.240 14.48	0.242 14.63	0.253 14.80
$\overline{T_a}$ t-ratio			-0.006 -11.05	-0.006 -11.58	-0.005 -8.16
$\phi/\overline{\phi}$ t-ratio				0.032 4.48	0.034 4.73
$\overline{k_t}$ t-ratio					-0.107 -2.53
std. error	0.123	0.120	0.116	0.116	0.115

Table 3.10: Stepwise Regression Results, Valentia

Variable	Step 1	2	3	4	5
k_t t-ratio	-1.564 -53.63	-1.604 -60.02	-1.585 -59.97	-1.604 -61.22	-1.591 -60.61
sin(α) t-ratio		0.277 18.04	0.214 12.36	0.153 8.01	0.166 8.61
$T_a \cdot \phi$ t-ratio			0.009 7.47	0.012 9.61	0.012 9.73
$\overline{\phi}$ t-ratio				-0.597 -6.91	-0.748 -8.00
$\overline{k_t}$ t-ratio					-0.213 -4.11
std. error	0.137	0.125	0.123	0.121	0.120

Table 3.11: Stepwise Regression Results, Copenhagen

Variable	Step 1	2	3	4	5
k_t t-ratio	-1.055 -33.18	-0.967 -31.63	-0.987 -33.58	-0.995 -35.15	-0.997 -35.30
ϕ/T_a t-ratio		0.591 13.99	0.793 17.88	1.043 21.50	1.102 21.18
sin(α) t-ratio			0.219 11.26	0.289 14.60	0.267 12.72
$T_{wb}/\overline{T_{wb}}$ t-ratio				-4.420 -10.85	-4.66 -11.27
$\overline{T_a}$ t-ratio					0.002 3.08
std. error	0.146	0.137	0.132	0.127	0.127

Table 3.12: Stepwise Regression Results, U.S. Data

Variable	Step 1	2	3	4	5
k_t t-ratio	-1.848 -144.6	-1.983 -161.8	-2.018 -171.8	-1.940 -156.7	-1.859 -119.3
sin(α) t-ratio		0.259 39.87	0.365 51.02	0.357 48.76	0.233 15.51
$\overline{T_a}$ t-ratio			-0.005 -29.68	-0.005 -31.60	-0.005 -31.58
$\phi/\overline{\phi}$ t-ratio				0.127 17.49	0.126 17.44
$k_t \cdot m$ t-ratio					-0.049 -8.55
std. error	0.138	0.127	0.121	0.119	0.119

Table 3.13: Stepwise Regression Results, All Data

Variable	Step 1	2	3	4	5
k_t t-ratio	-1.709 -164.8	-1.807 -177.0	-1.814 -182.8	-1.776 -178.8	-1.742 -171.7
sin(α) t-ratio		0.211 37.79	0.300 47.90	0.321 51.42	0.310 49.51
$\overline{T_a}$ t-ratio			-0.004 -28.48	-0.005 -30.73	-0.001 -3.69
$\phi/\overline{T_a}$ t-ratio				0.342 20.91	0.527 25.22
$\overline{\omega}$ t-ratio					-0.082 -14.08
std. error	0.142	0.135	0.131	0.129	0.128

The stepwise regression results on a yearly time period show that k_t is the single most important variable by being selected first in stepwise and by its high t-ratio. The next most important variable does not appear as straight forward as k_t because of the nature of the stepwise procedure. At a given step, the stepwise regression procedure will select the variable that has the highest t-ratio. Although other variables may have t-ratios that are nearly as large, they will not be selected. However, Minitab [39] has a feature which prints the best alternative variables as determined by the magnitude of their t-ratio. This feature was used to identify the second most important variable, sine of the solar altitude. In some cases (Albany, 1979-1981) $\sin(\alpha)$ was not selected as the second most important variable but its t-ratio was nearly as high as the variable actually selected. To illustrate the example, Table 3.14 lists the t-ratio results for cases when the sine of the solar altitude was not selected.

Table 3.14: Alternative Variable Results

Location	Variable Selected (t - ratio)	Alternative Variable (t - ratio)
Albany (1979)	$k_t \cdot m$ (-15.69)	$\sin(\alpha)$ (15.49)
Albany (1980)	$k_t \cdot m$ (-14.46)	$\sin(\alpha)$ (14.42)
Albany (1981)	$k_t \cdot m$ (-17.10)	$\sin(\alpha)$ (15.78)

It can be seen that the sine of the solar altitude has nearly the same magnitude of t-ratio as $k_t \cdot m$. Therefore, the sine of the solar altitude is the second most important variable. The most consistent third and fourth variables are the monthly average hourly ambient temperature and the ratio of the hourly relative humidity to the monthly average hourly relative humidity, respectively. Addition of a fifth variable does not substantially reduce the overall standard error of the model. Thus, the best four predictor variables to explain the deviations in the diffuse fraction are:

$$\hat{I}_d/I = f\left(k_t, \sin(\alpha), \overline{T_a}, \phi/\overline{\phi}\right)$$

Unfortunately, monthly average hourly data are not included in commonly used datasets [2, 7]. A correlation with monthly average hourly variables would force users to derive the necessary quantities from existing datasets. At this point, a decision was made to eliminate the use of monthly average hourly predictors and pursue a correlation based only on hourly values of the predictors. The impact of this decision will be investigated when the new set of predictor variables are selected.

The stepwise selection procedure was applied to the center interval of k_t using the set of predictors with the monthly average hourly predictors removed. On an hourly basis, the top four predictors were selected in a fashion similar to that described above. The best predictors to explain the deviations in the diffuse fraction are:

$$\hat{I}_d/I = f(k_t, \sin(\alpha), T_a, \phi)$$

This set of predictors provides the foundation for the remaining development and analysis of a new diffuse fraction correlation.

The next step in the diffuse fraction correlation development is to determine the best k_t intervals for piecewise fitting. The current interval is based on that of the Orgill and Hollands correlation. The appropriate k_t interval will minimize the standard error of the final correlation. Since the center interval of k_t contains the majority of data points, it was the primary region of concentration for determining the specific bounds on the intervals. A manual search technique was employed to find the best interval for k_t. The search routine varied the range of the center k_t interval until the overall standard error of the full correlation for the center interval was minimized. The center interval which minimized the standard error is $0.3 < k_t < 0.78$. The standard error for the correlation in the center interval is 0.129. In Table 3.13, the standard error for the correlation which included the monthly average predictors is 0.129 (based on the interval $0.35 < k_t < 0.75$). Thus, it appears that there is not a significant loss by not including the monthly average hourly predictor variables in the correlation. The three intervals of k_t for piecewise fitting and the number of data points in each interval are given in Table 3.15.

Table 3.15: Data Distribution In k_t Intervals

Interval	Number of Points	% of Total
$0 \leq k_t \leq 0.30$	4783	21.8
$0.3 < k_t < 0.78$	16286	74.3
$0.78 \leq k_t \leq 1.0$	854	3.9

The results of stepwise regression performed on the final k_t intervals are given in Tables 3.16 - 3.19.

Table 3.16: Stepwise Regression Results, $0 \leq k_t \leq 0.30$

Variable	Step 1	2	3	4
k_t t-ratio	-0.248 -28.52	-0.234 -25.36	-0.239 -25.75	-0.232 -24.97
ϕ t-ratio		0.018 4.52	0.020 5.08	0.020 4.91
$\sin(\alpha)$ t-ratio			0.015 4.42	0.024 6.65
T_a t-ratio				-0.0007 -6.39
std. error	0.0462	0.0461	0.0460	0.0458

Table 3.17: Stepwise Regression Results, $0.3 < k_t < 0.78$

Variable	Step 1	2	3	4
k_t t-ratio	-1.665 -211.4	-1.749 -219.6	-1.753 -224.9	-1.716 -217.3
sin(α) t-ratio		0.177 35.04	0.252 44.43	0.267 47.25
T_a t-ratio			-0.003 -26.94	-0.004 -29.51
ϕ t-ratio				0.106 20.32
std. error	0.138	0.133	0.130	0.129

Table 3.18: Stepwise Regression Results, $0.78 \leq k_t$

Variable	Step 1	2	3	4
sin(α) t-ratio	-0.219 -14.07	-0.272 -16.99	-0.239 -13.59	-0.256 -12.63
ϕ t-ratio		0.081 8.92	0.079 8.75	0.0734 4.73
k_t t-ratio			0.406 4.31	0.426 4.54
T_a t-ratio				0.00349 7.52
std. error	0.100	0.0960	0.0948	0.0936

The stepwise regression in each interval reveals some interesting behavior of the predictor variables. The relative importance of each variable is consistent with the exception of the last interval. Table 3.19 lists the order of importance of each predictor and its associated sign (indicating if the variable is negatively or positively correlated with the diffuse fraction).

Table 3.19: Relative Importance of Predictors

Order	Low	k_t Interval Middle	High
1	k_t (-)	k_t (-)	sin(α) (–)
2	sin(α) (+)	sin(α) (+)	T_a (+)
3	T_a (–)	ϕ (+)	ϕ (+)
4	ϕ (+)	T_a (–)	k_t (+)

The clearness index is the most important variable in the low and middle intervals but at the high interval, the significance of the clearness index decreases dramatically. At the low and middle interval, k_t is negatively correlated with the diffuse fraction thus, an increase in the clearness index (clear skies) causes a decrease in the diffuse fraction. At high intervals there is an inversion in the sign of the k_t coefficient implying that a further increase in the clearness index above 0.78 will increase the fraction of solar radiation diffusely scattered. This situation could arise in the following scenario: highly intermittent cloudy sky conditions with direct solar radiation reaching the measuring surface unimpeded and only a

portion of the diffuse blocked by the clouds. A significant portion of the incident radiation is reflected from the earth's surface to the clouds and back to the measuring instrument. Thus, the increase in diffuse radiation due to internal reflection of the incident total radiation causes the diffuse fraction to increase with apparent increasing clearness.

The solar altitude effects are not as strong under cloudy skies (low values of k_t) but under clear skies (high values of k_t), the solar altitude becomes the dominant predictor variable. For clear sky conditions, the diffuse fraction increases for decreasing solar altitude angles due to the longer path length required for radiation to travel. These results are consistent with those found by Skartveit and Olseth [34]. The only problem with the high interval of k_t is the apparent discontinuity of the predicted diffuse fraction caused by the coefficients of k_t, sine of solar altitude, and ambient temperature changing their signs. The sparsity of data in this interval does not greatly contribute to understanding this peculiar effect.

The effect of relative humidity and ambient temperature on the diffuse fraction are consistent in the low and middle intervals of k_t. When the ambient temperature is constant and relative humidity increases, the diffuse fraction increases because there is more moisture in the atmosphere scattering incident radiation. A decrease in ambient temperature means the air will hold less moisture. Thus, for constant relative humidity, a decrease in the ambient temperature causes the diffuse fraction to decrease because there is less moisture in the

atmosphere available for scattering incident radiation.

The appropriate intervals of k_t have been selected as well as the final set of predictors. The final version of the hourly diffuse fraction correlation was determined by applying the method of least squares to each k_t interval. The results of the fitted models in each interval along with the appropriate statistical tests are presented below (Appendix B contains further information regarding the techniques used in this statistical analysis).

Interval: $0 \leq k_t \leq 0.3$.

$$\hat{I}_d/I = 1.000 - 0.232\,k_t + 0.0239\sin(\alpha) - 0.000682\,T_a + 0.0195\,\phi \qquad (3.19)$$

The equation carries a subsequent constraint $I_d/I \leq 1.0$. The ANOVA (analysis of variance) is given in Table 3.20 (for more information regarding analysis of variance, see Appendix B).

Table 3.20: Analysis of Variance, $0 \leq k_t \leq 0.3$

Source	d.f.	Sum Sq.	Mean Sq.	F
Regression I bo	4	1.90672	0.47668	227.087
Residual	4778	9.83642	0.00210	
Total, corrected	4782	11.74314		

The null hypothesis for testing the overall significance (at a 95% confidence level) of the fit is given by:

$$H_o: \beta_0 = \beta_1 = \beta_2 = \beta_3 = \beta_4 = 0$$

Comparing the calculated F-statistic with the appropriate F-distribution point at a 95% confidence level [40],

$$F = 227.08,\ F_{5,\infty} = 2.21$$

The overall regression is highly significant and the null hypothesis is rejected. In other words, all parameters in the fitted equation are not zero. The test does not indicate if a particular parameter is zero. Partial F-tests are performed to determine if each parameter is significant. If the parameter is not significant, it will be removed from the fitted equation. In general, the null hypothesis and alternative, respectively for the partial F-tests are given by:

$$H_o: \beta_i = 0,\ H_1: \beta_i \neq 0$$

Since there is only one degree of freedom in the null hypothesis, a t-test can be performed by using the following relationship given by Draper and Smith [40]:

$$F_{1,\nu_2} = t^2_{\nu_2}$$

At a 95% confidence level, the individual parameters must have a calculated t-statistic greater than t = abs(1.96). The results of the t-statistics calculated for each parameter are given below.

Predictor	t-statistic	Result
constant	230.91	significant
k_t	-24.97	significant
sin(α)	6.65	significant
T_a	-6.39	significant
ϕ	4.91	significant

Thus, all parameter estimates are statistically significant at a 95% level and none will be excluded from the final correlation.

Interval: $0.3 < k_t < 0.78$.

$$\hat{I}_d/I = 1.329 - 1.716\,k_t + 0.267\sin(\alpha) - 0.00357\,T_a + 0.106\,\phi \qquad (3.20)$$

Equation (3.20) has the subsequent constraints: $I_d/I \leq 0.97$ **and** $I_d/I \geq 0.1$. The $I_d/I \leq 0.97$ constraint is used to ease the transition from the lower k_t interval to the middle interval.

Table 3.21: Analysis of Variance, $0.3 < k_t < 0.78$

Source	d.f.	Sum Sq.	Mean Sq.	F
Regression I bo	4	894.29	223.57	13483.0
Residual	16281	269.79	0.02	
Total, corrected	16285	1164.08		

Overall regression is highly significant at a 95% level. The t-statistics for each variable are given below.

Predictor	t-statistic	Result
constant	216.67	significant
k_t	-217.28	significant
sin(α)	47.25	significant
T_a	-29.51	significant
ϕ	20.32	significant

All parameter estimates are statistically significant at a 95% level and none will be excluded from the final correlation.

Interval: $0.78 \leq k_t$.

$$\hat{I}_d/I = -0.0312 + 0.426\,k_t - 0.256\sin(\alpha) + 0.00349\,T_a + 0.0734\,\phi \qquad (3.21)$$

Equation (3.21) has the subsequent constraint: $I_d/I \geq 0.1$.

Table 3.22: Analysis of Variance, $0.78 < k_t$

Source	d.f.	Sum Sq.	Mean Sq.	F
Regression I bo	4	3.1254	0.7813	87.20
Residual	849	7.6028	0.00896	
Total, corrected	853	10.7282		

Overall regression is highly significant at a 95% level. The t-statistics for each variable are given below.

Predictor	t-statistic	Result
constant	-0.39	not signif.
k_t	4.54	significant
$\sin(\alpha)$	-12.63	significant
T_a	7.52	significant
ϕ	4.73	significant

Since the t-statistic for the constant is not significant, it will not be included in the final correlation.

The distributional tests (t-tests) performed will not be valid until the proper diagnostic tests are performed. The diagnostic tests consist primarily of residual plots to assure that the underlying assumptions made during the t and F-tests are not violated. The hypothesis tests performed on the models assume the residuals are normally distributed with mean zero and constant variance.

$$\varepsilon_i \sim N(0, \sigma^2)$$

Two methods to test for normally distributed residuals include residual histograms and normal probability plots. The residual histograms should look like a normal distribution centered at 0. The normal probability plot should produce a straight line. Figure 3.8 shows both the histogram and normal probability plots of standardized residuals for the center interval of k_t. The data in the upper and lower intervals are not as normal due to the subsequent constraints placed on the models.

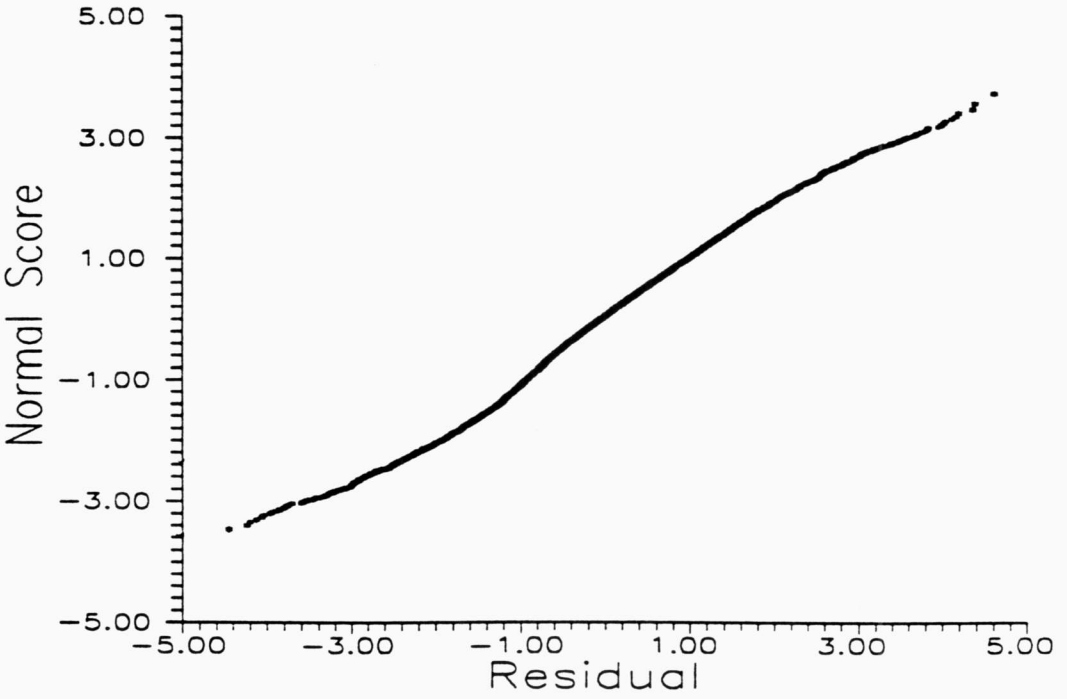

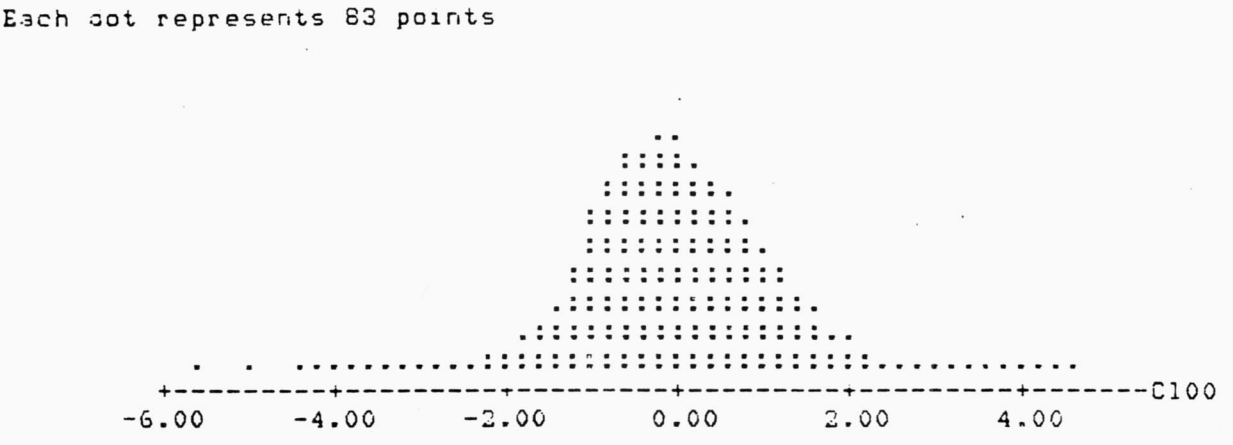

Figure 3.8: Normal probability plot and residual histogram

The remaining diagnostics will consist of residuals being plotted against time, predictors, and predicted values of the diffuse fraction. In all cases, the points on each plot should appear as a band of noise centered at a residual value of 0. There should not be any linear, curvilinear, or funnel shapes in the residual plots. For more information on residuals for diagnostic analysis see Draper and Smith [40] and Belsley, Kuh, and Welsch [41]. A sample residual plot of each type will be presented for illustration purposes. The remaining residual plots are available for inspection in Appendix C.

To determine of seasonal or time dependent trends exist, the residuals are plotted in time series. Figure 3.9 is a time series plot of residuals on an hourly and daily basis for Albany data. The plots appear to be acceptable. No noticeable time dependencies are apparent from the time series plots. Figure 3.10 - 3.11 plots residuals against each predictor variable for Albany. The plots of residual vs. k_t appear abnormal due to the piecewise fit. If the plot is viewed within each k_t interval, it appears acceptable. The plots of the residuals against the other predictors appear acceptable. The final plot in Figure 3.12 shows the residuals against the predicted diffuse fraction values for Albany. The plot appears odd due to the subsequent constraints placed on the fitted equations. On an overall basis, the diagnostic plots are acceptable and support the derived correlation.

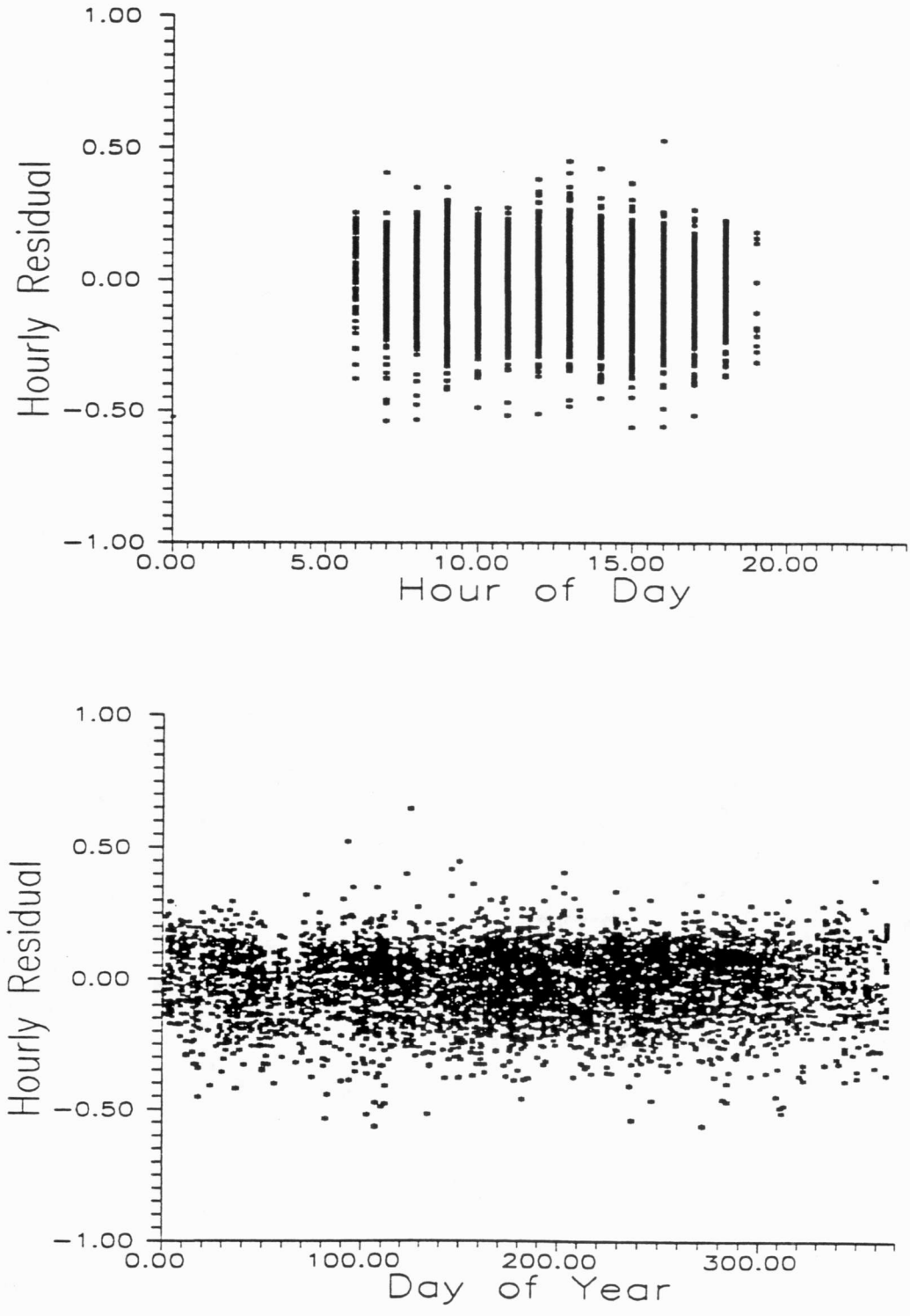

Figure 3.9: Time series plot of residuals, Albany 1979-1982

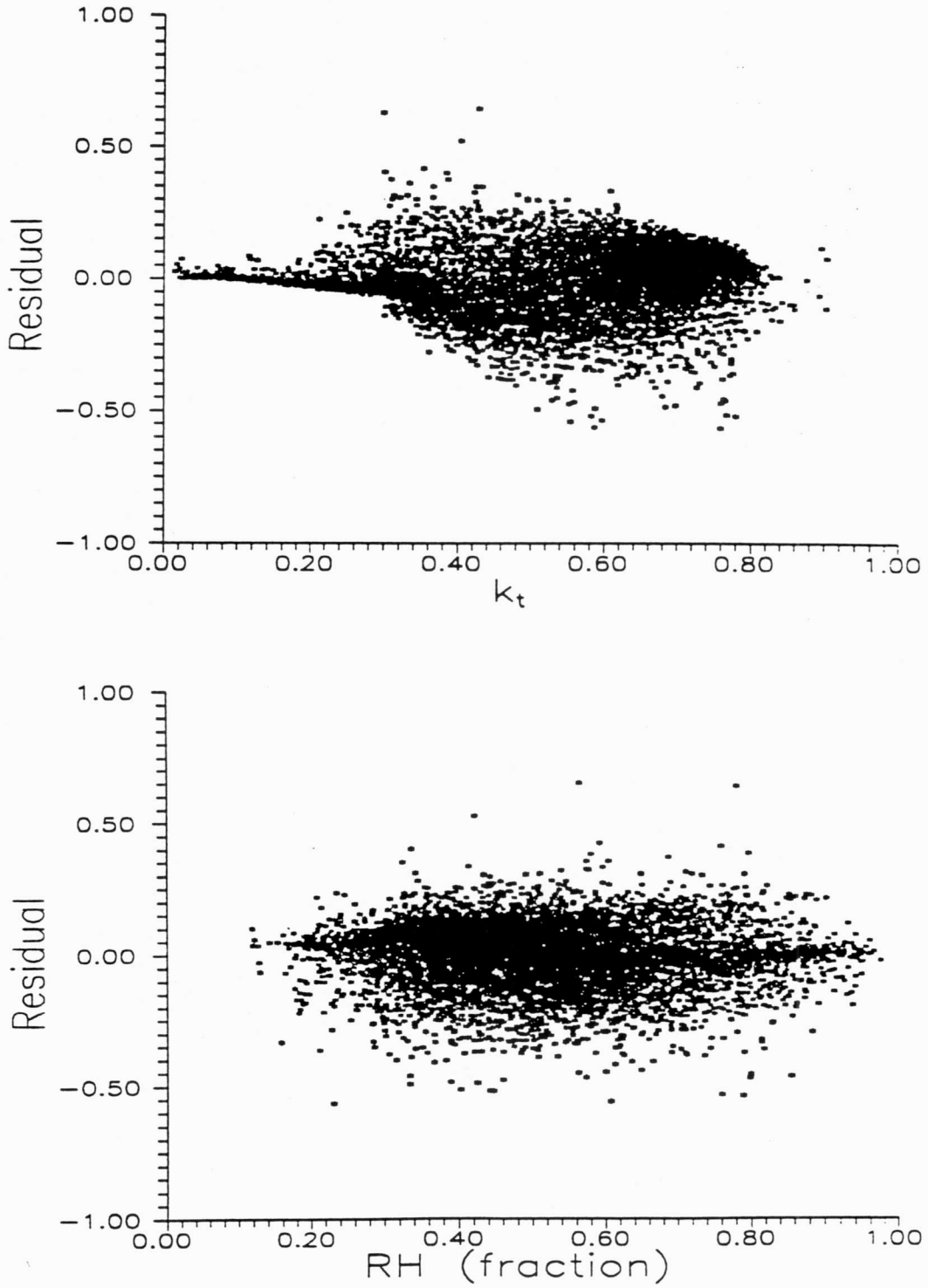

Figure 3.10:Residuals vs. predictors, Albany 1979-1982

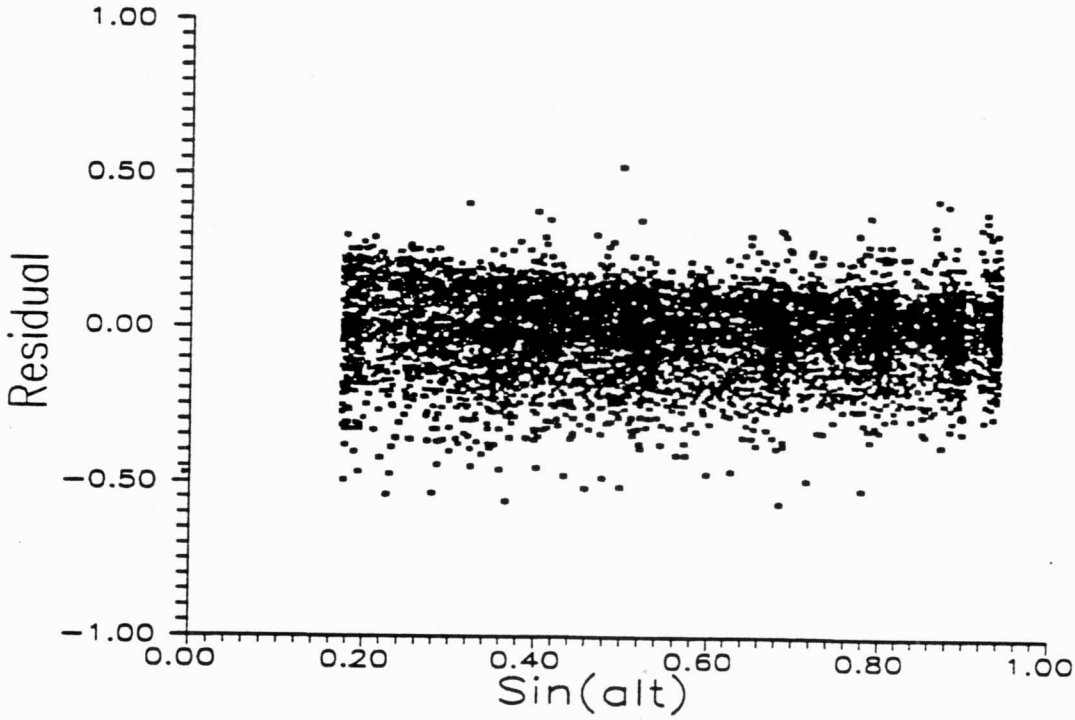

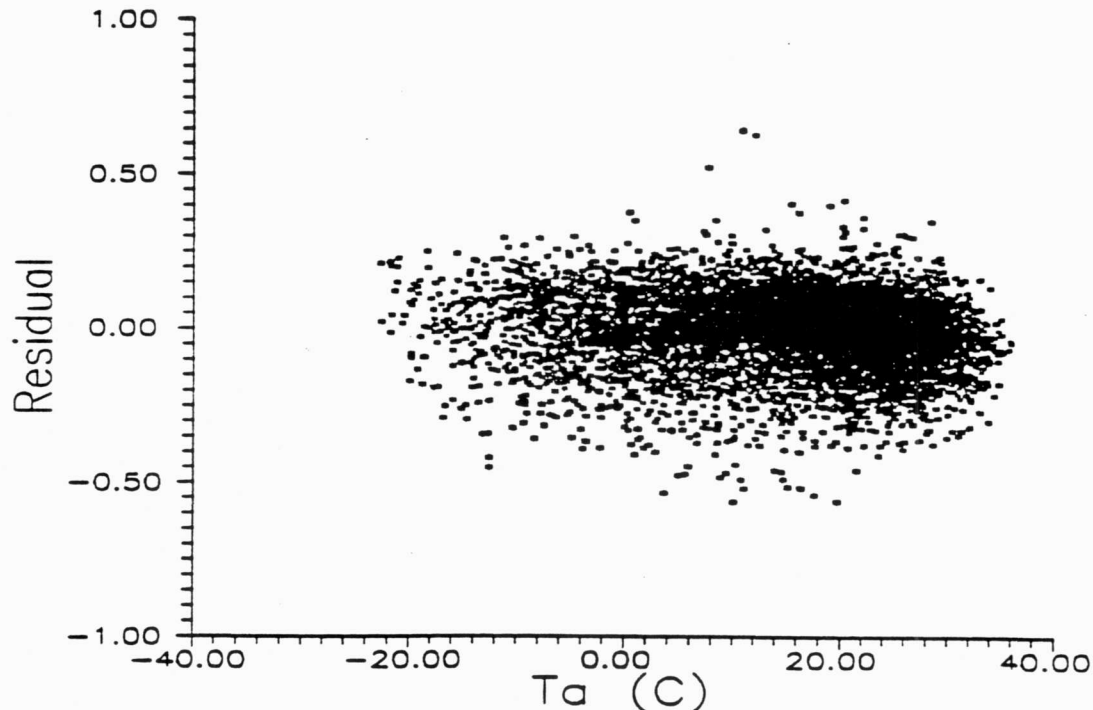

Figure 3.11: Residuals vs. predictors, Albany 1979-1982

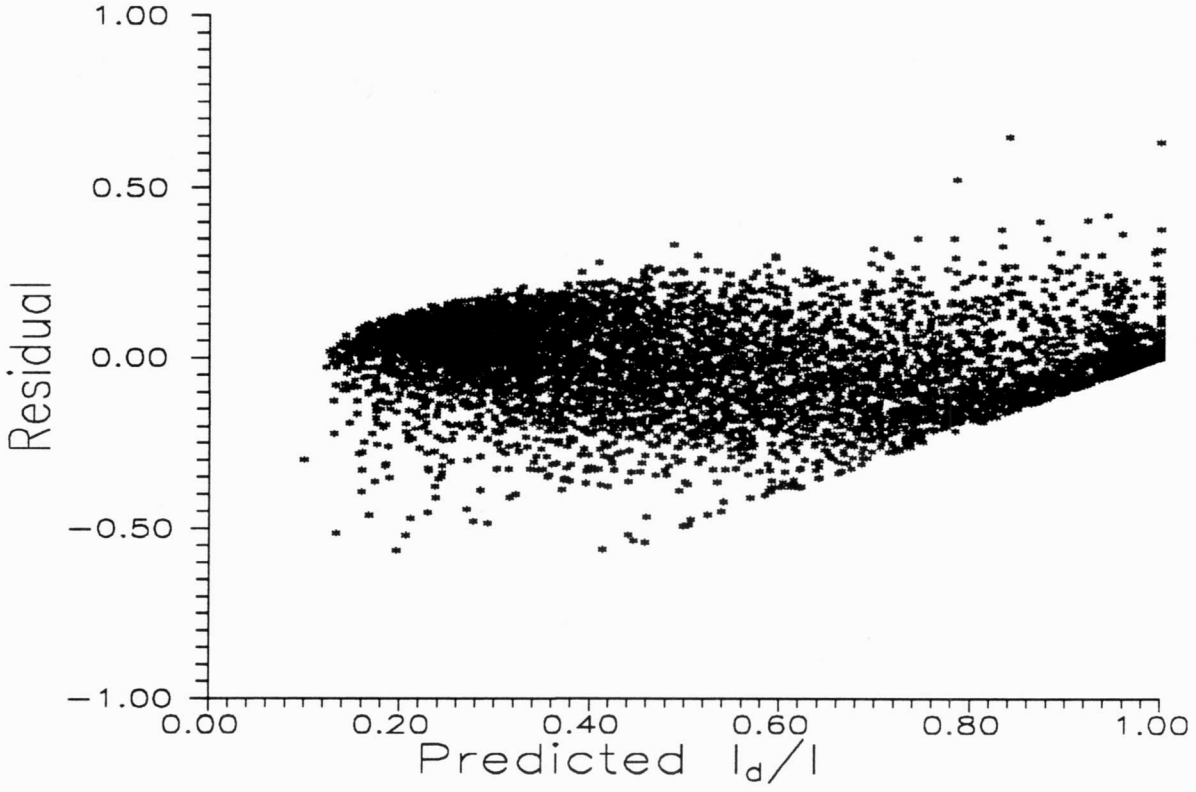

Figure 3.12: Residual vs. predicted diffuse fraction, Albany 1979-1982

The final version of the correlation is given below.

Interval: $0 \le k_t \le 0.3$; Constraint: $I_d/I \le 1.0$.

$$\hat{I}_d/I = 1.000 - 0.232\,k_t + 0.0239\sin(\alpha) - 0.000682\,T_a + 0.0195\,\phi \qquad (3.19)$$

Interval: $0.3 < k_t < 0.78$; Constraint: $I_d/I \le 0.97$ and $I_d/I \ge 0.1$.

$$\hat{I}_d/I = 1.329 - 1.716\,k_t + 0.267\sin(\alpha) - 0.00357\,T_a + 0.106\,\phi \qquad (3.20)$$

Interval: $0.78 \le k_t$; Constraint: $I_d/I \ge 0.1$.

$$\hat{I}_d/I = 0.426\,k_t - 0.256\sin(\alpha) + 0.00349\,T_a + 0.0734\,\phi \qquad (3.21)$$

At this point, a simple piecewise correlation exists which gives the hourly diffuse fraction as a function of hourly clearness index, solar altitude, ambient temperature, and relative humidity. Although hourly ambient temperature and relative humidity are commonly measured climatic quantities (or can be calculated from measured quantities), they may not be available in some data sets. It would be desirable to provide a reduced form of the current correlation for use when hourly ambient temperature and/or relative humidity data are not available. The bias for each of the current model parameters is calculated to determine the new parameters when hourly ambient temperature and/or relative humidity data are not available. The result is a piecewise model which provides estimates of the hourly diffuse fraction as a function of the clearness index and solar altitude angle.

Interval: $0 \le k_t \le 0.3$; Constraint: $Id/I \le 1.0$

$$\hat{I}_d/I = 1.020 - 0.254\,k_t + 0.0123\sin(\alpha) \qquad (3.22)$$

Interval: $0.3 < k_t < 0.78$; Constraint: $Id/I \leq 0.97$ and $Id/I \geq 0.1$.

$$\hat{I}_d/I = 1.400 - 1.749\,k_t + 0.177\sin(\alpha) \tag{3.23}$$

Interval: $0.78 \leq k_t$; Constraint: $Id/I \geq 0.1$

$$\hat{I}_d/I = 0.486\,k_t - 0.182\sin(\alpha) \tag{3.24}$$

Therefore, when hourly ambient temperature and or hourly relative humidity are not available, the correlation given by equations 3.22-3.24 should be used for estimating the hourly diffuse fraction.

A final correlation which is a function of k_t only was also developed. This was done to allow direct comparison to the Liu and Jordan type correlations presented in section 3.2.1. The reduced correlation is given below.

Interval: $0 \leq k_t \leq 0.3$; Constraint: $I_d/I \leq 1.0$.

$$\hat{I}_d/I = 1.020 - 0.248\,k_t \tag{3.25}$$

Interval: $0.3 < k_t < 0.78$

$$\hat{I}_d/I = 1.45 - 1.67\,k_t \tag{3.26}$$

Interval: $0.78 \leq k_t$

$$\hat{I}_d/I = 0.147 \tag{3.27}$$

The correlation is plotted in Figure 3.13 along with the Liu and Jordan type correlations introduced in section 3.2.1. The derived correlation based on k_t is similar to Orgill and Hollands [9] and Erbs [10].

3.2.2.3 Model Performance

An obvious question at this point is: does the new hourly diffuse fraction correlation provide any improvement over the current Liu and Jordan type correlations? A simple composite residual sum squares (CRSS) comparison is used to quantify the improvement of the new hourly diffuse fraction correlation over current Liu and Jordan type models. In an effort to provide a fair comparison between the new hourly diffuse fraction correlation and the current Liu and Jordan type models, the reduced correlation based on k_t (given by equations 3.25 - 3.27) derived from the existing dataset will be included in all model comparisons. The reduced model will be referred to as "ktcorr" in the remainder of this thesis. By comparing the ktcorr model with the new diffuse fraction correlation, the relative merit of added climatic and geometric terms in the new model will be directly assessed. The reduced correlation based on k_t and sine of solar altitude (given by equations 3.22 - 3.24) will also be included in the correlation comparison. The model will be identified by DTR(k_t). The only other existing model that will be included in the model comparisons will be the Erbs model as given in section 3.2.1.3. Location and seasonal effects are noted.

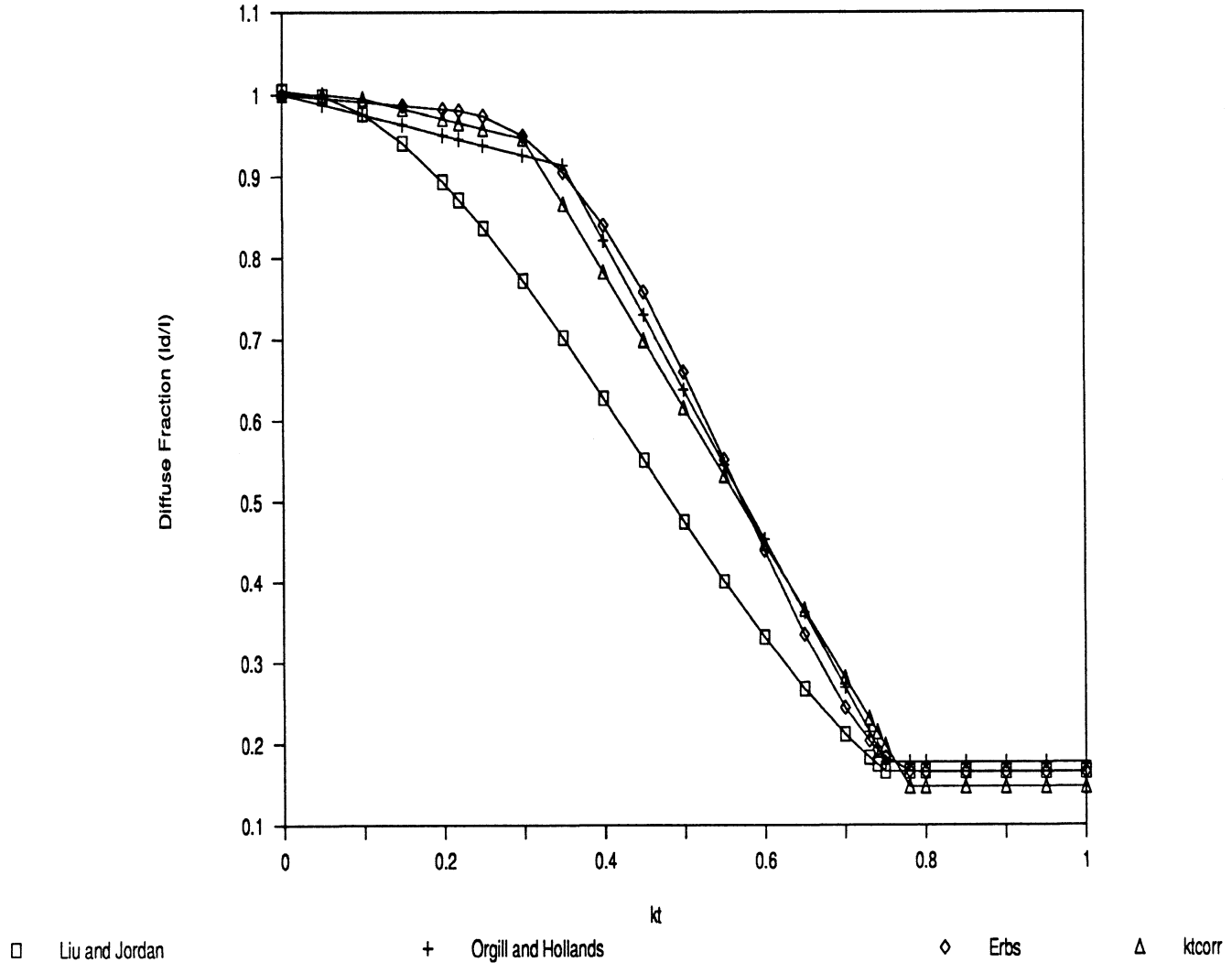

Figure 3.13: Diffuse fraction including ktcorr

The CRSS is calculated by the following relationship:

$$CRSS = \sum_{location} \sum_{year} \sum_{hour} \left(\frac{\hat{I}_d}{I} - \frac{I_d}{I_{meas}} \right)^2 \qquad (3.29)$$

Applying equation 3.29 to the complete dataset yielded the results listed in Table 3.23.

Table 3.23: Composite Residual Sum Squares Results

Location	New Corr.	DTR(k_t)	ktcorr	Erbs
Albany, '79	33.04	35.67	38.16	37.01
Albany, '80	35.42	36.05	39.64	37.73
Albany, '81	27.37	29.72	32.96	30.99
Albany, '82	23.38	25.07	28.80	29.54
Cape	45.85	50.63	55.29	57.97
Valentia	37.95	41.04	46.37	47.24
Hamburg	34.75	34.51	35.59	37.30
Copenhagen	55.49	58.52	65.78	77.64
Total	293.25	311.21	342.59	355.42

The new hourly diffuse fraction correlation reduces the residual sum squares of the correlation based on k_t only (derived from the same dataset) by 14.4%. The reduced hourly diffuse fraction correlation shows a 9% improvement over ktcorr.

As pointed out in section 3.2.2.1, location differences were observed in the plots of diffuse fraction vs. clearness index for each data set. The location

differences are quantified here in the form of residual sum squares for each location. The variation in the residual sum squares for each location suggests that the correlation is not location independent. Copenhagen exhibits the largest residual sum square. The peculiarities of the Copenhagen data noted in section 3.2.2.1 explain the high residual but the unusual behavior of the data in that particular data set remains unexplained.

To observe potential seasonal effects, the residual sum squares is plotted on a monthly basis. Three histograms are presented to show the typical trends in the monthly residual sum squares for each of the correlations listed in Table 3.23. Figure 3.14 shows the monthly residual sum squares for Albany, 1979, 1980 data. Figure 3.15 plots monthly residual sum squares for Hamburg. The plots are representative of the other locations and suggest that errors tend to be higher in the spring and summer months. Seasonal effects were not apparent in the plots of residuals in time order (Figure 3.9). No attempt is made to account for location or seasonal effects. The author feels that the current correlation is acceptable.

3.3 Conclusions

Two methods for calculating the beam and diffuse radiation were introduced in this chapter. The first method uses Lambert's law to model the monochromatic beam radiation passing through a cloudless atmosphere (formally identified as the radiative transfer equation). The second method estimates the diffuse fraction of the global horizontal radiation by means of a spectrally independent empirical model derived from extensive datasets of radiation measurements.

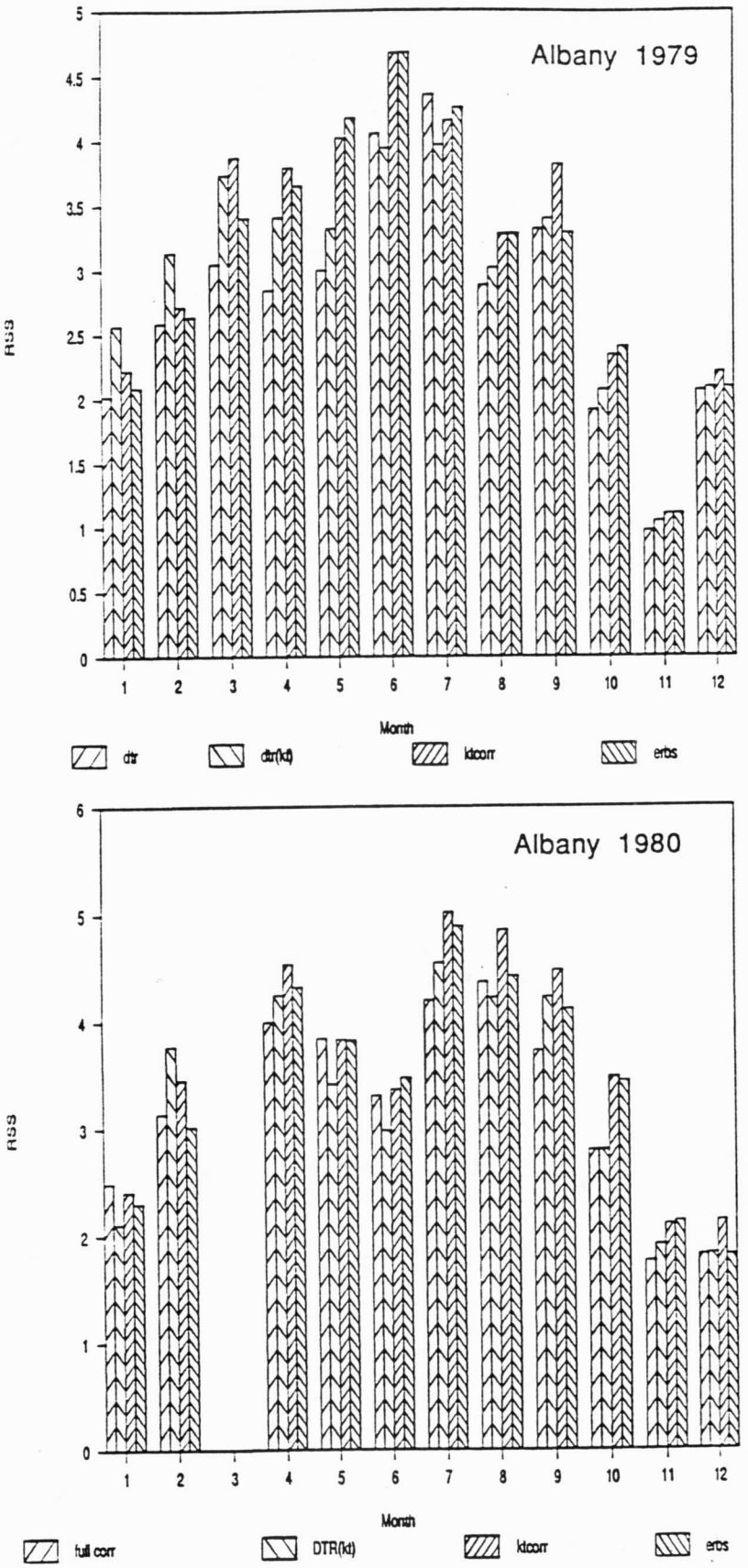

Figure 3.14: Monthly residual sum squares for Albany 1979, 1980

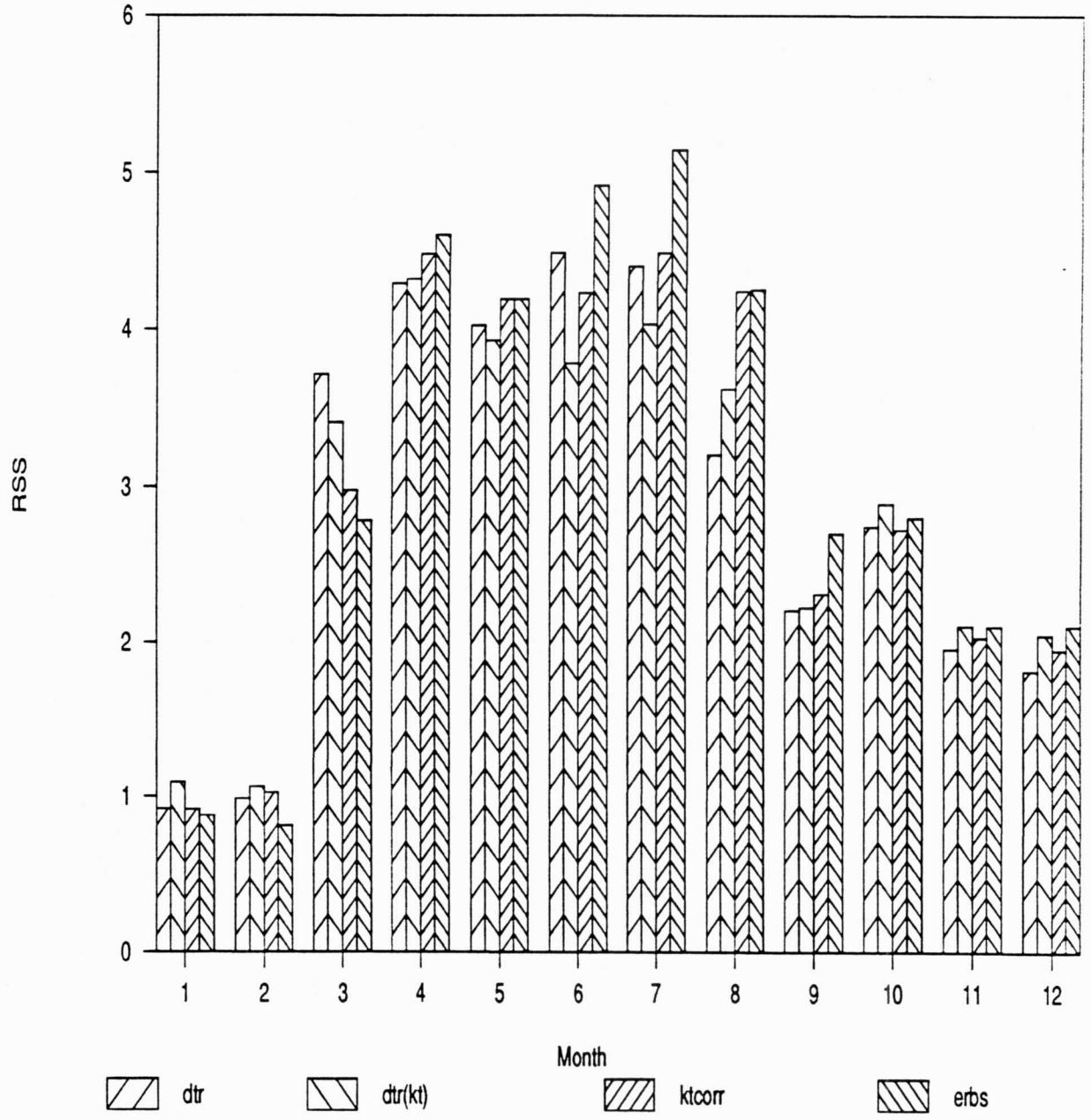

Figure 3.15: Monthly residual sum squares for Hamburg data

The radiative transfer equation was developed for a cloudless sky with four constituents responsible for absorbing and scattering radiation. The difficulty in this method arises in determining the vertical optical depths for each of the atmospheric constituents that absorb and scatter radiation. The vertical optical depths for a given constituent will vary with temperature and pressure. The final solution to the radiative transfer equation is computationally intensive because it must be integrated over all wavelengths.

The second method uses empirical spectrally independent models to estimate the diffuse fraction of the global horizontal radiation (diffuse fraction correlations). Diffuse fraction correlations are derived from large databases of actual radiation measurements. The fitted diffuse fraction models are very simple and well suited for use in estimating radiation inputs for hourly simulation of energy systems. The drawback associated with current diffuse fraction correlations is the high standard error of estimating the diffuse fraction.

The goal of this chapter was to reduce the standard error of the current Liu and Jordan type correlations by including additional predictor variables in the model. Stepwise regression is used to reduce a large set of potential predictor variables down to four significant predictors. The significant predictors include hourly values of clearness index, sine of solar altitude, ambient temperature, and relative humidity. The final version of the piecewise correlation is given on p. 76 by equations 3.19-3.21. In the event that hourly ambient temperature and or

hourly relative humidity are not available, a reduced form of the correlation was derived to predict the diffuse fraction as a function of k_t and sine of the solar altitude (equations 3.22-3.24).

The improvement of the new correlation is demonstrated in section 3.2.2.3. The new correlation reduced the composite residual sum of squares by 14.4% when compared to a k_t correlation derived from the same dataset. The reduced form of the correlation reduces the composite residual sum squares by 9.2%. Some location and seasonal dependencies were suggested but their effects are considered to be negligible to the correlation's overall performance.

Chapter 4 Tilted Surface Models

Simulation of solar energy systems requires knowing the total radiation incident on the system's collecting surface in a specified time interval. An hour time step is the most common interval used in system simulations but simulations are not limited to hourly intervals. Consistent with the notation used by Duffie and Beckman [5], I indicates an hourly time interval of radiation. Although not explicitly stated, the intervals discussed herein are assumed to be hourly intervals. Most collecting devices associated with solar energy systems are tilted at some angle, β, with respect to the horizontal. Due to the lack of tilted surface solar radiation data, models are commonly employed to estimate the radiation incident on the collector's surface. Estimating the radiation on a tilted surface requires knowing the division of global horizontal radiation into its beam and diffuse components. In general, hourly global radiation measurements are available; hourly measurements of horizontal diffuse (or beam) radiation are not as widely available. If diffuse (or beam) radiation measurements are not available, the methods described in Chapter 3 can be used to estimate the hourly diffuse radiation. In this chapter, methods for projecting the horizontal radiation components onto a tilted surface are presented and evaluated.

The total radiation on a tilted surface is composed of three elements: beam, diffuse, and ground reflected.

$$I_T = I_{b,T} + I_{d,T} + I_{g,T} \tag{4.1}$$

where: I_T represents the total radiation on a tilted surface; $I_{b,T}$, $I_{d,T}$, and $I_{g,T}$ represent the respective beam, diffuse, and ground reflected radiation components on a tilted surface. The methods for projecting each radiation component onto a tilted surface are discussed below.

4.1 Beam Radiation

Projecting the beam radiation onto a tilted surface is accomplished by geometry. Duffie and Beckman [5] define the geometric factor, R_b as the ratio of beam radiation on a tilted surface to the beam radiation on a horizontal surface. R_b, as given in Chapter 1,

$$R_b = \frac{I_{b,T}}{I_b} = \frac{\cos\theta}{\cos\theta_z} \tag{1.2}$$

Thus, the beam radiation on a tilted surface is,

$$I_{b,T} = I_b \cdot R_b \tag{4.2}$$

When calculated values of either θ or θ_z exceed 90°, the beam radiation on the tilted surface will be zero. When θ is greater than 90°, the sun is behind the collecting surface. When θ_z is greater than 90°, the sun is below the horizon.

4.2 Diffuse Radiation

Diffuse radiation is the most difficult and challenging component to model or project onto a tilted surface. Chapter 1 introduced the diffuse sub-components consisting of circumsolar, horizon brightening, and isotropic sky diffuse. Several models have been proposed to estimate the diffuse radiation on a tilted surface, not all of which account for these three diffuse sub-components. Three existing tilted surface models are presented: isotropic, Hay and Davies [21], and Perez [20], et al. A new model based on the work of Hay and Davies, Temps and Coulson [4], and Klucher [16] is developed and evaluated with the above models.

4.2.1 Isotropic Model

The isotropic model [14] is the simplest of the tilted surface models. This model assumes the diffuse radiation is uniformly distributed over the complete sky dome. When integration is performed over the complete sky dome in the collector's field of view, the following view factor is obtained [4],

$$f_{c,s} = \cos^2(\beta/2) = \frac{1+\cos(\beta)}{2} \tag{4.3}$$

where β is the surface slope. Thus, the diffuse radiation on a tilted surface by the isotropic sky model is given by,

$$I_{d,T} = I_d\left(\frac{1+\cos(\beta)}{2}\right) \tag{4.4}$$

Under completely cloudy skies, the isotropic sky model becomes a good approximation. As skies become clearer, the validity of the isotropic sky model deteriorates due to the presence of anisotropic effects including: increase in intensity of diffuse radiation near the sun (circumsolar diffuse) and near the horizon (horizon brightening).

4.2.2 Hay and Davies Model

Hay and Davies [21] developed a model to predict the tilted surface diffuse which accounts for both circumsolar and isotropic diffuse. This model will be referred to as the "Hay" model. Realizing that the anisotropic behavior of circumsolar diffuse becomes more pronounced under clear sky conditions, Hay and Davies defined an "anisotropy index" to weight the circumsolar and isotropic radiation components. The anisotropy index is given by,

$$AI = \frac{I_{bn}}{I_{on}} \tag{4.5}$$

where: I_{bn} is the hourly direct normal beam radiation and I_{on} is the hourly extraterrestrial radiation at normal incidence. The anisotropy index defines a portion of the diffuse radiation to be treated as circumsolar with the remaining portion considered isotropic. The circumsolar diffuse on a tilted surface is:

$$I_{T,cir} = I_d \cdot AI \cdot \frac{\cos\theta}{\cos\theta_z} = I_d\,(AI \cdot R_b) \tag{4.6}$$

Since the circumsolar diffuse radiation originates from a region in the neighborhood around the sun, it is projected onto the tilted surface in the same fashion as beam radiation. In other words, the directional dependence of circumsolar diffuse is lumped with the directional dependence of beam radiation. The remaining diffuse radiation is treated as isotropic diffuse.

$$I_{T,iso} = I_d \cdot (1 - AI) \cdot \left(\frac{1 + \cos\beta}{2} \right) \tag{4.7}$$

The complete Hay model is,

$$I_{d,T} = I_d \left[(1 - AI) \cdot \left(\frac{1 + \cos\beta}{2} \right) + AI \cdot R_b \right] \tag{4.8}$$

Under clear skies, the anisotropy index will be high and the circumsolar diffuse is weighted heavier than the isotropic diffuse. Under cloudy skies, the anisotropy index goes to zero and the model will treat all diffuse radiation isotropically. This behavior is consistent with diffuse sky measurements made by Temps and Coulson [4] (and others as given in Hay and McKay [8]). Their measurements show that diffuse radiation is directionally dependent under clear skies and the directional dependence diminishes under cloudy skies.

The Hay model is very simple and quite elegant in its formulation of tilted surface diffuse radiation but there are potential weaknesses in the model. The Hay model does not include the anisotropic effect of horizon brightening. This could cause the model to underestimate the radiation on a tilted surface. Another

weakness is observed for cases when the angle of incidence, θ, is greater than 90°. When θ is greater than 90°, the circumsolar diffuse is set equal to zero because the sun is not the collector's field of view. However, if the anisotropy index is not zero, the Hay model will predict a lower value of tilted surface radiation than the isotropic sky model.

4.2.3 Perez, et al. Model

Perez et al. [20] proposes a new simplified version of a previous "Perez" anisotropic model [35] to estimate the diffuse radiation on a tilted surface. The new version of the anisotropic model will be referred to as the "Perez" model. The Perez model incorporates three components to account for circumsolar diffuse, horizon diffuse, and isotropic diffuse.

The sky is modeled by superimposing a circumsolar region and a horizon band on an isotropic background. Geometrically, the circumsolar region has a half angle of 25° and the horizon region is assumed to be infinitesimally thin at a 0° elevation. The contribution of diffuse radiation from the circumsolar, isotropic, and horizon regions is determined by two empirically derived coefficients (reduced brightness coefficients). The coefficients represent the normalized contribution of circumsolar diffuse and horizon diffuse to the total horizontal diffuse radiation. Perez derived the reduced brightness coefficients using two years of data from Carpentras, France and two years of data from Trappes, France. The Perez model is represented by the following:

$$I_{d,T} = I_d\left[(1 - F_1') \cdot \left(\frac{1+\cos\beta}{2}\right) + F_1' \cdot \left(\frac{a}{c}\right) + F_2' \sin\beta\right] \tag{4.9}$$

where: a/c is a weighted circumsolar solid angle; F_1' and F_2' are the reduced brightness coefficients representing the normalized contribution of circumsolar diffuse to the diffuse radiation on a horizontal surface (I_d) and the normalized contribution of horizon diffuse to I_d. The first term within the brackets represents the diffuse radiation received on a tilted surface from the isotropic portion of the sky dome. The second term is the contribution of circumsolar diffuse and the last term represents the contribution of horizon brightening diffuse.

The reduced brightness coefficients are a function of three parameters: zenith angle, sky clearness, and sky brightness. Perez defines the following as the sky clearness parameter,

$$\varepsilon \equiv \frac{(I_d + I_{bn})}{I_d} \tag{4.10}$$

where I_{bn} is the hourly direct normal radiation. The sky brightness parameter is defined by,

$$\Delta \equiv \frac{I_d}{I_o} \tag{4.11}$$

where I_o is the hourly extraterrestrial radiation on a horizontal surface. Once the zenith angle, sky clearness, and sky brightness parameters are calculated, the reduced brightness coefficients can be found by the following equations:

$$F_1' = F_{11}'(\varepsilon) + F_{12}'(\varepsilon) \cdot \Delta + F_{13}'(\varepsilon) \cdot \theta_z \tag{4.12}$$

$$F_2' = F_{21}'(\varepsilon) + F_{22}'(\varepsilon) \cdot \Delta + F_{23}'(\varepsilon) \cdot \theta_z \tag{4.13}$$

where θ_z is in radians. The intermediate coefficients, F_{11}, F_{12}, etc. are given by Table 4.1 depending on the value of ε.

Table 4.1: Intermediate Brightness Coefficients *

epsilon bin	Upper Limit	F_{11}	F_{12}	F_{13}	F_{21}	F_{22}	F_{23}
1	1.056	-0.011	0.748	-0.080	-0.048	0.073	-0.024
2	1.253	-0.038	1.115	-0.109	-0.023	0.106	-0.037
3	1.586	0.166	0.909	-0.179	0.062	-0.021	-0.050
4	2.134	0.419	0.646	-0.262	0.140	-0.167	-0.042
5	3.230	0.710	0.025	-0.290	0.243	-0.511	-0.004
6	5.980	0.857	-0.370	-0.279	0.267	-0.792	0.076
7	10.08	0.734	-0.073	-0.228	0.231	-1.180	0.199
8	-	0.421	-0.661	0.097	0.119	-2.125	0.446

* Coefficients for a circumsolar half angle of α= 25°.

The ratio a/c represents a weighted circumsolar solid angle. The "a" parameter is the circumsolar solid angle weighted by its average incidence on the tilted surface. The "c" parameter is the circumsolar solid angle weighted by its average incidence on a horizontal surface. Perez provides functional forms for "a" and "c" which depend on the angle of incidence, zenith angle, and circumsolar half angle. Since the Perez model requires the ratio a/c, the functional forms for "a" and "c" were combined and reduced to the five cases presented below.

i.) $\theta < \frac{\pi}{2} - \alpha, \qquad \theta_z < \frac{\pi}{2} - \alpha$

$$\frac{a}{c} = \frac{\cos\theta}{\cos\theta_z} = R_b$$

ii.) $\frac{\pi}{2} - \alpha < \theta < \frac{\pi}{2} + \alpha, \qquad \theta_z < \frac{\pi}{2} - \alpha$

$$\frac{a}{c} = \frac{(\frac{\pi}{2} - \theta + \alpha)\sin(\frac{\pi}{4} - \frac{\theta}{2} + \frac{\alpha}{2})}{2\alpha\cos\theta_z}$$

iii.) $\theta > \frac{\pi}{2} + \alpha$

$$\frac{a}{c} = 0$$

iv.) $\theta < \frac{\pi}{2} - \alpha, \qquad \theta_z > \frac{\pi}{2} - \alpha$

$$\frac{a}{c} = \frac{\cos\theta}{\sin\left(\frac{\pi}{4} - \frac{\theta_z}{2} + \frac{\alpha}{2}\right)}$$

v.) $\frac{\pi}{2} - \alpha < \theta < \frac{\pi}{2} + \alpha, \qquad \theta_z > \frac{\pi}{2} - \alpha$

$$\frac{a}{c} = \frac{(\frac{\pi}{2} - \theta + \alpha) \quad \sin(\frac{\pi}{4} - \frac{\theta}{2} + \frac{\alpha}{2})}{2\alpha \quad \sin\left(\frac{\pi}{4} - \frac{\theta_z}{2} + \frac{\alpha}{2}\right)}$$

In the first case (i), the complete circumsolar region is in the tilted surface's field of view and the weighted solid angle reduces to the familiar R_b factor. The second case (ii) represents the situation when part of the circumsolar region is behind the collector. In the third case (iii), the entire circumsolar region is out of the collector's field of view; therefore, the contribution from circumsolar diffuse will be zero. The fourth case (iv) occurs when part of the circumsolar region is obscured by the horizon and the last case (v) results when part of the circumsolar region is obscured by the horizon and part of the circumsolar region is behind the collector surface.

In summary, there are four major steps in estimating the tilted surface diffuse radiation by the Perez model:

1. Calculate the sky brightness, sky clearness, and zenith angle parameters.

2. Enter Table 4.1 in the appropriate ε bin. Use the intermediate brightness coefficients, F_{11}, F_{12}, etc. along with Δ and θ_z (in radians) to find the reduced brightness coefficients by equations 4.12 and 4.13.

3. Calculate the angle of incidence, θ. Find the proper a/c case based on the values of θ and θ_z (using a circumsolar half angle of α=25°). Calculate the weighted circumsolar solid angle, a/c.

4. Substitute the reduced brightness coefficients, weighted circumsolar solid angle, surface slope, and horizontal diffuse into equation 4.9 to find the diffuse radiation on a tilted surface.

The Perez model is quite complex when compared to the isotropic or Hay models. The Perez model also relies heavily on the empirically derived reduced brightness coefficients; this could make the model location dependent. Because of the large circumsolar region, the model is limited to collectors that have a wide field of view, e.g. flat plate collectors.

4.2.4 New Tilted Surface Model

The new model is the result of modifications made to the Hay model. As indicated in section 4.2.2, the Hay model does not account for horizon brightening diffuse. Preliminary calculations of predicted radiation incident on south facing surfaces indicated that the Hay model was underpredicting the measured tilted

surface radiation. The author believes that the underpredicting nature of the Hay model is partly due to the absence of a horizon brightening term in the model. Thus, the accuracy of the Hay model may be improved by the addition of a horizon brightening factor.

In their study of clear sky radiance distributions, Temps and Coulson [4] approximated the horizon brightening effects by applying a correction factor of $[1+\sin^3(\beta/2)]$ to the isotropic diffuse radiation. A similar correction factor was applied to account for the circumsolar diffuse in their model. The correction factors pertained to clear sky conditions only. Klucher [16] modified the Temps and Coulson clear sky model by introducing a modulating factor, $F = [1 - (I_d/I)^2]$. This modulating factor forced the anisotropic correction factors to approach 1 under cloudy sky conditions. Thus, under cloudy sky conditions, the model would revert back to the isotropic sky model.

The horizon brightening correction factor suggested by Temps and Coulson was applied to the isotropic term in the Hay model. A new modulating factor was defined to account for the sky cloud conditions. The factor $f=\sqrt{I_b/I}$ was used to modulate the Temps and Coulson horizon brightening term. The isotropic term in the Hay model becomes,

$$I_{T,iso,hor} = I_d\left[(1-AI)\cdot\left(\frac{1+\cos\beta}{2}\right)\cdot(1+f\sin^3(\beta/2))\right] \qquad (4.14)$$

The new modified Hay model becomes,

$$I_{d,T} = I_d \left[(1 - AI) \cdot \left(\frac{1 + \cos\beta}{2} \right) \cdot (1 + f \sin^3(\beta/2)) + AI \cdot R_b \right] \quad (4.15)$$

The first term in brackets represents the isotropic diffuse corrected to include horizon brightening. The second term represents the contribution of circumsolar diffuse. Under cloudy skies, the modulating factor and the anisotropy index go to zero and the model reverts to the isotropic model. Under partly cloudy skies, the modulating function and anisotropy index are non-zero; therefore, the isotropic term is corrected to account for horizon brightening. In other words, the contribution of horizon brightening is added to the isotropic portion of the diffuse radiation.

The new model will always predict equal or greater values of tilted surface diffuse radiation when compared to the original Hay model. The new model remains relatively simple but weaknesses still exist. The weaknesses of the Hay model discussed in section 4.2.2 regarding incidence angles greater than 90° and non-zero anisotropy index still exists but its effect is mitigated by the addition of the horizon correction term. The addition of this term will cause the new model to predict higher values of tilted surface radiation compared to the original Hay model under the same circumstances. Another problem is attributed to the model's behavior under clear sky conditions. For increasing clear skies (anisotropy index approaching 1), the isotropic term is forced to zero. Consequently, there will be no contribution of diffuse radiation by horizon brightening. This is not expected to cause large errors because under clear sky conditions, the magnitude of the horizontal diffuse is small.

4.3 Ground Reflected Radiation

A common method for calculating the ground reflected radiation incident on a tilted surface is to assume that the foreground in the collector's field of view behaves as an isotropic reflector. Other authors have proposed anisotropic ground reflectance models [4,42,43] but the lack of experimental data has hampered their validation. Therefore, the ground reflected radiation is assumed to be isotropic. Calculating the ground reflected radiation requires knowing the collector to ground view factor. Recall, the surface to sky view factor for calculating the isotropic diffuse is $\cos^2(\beta/2)$. Thus, the collector to ground view factor is given by,

$$f_{c,g} = 1 - \cos^2(\beta/2) = 1 - \left(\frac{1+\cos\beta}{2}\right) = \left(\frac{1-\cos\beta}{2}\right) \tag{4.16}$$

The isotropic ground reflected radiation is obtained by [5],

$$I_{g,T} = I\,\rho_g \left(\frac{1-\cos\beta}{2}\right) \tag{4.17}$$

where ρ_g is the surface albedo (reflectance). The above relationship for calculating ground reflected radiation assumes the foreground is a long horizontal surface with a constant albedo that reflects incident radiation uniformly in all directions.

Liu and Jordan [44] recommend ρ_g = 0.2 as a typical average albedo for ground without snow cover and ρ_g = 0.7 for ground with fresh snow cover. Albedos for more specific surfaces are reported by Hunn and Calafell [45].

4.4 Tilted Surface Model Evaluation

It has been routine practice [8,16,17,18,19,35,36,42,43] to assess tilted surface model performance by comparing predicted tilted surface radiation to measured tilted surface radiation for surfaces of various slope/azimuth orientations. Usually root mean square difference (RMSD) and mean bias difference (MBD) statistics are formed to quantify individual model performance. Comparing predicted and measured values of tilted surface radiation does not provide a good indication of a model's performance when used for solar energy system simulations.

van den Brink [18] uses various reference systems (dwellings with and without active solar, swimming pools, etc.) to explore effects on the auxiliary energy required for a given system when using measured and model predicted values of tilted surface radiation. Bugler [12] compares the calculated heat output of a typical flat plate collector using measured and model predicted values of tilted surface radiation. These methods lack the generality to extend the results to other types of collecting devices and solar energy systems. From a thermal system point of view, it is of interest to compare a model's ability to estimate the utilizable energy on a tilted surface at different critical radiation levels. Utilizable energy provides a means of comparing the tilted surface model performance independent of a particular system. Thus, it is a more general method for comparing individual model performance.

The goal is to determine which tilted surface model performs the best (in the context of solar energy systems). All models share the same techniques for calculating the beam and ground reflected radiation on a tilted surface. The data sets used in this study are discussed and the results of the model evaluation are presented.

4.4.1 Data Sets Used

Four years of hourly radiation data from Albany, New York and one year of hourly data from San Antonio, Texas (Trinity) provided the basis for comparing the tilted surface radiation models. The two data sets have five common surface slope/azimuth orientations: 43°s, 90°n, 90°s, 90°e, 90°w. The actual pyranometer slope difference at Trinity (β=40°) and Albany (β=43°) is assumed negligible for purposes of model comparison.

Both radiation monitoring sites use artificial horizons affixed to the tilted surface pyranometers to reduce the ground reflected radiation component. At Albany, the artificial horizons completely eliminated the ground reflected radiation ($\rho_g = 0$). At Trinity, the artificial horizons reduced the ground reflected radiation to an effective albedo of $\rho_g = 0.05$.

In addition to the data quality control checks discussed in section 2.3, a tolerance was imposed on the predicted values of tilted surface radiation. The tolerance limits the absolute deviation of the predicted value of tilted surface radiation from the measured value of tilted surface radiation to be no greater than

200 kJ/m² + 10% of the measured tilted surface radiation. The hour was omitted if the tolerance was exceeded. A similar tolerance was used by Hay and McKay [19]. This assures that some consistency exists between the horizontal measurements and the tilted surface measurements.

4.4.2 Results

All tilted surface models were compared on the basis of monthly average hourly utilizable energy. Throughout the remainder of this thesis when utilizable energy is mentioned, monthly average hourly utilizable energy is implied. The monthly average hourly utilizable energy is given by,

$$UE = \frac{1}{n} \sum_{n} (I_T - I_{T,c})^+ \tag{4.18}$$

where: n is the number of hours summed, I_T is the total hourly radiation on a tilted surface (measured or predicted), $I_{T,c}$ is the critical radiation level, and the + indicates that only positive differences are summed. The utilizable energy measured is obtained by using the actual tilted surface measurements in equation 4.18. The utilizable energy predicted is found by using the estimated tilted surface radiation in equation 4.18.

Utilizable energy measured and utilizable energy predicted were calculated for all surface slope/azimuth orientations over a wide range of critical radiation levels at each surface orientation. The following root mean square difference (RMSD) and mean bias difference (MBD) statistics were calculated,

$$RMSD = \left[\frac{1}{n} \sum_{n} (UE_{meas} - UE_{pred})^2 \right]^{1/2} \tag{4.19}$$

$$MBD = \frac{1}{n} \sum_{n} (UE_{meas} - UE_{pred}) \tag{4.20}$$

where: UE_{meas} is the utilizable energy measured and UE_{pred} is the utilizable energy predicted by a given model. Because the tilted surface measurements are not without error, the nomenclature root mean square difference and mean bias difference is used rather than root mean square error and mean bias error.

The RMSD provides a measure of a model's short term prediction performance. The MBD is a measure of a model's long term prediction performance; because over a long period, cancellation of overpredicted and underpredicted utilizable energy will allow the statistic to go to zero. However, the RMSD does not allow cancellation and a few large deviations or differences in the UE_{meas} and UE_{pred} can inflate the statistic. Both statistics will be used to evaluate all tilted surface models. A tilted surface model with good performance will have a low RMSD and near zero MBD. The problem here is determining what are low values of RMSD or MBD. This problem is resolved by normalizing the RMSD and

MBD statistics with respect to the utilizable energy measured.

$$NRMSD = \frac{RMSD}{UE_{meas}} \tag{4.21}$$

$$NMBD = \frac{MBD}{UE_{meas}} \tag{4.22}$$

The normalized root mean square difference (NRMSD) and normalized mean bias difference (NMBD) statistics were formed for each tilted surface model predicting the utilizable energy on five surface orientations over a range of critical radiations levels. The inputs to the tilted surface models are measured values of global horizontal and diffuse radiation on a horizontal surface. Table 4.2 shows the surface orientations and critical levels used in forming the NRMSD and NMBD statistics.

Table 4.2: Tilted Surface Model Parameters

Location/Year	Slope/Azimuth	I_{tc} (increment), kJ/m²
Albany, 1979	43°s	0 - 2500 (500)
Albany, 1980	43°s	0 - 2500 (500)
	90°s	0 - 1500 (500)
	90°w	0
	90°e	0 - 500 (500)
	90°n	0
Albany, 1981	43°s	0 - 2500 (500)
	90°s	0 - 1500 (500)
	90°w	0
	90°e	0
	90°n	0
Albany, 1982	43°s	0 - 2500 (500)
	90°s	0 - 1500 (500)
	90°w	0
	90°e	0
	90°n	0
Trinity, 1980	43°s	0 - 2500 (500)
	90°s	0 - 1000 (500)
	90°w	0
	90°e	0 - 500 (500)
	90°n	0

The resulting NRMSD and NMBD statistics for each model for all surface orientations are graphically presented in Figure 4.1 for the hour 10-11:00 am. The NRMSD results indicate that the anisotropic models (Hay, Perez, and new model) show similar performance but the isotropic model exhibits much larger differences from the utilizable energy measured. The NMBD results show that the isotropic, Hay, and new model are underpredicting the utilizable energy while the Perez model overpredicts the utilizable energy on an overall basis.

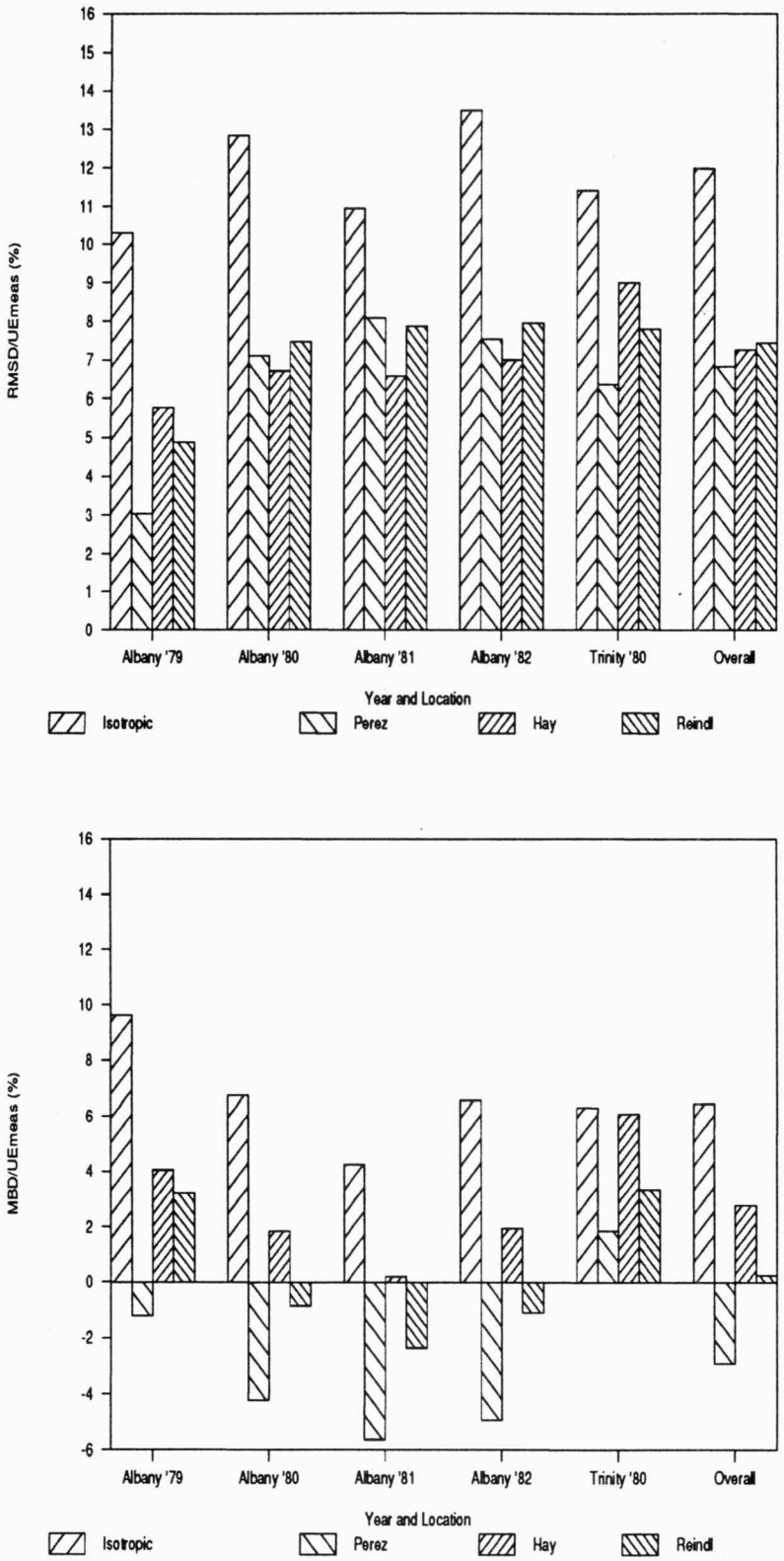

Figure 4.1: Normalized root mean square difference and normalized mean bias difference for all surface orientations, 10-11:00 am

Most collecting devices for solar energy systems are oriented south facing. It is useful to observe the model's performance when applied only to south facing surface orientations. The NRMSD and NMBD statistics were calculated using the two available south facing surface orientations (43°s and 90°s) at the critical levels indicated in Table 4.2. The results are shown in Figure 4.2. On an overall basis, the NRMSD was reduced by about 2% for each model. The NMBD revealed some interesting results. When compared to the results in Figure 4.1 (all surface orientations), the NMBD for the isotropic model increased. This indicates that the isotropic model overpredicts for non-south facing surface orientations. For south facing surfaces, the NMBD for the Perez model decreased when compared to Figure 4.1. The margin of overprediction by the Perez model is reduced for south facing surfaces when compared to its performance for all surface orientations. The Hay and new model have larger underpredicting differences for south facing surfaces. This indicates that the Hay and new (Reindl) model overpredict for non-south orientations. It is clear that all models overpredict the utilizable energy for non-south surface orientations. Another NMBD peculiarity is noted in the Trinity results. All models underpredict the utilizable energy at Trinity. The author attributes this to possible uncertainty in the reported value of effective ground reflectance associated with the artificial horizons. A value of reflectance ρ_g =0.05 is reported but if the actual reflectance was higher, the measuring instrument would receive more energy due to ground reflectance causing the measured utilizable energy to be higher. This would explain the consistent underprediction of utilizable energy by each model for Trinity.

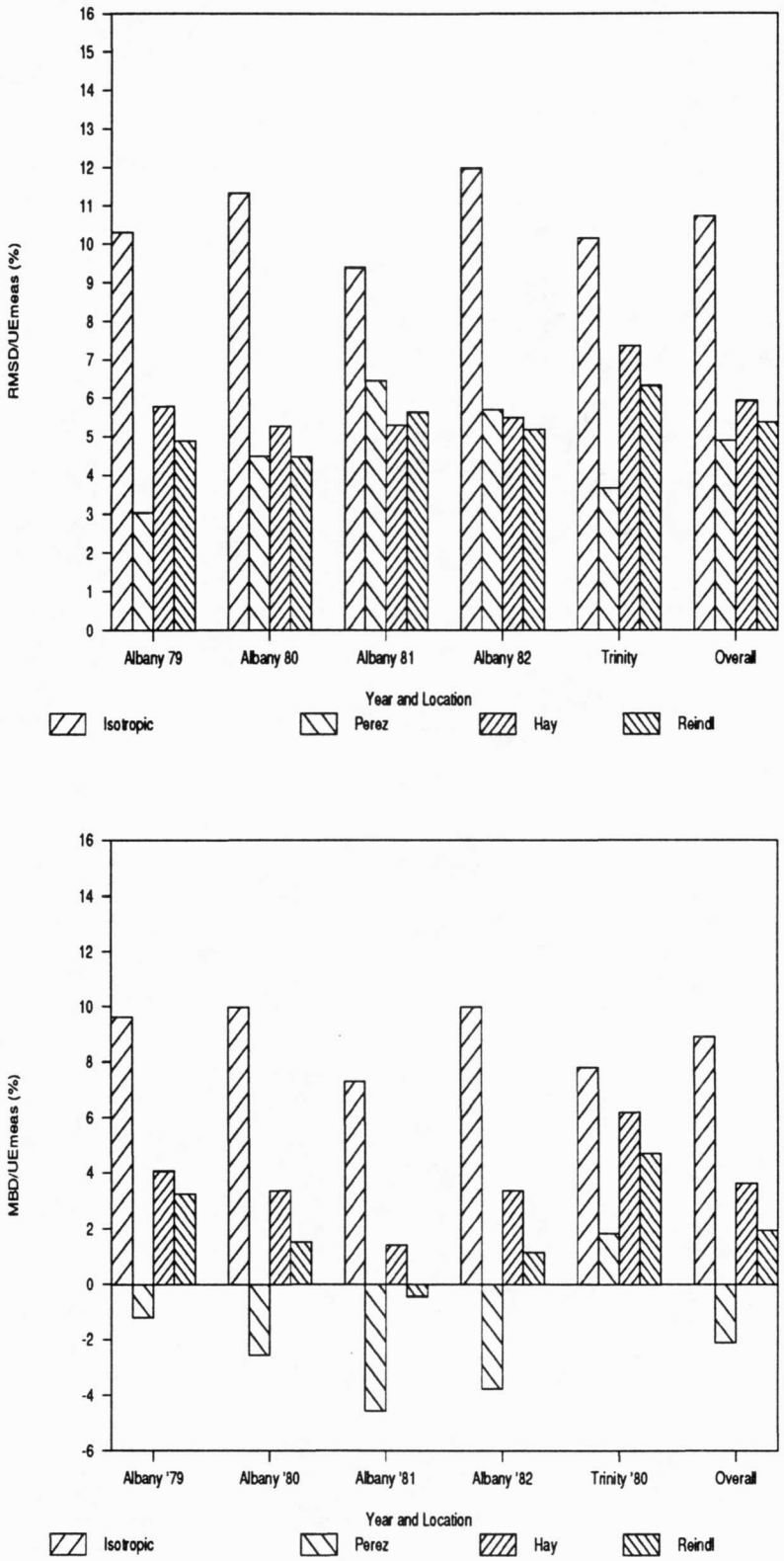

Figure 4.2: Normalized root mean square difference and normalized mean bias difference for south facing surface orientations, 10-11:00 am

Up to this point, the model performance was evaluated for various surface orientations and a range of critical radiation levels. To observe the effects of critical radiation level on model performance, NRMSD and NMBD statistics were calculated for a 43° south facing surface at critical levels of 0 and 1000 kJ/m². The results are shown in Figures 4.3a, and 4.3b. It can be seen that the models which tend to underpredict (isotropic, Hay, new model) have an increased difference when going from 0 to 1000 kJ/m² critical radiation level. This can be explained by examining the method for calculating the RMSD and MBD. Both the RMSD and MBD contain the difference between the utilizable energy measured and utilizable energy predicted.

$$(UE_{meas} - UE_{pred})$$

Substituting the definition of utilizable energy,

$$\Delta UE = \frac{1}{n}\left[\sum_{n} (I_{T,m} - I_{T,c})^{+} - \sum_{n} (I_{T,p} - I_{T,c})^{+} \right]$$

where: $I_{T,m}$ is the measured tilted surface radiation; and $I_{T,p}$ is the tilted surface radiation predicted by a given model. If the predicted value of tilted surface radiation exceeded the critical radiation level for the same hours which the measured tilted surface radiation exceeded the critical level, the critical radiation level would effectively cancel out of the difference. That is, if $I_{T,p} > I_{T,c}$ when $I_{T,m} > I_{T,c}$, the following results,

$$\Delta UE = \frac{1}{n^*}\left[\sum_{n^*} I_{T,m} - \sum_{n^*} I_{T,c} - \sum_{n^*} I_{T,p} + \sum_{n^*} I_{T,c} \right]$$

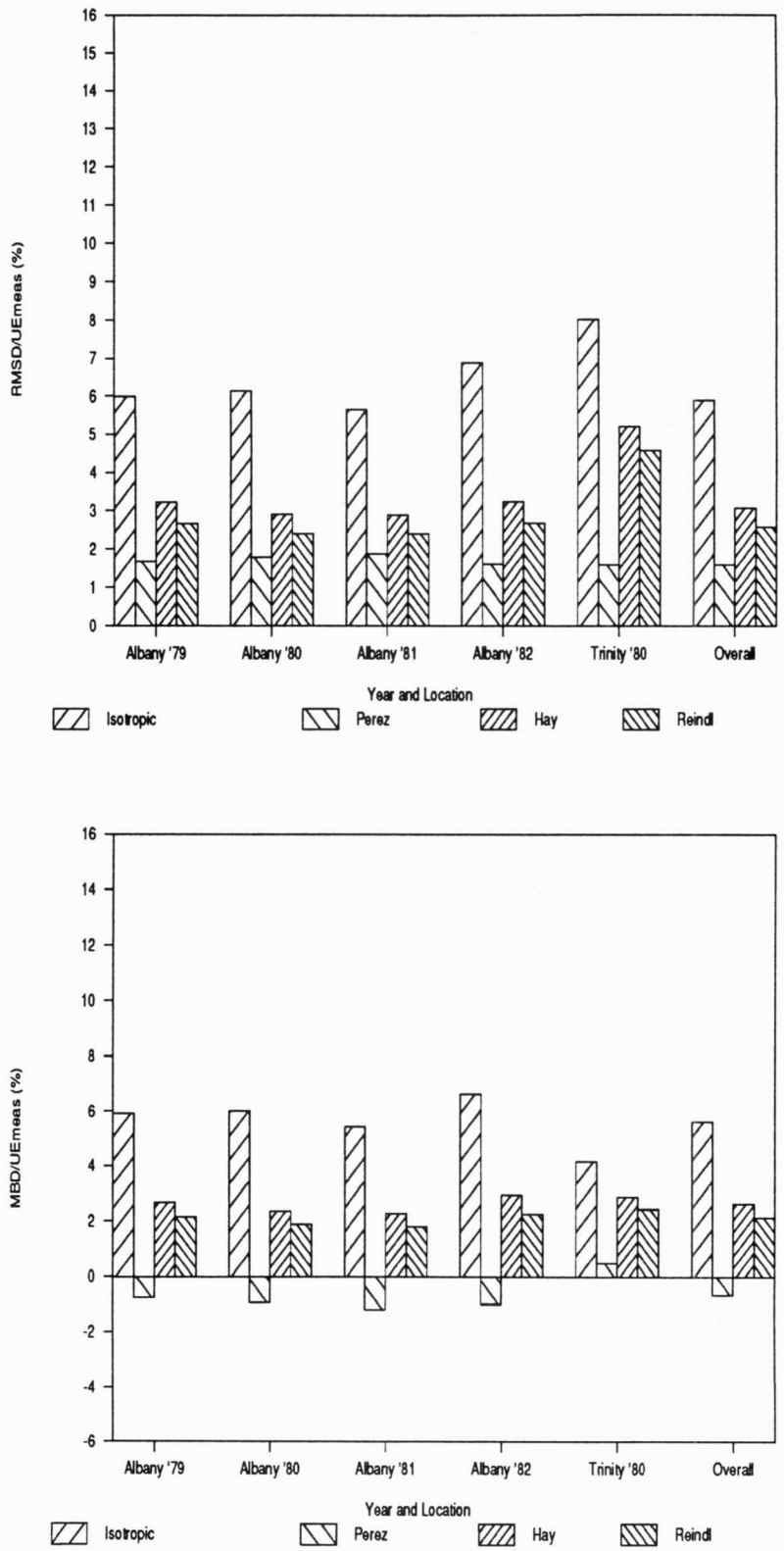

Figure 4.3a: Normalized root mean square difference and normalized mean bias difference for 43° south facing surface, Itc=0, 10-11:00 am

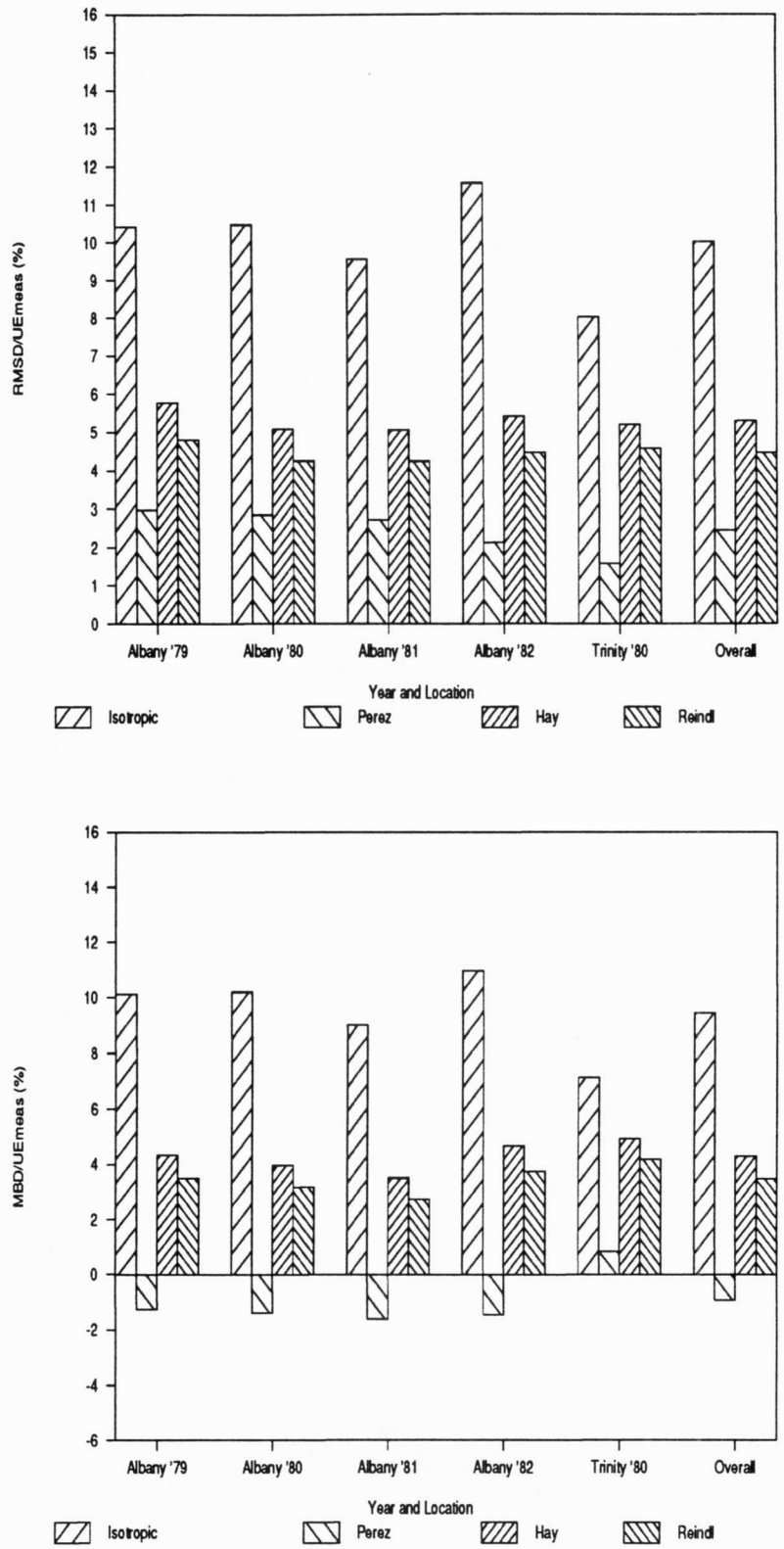

Figure 4.3b: Normalized root mean square difference and normalized mean bias difference for 43° south facing surface, Itc=1000 kJ/m², 10-11:00 am

$$\Delta UE = \frac{1}{n^*}\left[\sum_{n^*}(I_{T,m} - I_{T,p})\right]$$

However, a model that underpredicts the tilted surface radiation will cause the summation of ΔUE to increase rapidly if the underpredicted value of tilted surface radiation does not exceed the critical level when the measured tilted surface radiation exceeds the critical level. That is, if if $I_{T,p} < I_{T,c}$ when $I_{T,m} > I_{T,c}$, the following results,

$$\Delta UE = \frac{1}{n^*}\left[\sum_{n^*}(I_{T,m} - I_{T,c}) - 0\right]$$

causing the RMSD and MBD statistics to inflate quickly. This may be the reason why the NRMSD and NMBD increased for the isotropic, Hay, and new model as the critical level increased to 1000 kJ/m².

The effect of changing the surface slope from 43°s to 90°s was also investigated. Figure 4.4 illustrates the NRMSD and NMBD statistics for a 90° south facing surface with a critical radiation level of 0. When compared to Figure 4.3a, the Perez model shows the sharpest increase in the NRMSD due to the model overpredicting the utilizable energy by a greater margin for a vertical surface.

Seasonal variations in model performance are investigated by observing the NRMSD and NMBD on a monthly basis.

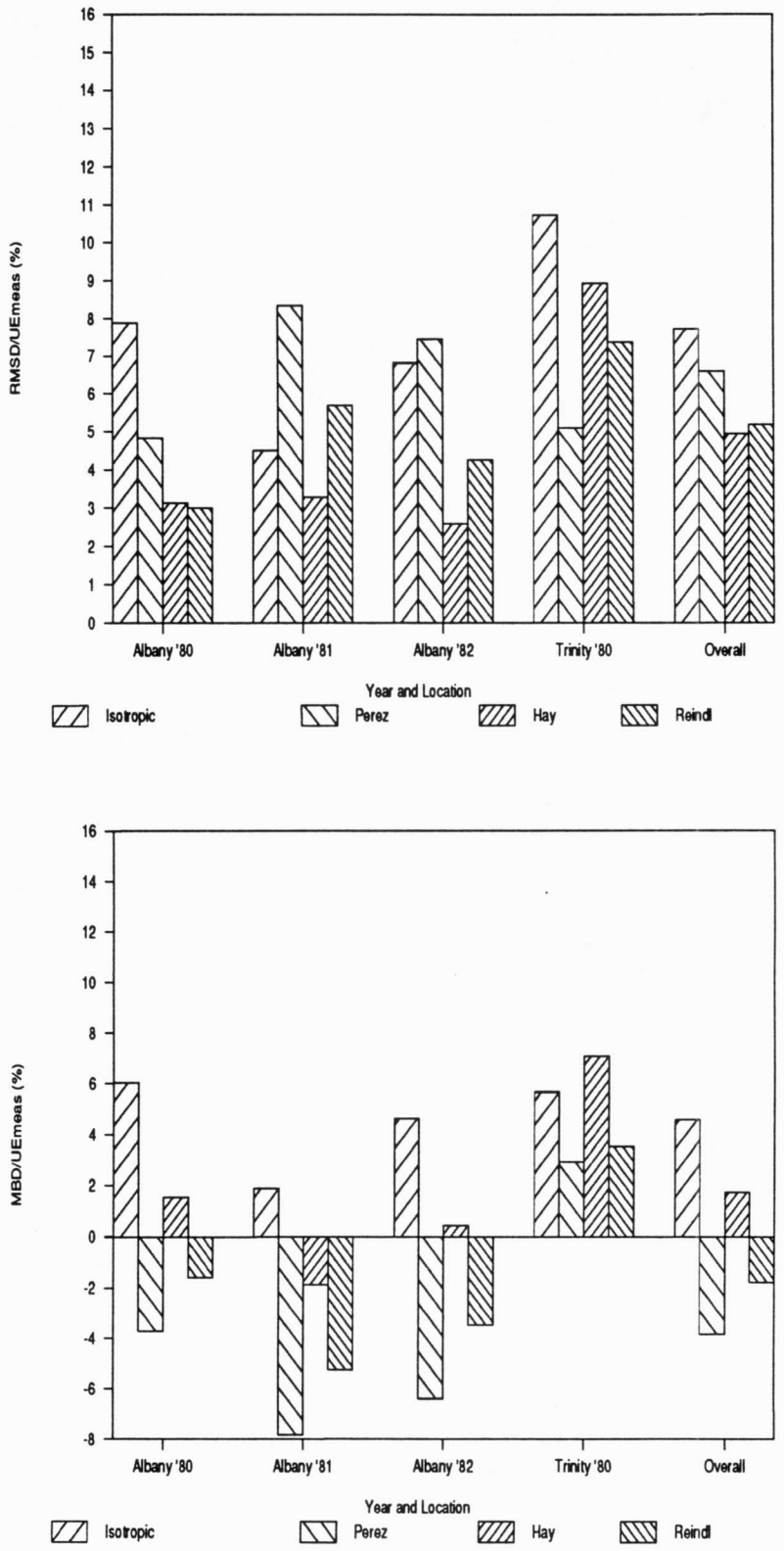

Figure 4.4: Normalized root mean square difference and normalized mean bias difference for 90° south facing surface, Itc=0, 10-11:00 am

The monthly variation in the utilizable energy measured and the utilizable energy predicted by each model at critical radiation levels of 0 and 1000 kJ/m² for Albany, 1980 (β = 43°s) is plotted in Figures 4.5 and 4.6, respectively. The NRMSD and NMBD statistics for the same location and surface orientation are plotted on a monthly basis in Figures 4.7 and 4.8 for critical radiation levels of 0 and 1000 kJ/m². The Perez model tends to overpredict the utilizable energy in the summer months. The NRMSD for Perez is the highest in the winter months. The RMSD for the Hay and new model indicate that both are more accurate in the winter months. The NMBD shows that both Hay and new model tend to underpredict the utilizable energy nearly all year round. The isotropic model consistently underpredicts.

The previous analysis probed model performance using tilted surface model inputs of measured global horizontal radiation and measured horizontal diffuse radiation. In cases when measured diffuse radiation on a horizontal surface is not available, correlations such as those presented in Chapter 3 must be used to estimate the diffuse radiation on a horizontal surface. To explore the effects of using a diffuse fraction correlation on the resulting utilizable energy predicted by each tilted surface model, the full diffuse fraction correlation developed in Chapter 3 (equations 3.19-3.21) is used to estimate the diffuse radiation on a horizontal surface for input to the tilted surface models. The NRMSD and NMBD statistics are formed for each measured tilted surface orientation and a range of critical levels. Table 4.3 shows the surface slopes and ranges of critical levels used to generate the above statistics.

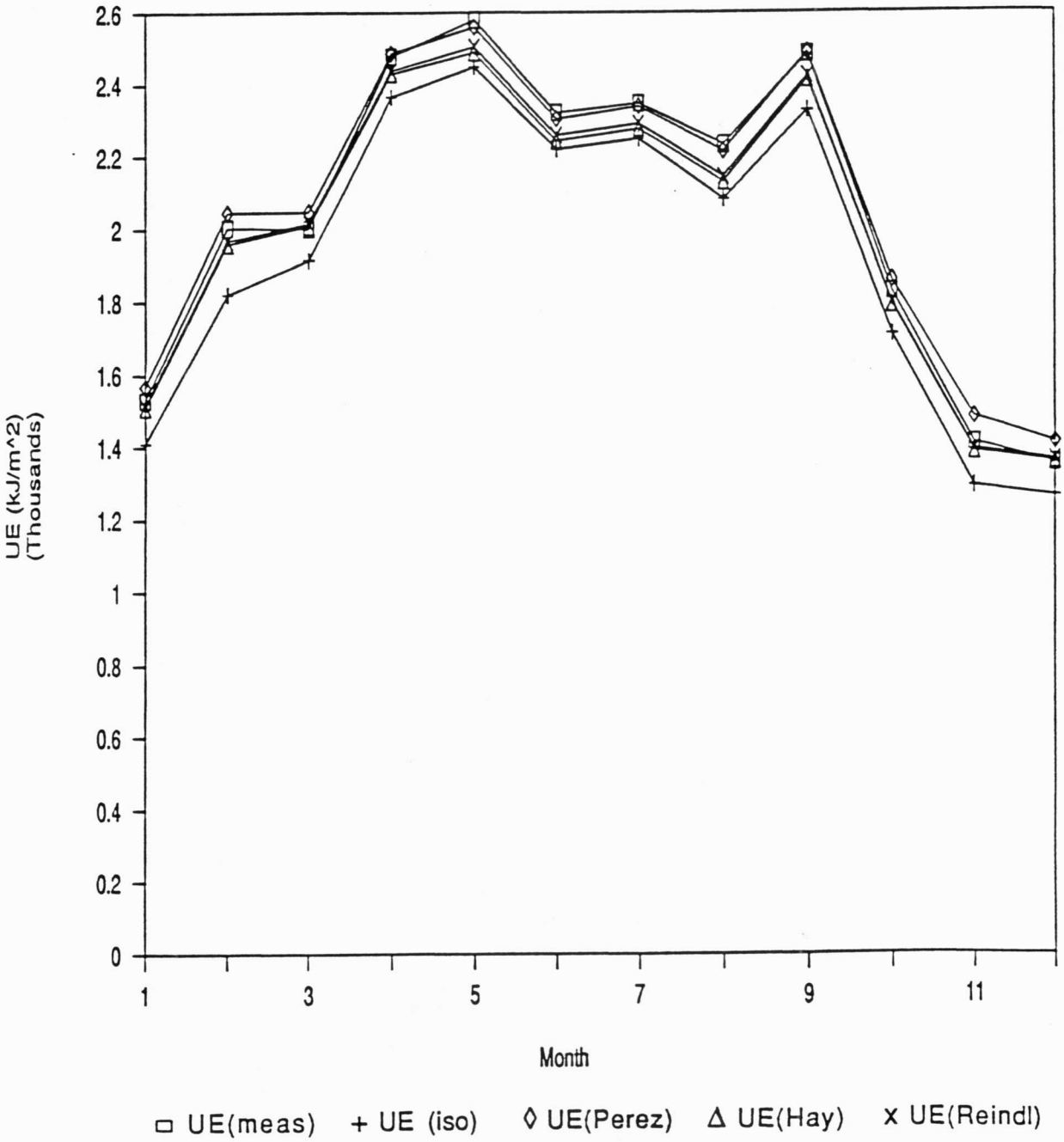

Figure 4.5: Monthly variation in utilizable energy, Albany 1980, Itc=0, slope=43°s, 10-11:00am

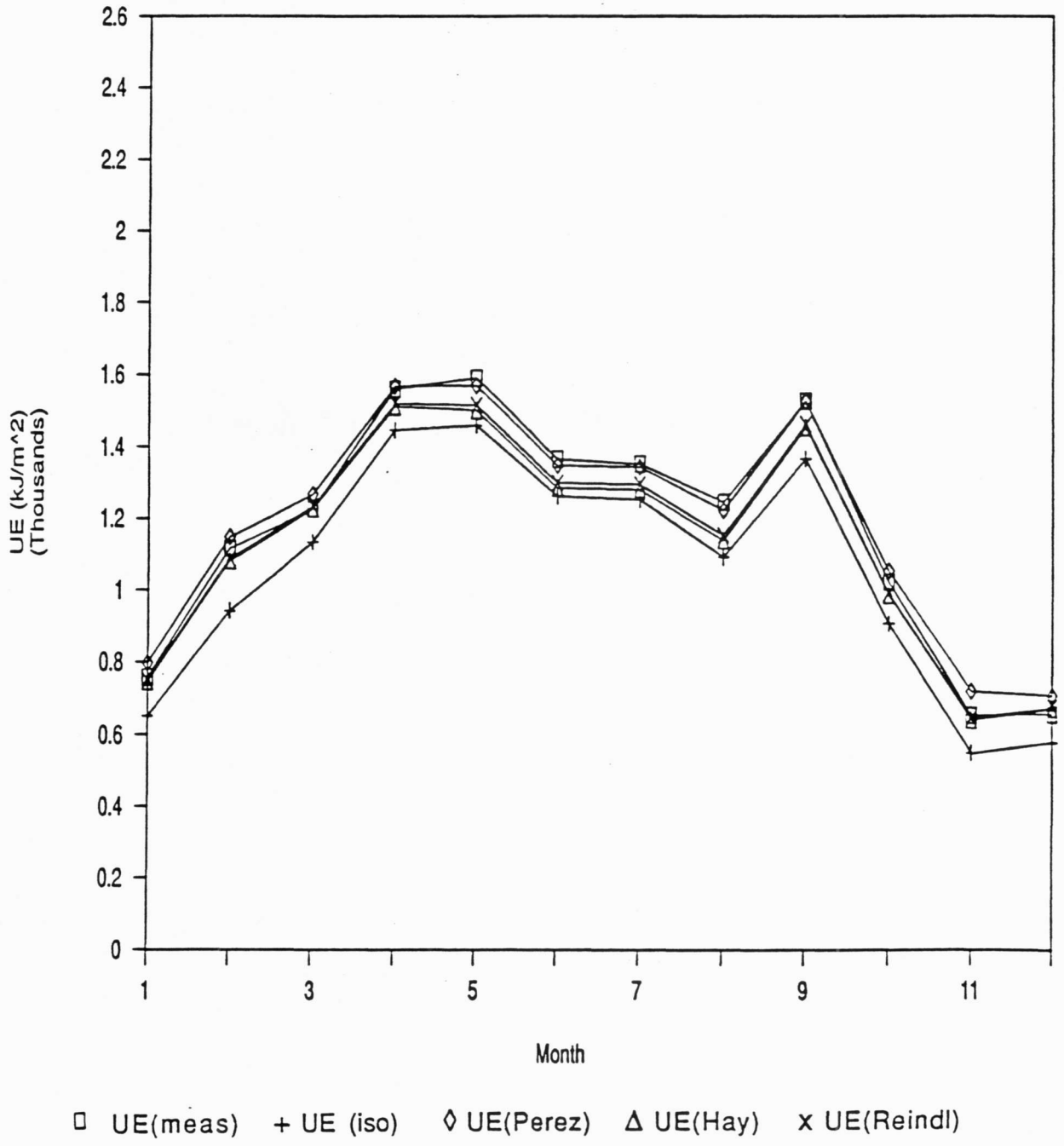

Figure 4.6: Monthly variation in utilizable energy, Albany 1980, Itc=1000 kJ/m^2, slope=43°s, 10-11:00am

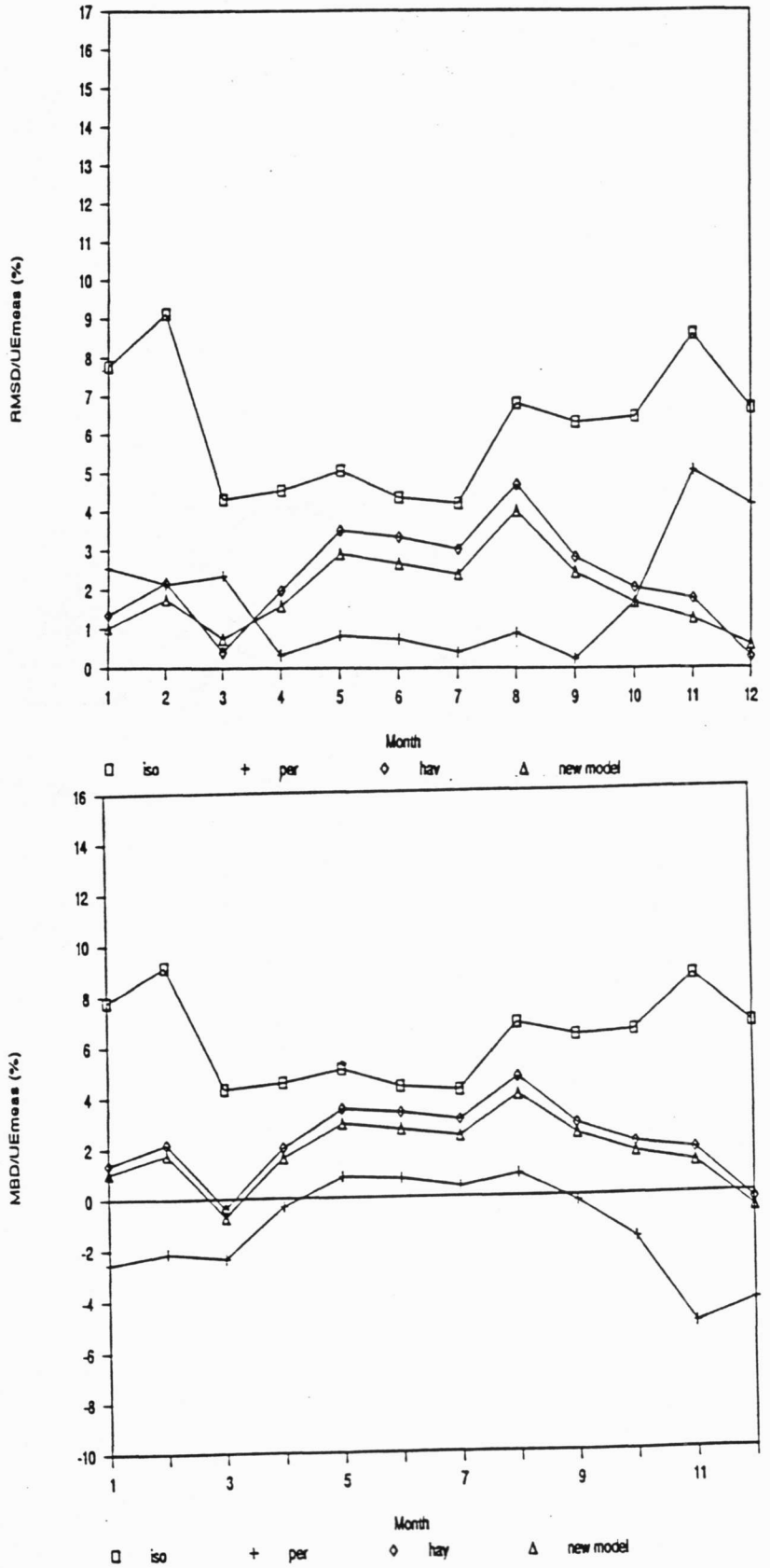

Figure 4.7: Normalized root mean square difference and normalized mean bias difference for Albany 1980, ltc=0, slope=43°s, 10-11:00am

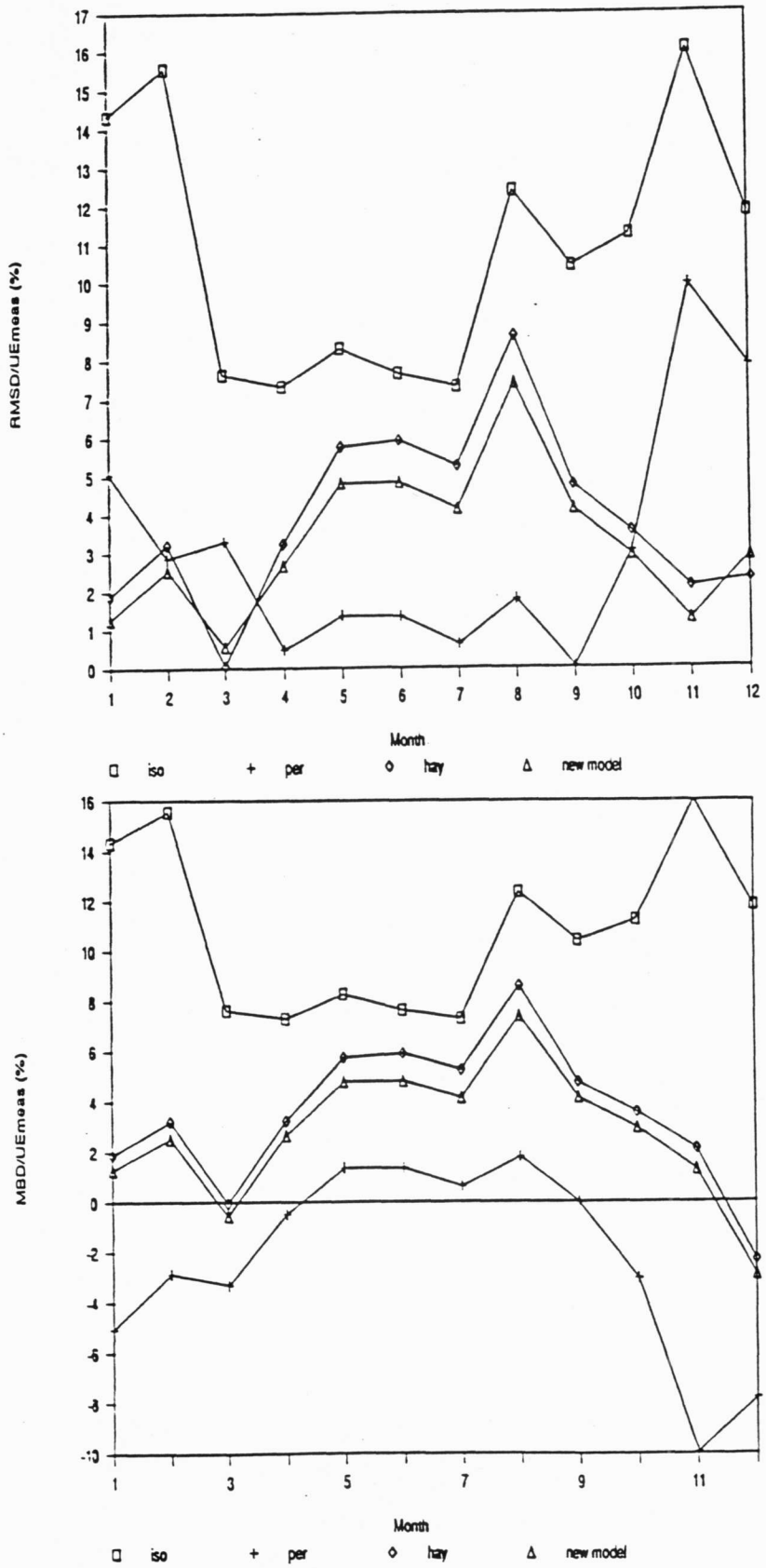

Figure 4.8: Normalized root mean square difference and normalized mean bias difference for Albany 1980, Itc=1000 kJ/m^2, slope=43°,10-11:00am

Table 4.3: Tilted Surface Model Parameters (using predicted horizontal diffuse)

Location/Year	Slope/Azimuth	I_{tc} (increment), kJ/m²
Albany, 1979	43°s	0 - 2500 (500)
Albany, 1980 (excluding March)	43°s	0 - 2500 (500)
	90°s	0 - 1000 (500)
	90°w	0
	90°e	0 - 500 (500)
	90°n	0
Albany, 1981 (excluding March)	43°s	0 - 2500 (500)
	90°s	0 - 1000 (500)
	90°w	0
	90°e	0 - 500 (500)
	90°n	0
Albany, 1982 (excluding Jan, Feb, and March)	43°s	0 - 2500 (500)
	90°s	0 - 1000 (500)
	90°w	0
	90°e	0 - 500 (500)
	90°n	0

Due to instrumentation problems, five months of data from Albany and all of the Trinity data were not available to include in the NRMSD and NMBD. The results of the NRMSD and NMBD statistics for all surface orientations are shown in Figure 4.9. Interestingly, the results are not greatly influenced by the use of an empirical correlation to estimate the diffuse radiation on a horizontal surface. Figure 4.10 displays the results for south facing orientations only. Again, the use of the diffuse fraction correlation does not have a great impact on the predicted utilizable energy as implied by the magnitude of the NRMSD and NMBD statistics.

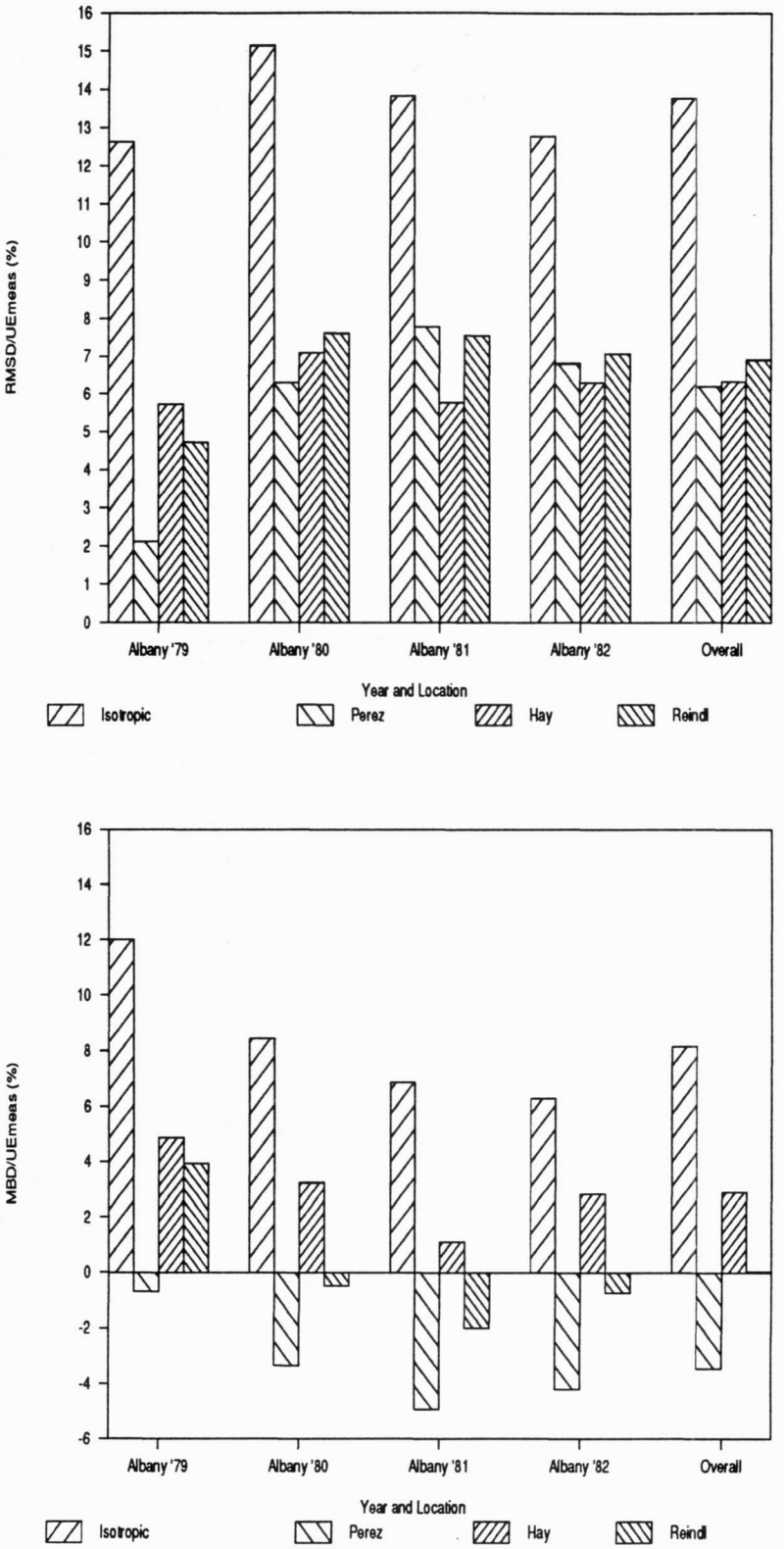

Figure 4.9: Normalized root mean square difference and normalized mean bias difference for all surface orientations using full correlation (eq. 3.19-3.21) to estimate horizontal diffuse, 10-11:00

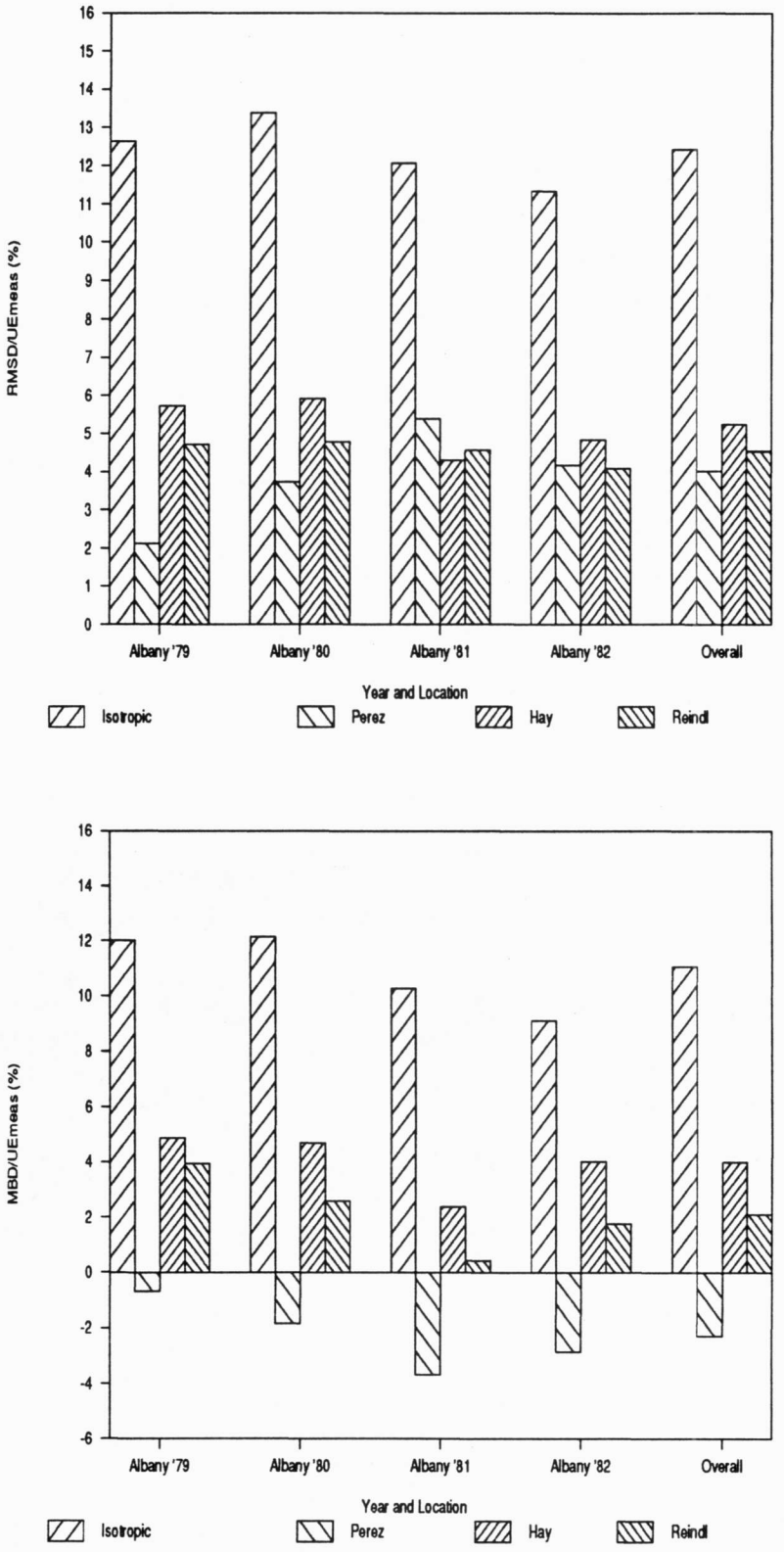

Figure 4.10: Normalized root mean square difference and normalized mean bias difference for south facing surfaces using full correlation (eq. 3.19-3.21) to estimate horizontal diffuse, 10-11:00 am

Another diffuse fraction correlation was developed in Chapter 3 (equations 3.22-3.24). The reduced diffuse fraction correlation was intended for use when ambient temperature and or relative humidity data are not available for input to the full diffuse fraction correlation. The NRMSD and NMBD statistics were computed for each location using the surface slopes and critical radiation levels listed in Table 4.1. The results for all surface orientations and south facing orientations are given in Figures 4.11 and 4.12, respectively. On an overall basis, the use of the reduced diffuse fraction correlation to estimate the horizontal diffuse radiation did not significantly affect the utilizable energy predicted by any given model.

The last comparison uses the Orgill and Hollands correlation to predict the hourly diffuse radiation on a horizontal surface. The NRMSD and NMBD statistics were formed for each location using the surface orientations and critical levels given by Table 4.1. The results for all surface orientations and south facing orientations are shown in Figures 4.13 and 4.14, respectively. There is no significant difference in the utilizable energy predicted when using the Orgill and Hollands correlation to predict the diffuse radiation on a horizontal surface for input to the tilted surface models.

An additional data set which includes 4 locations with approximately 6 months of data from each location was available for model comparisons. Because the data sets did not include complete years of data, the author hesitates to base solid conclusions on their results. However, NRMSD and NMBD results from these four locations are included in Appendix D. The results from this additional data set do not alter the current conclusions of model performance.

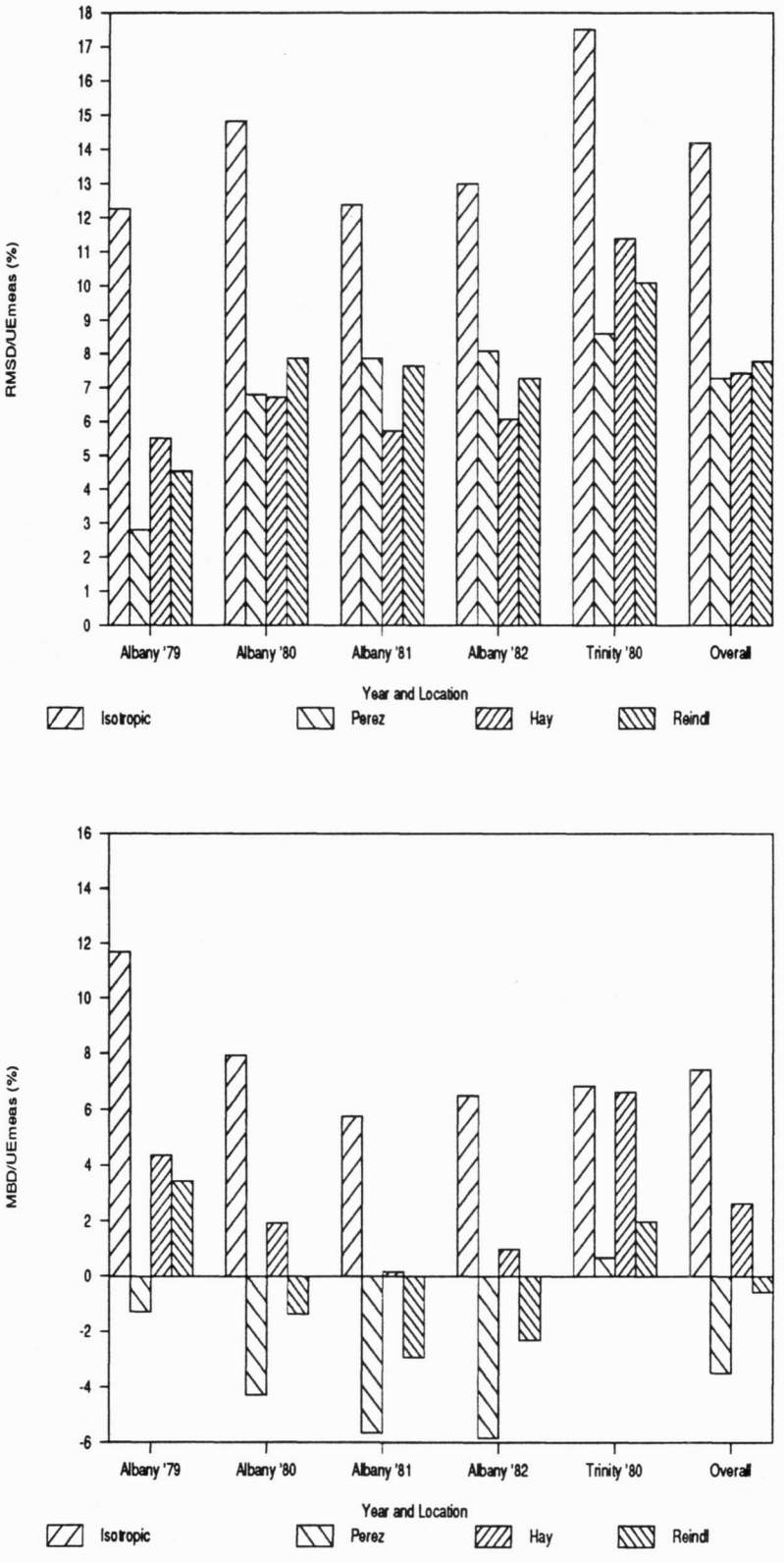

Figure 4.11: Normalized root mean square difference and normalized mean bias difference for all surface orientations using reduced correlation (eq. 3.22-3.24) to estimate horizontal diffuse, 10-11:00

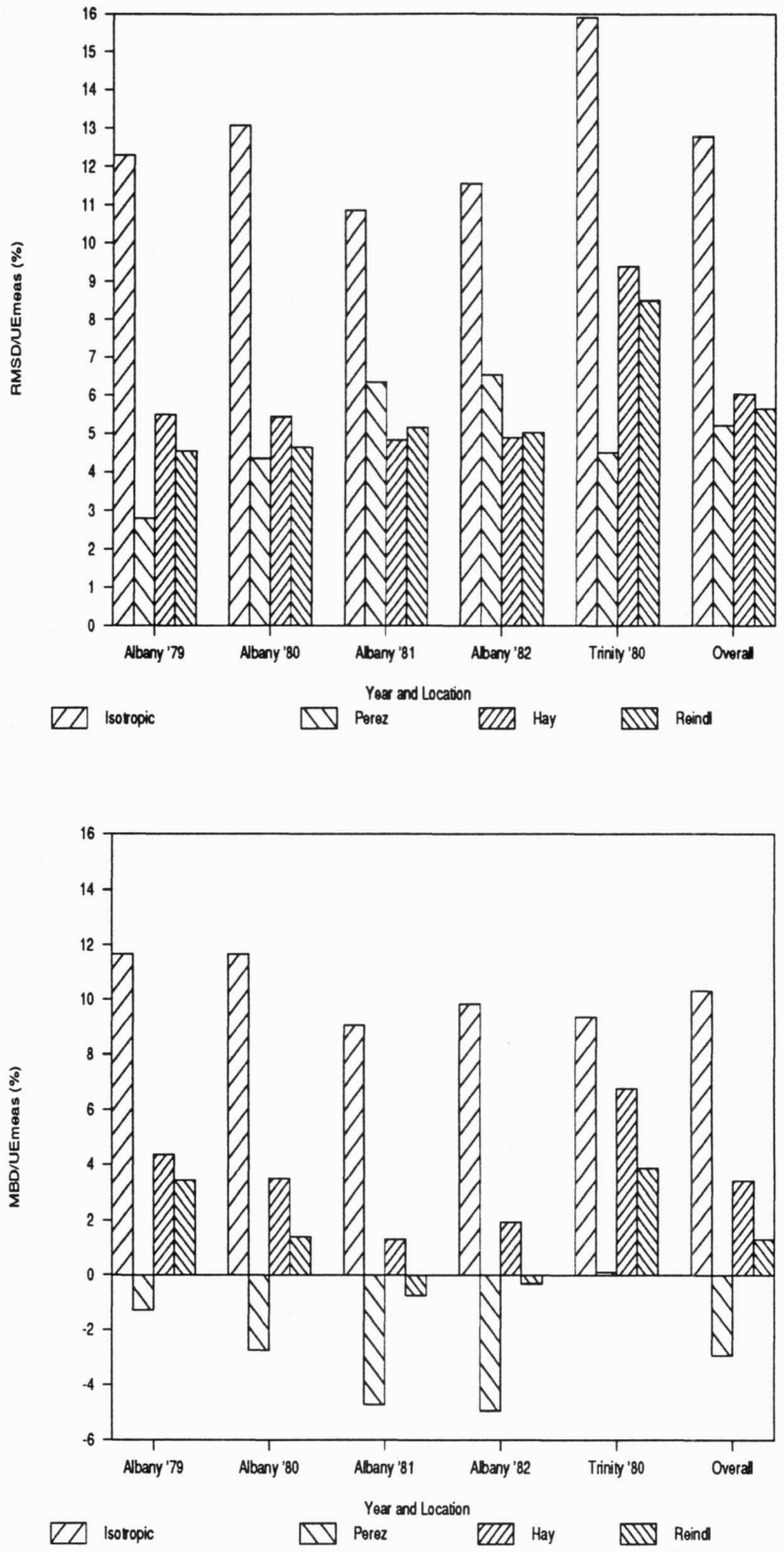

Figure 4.12: Normalized root mean square difference and normalized mean bias difference for south facing surfaces using reduced correlation (eq. 3.22-3.24) to estimate horizontal diffuse, 10-11:00

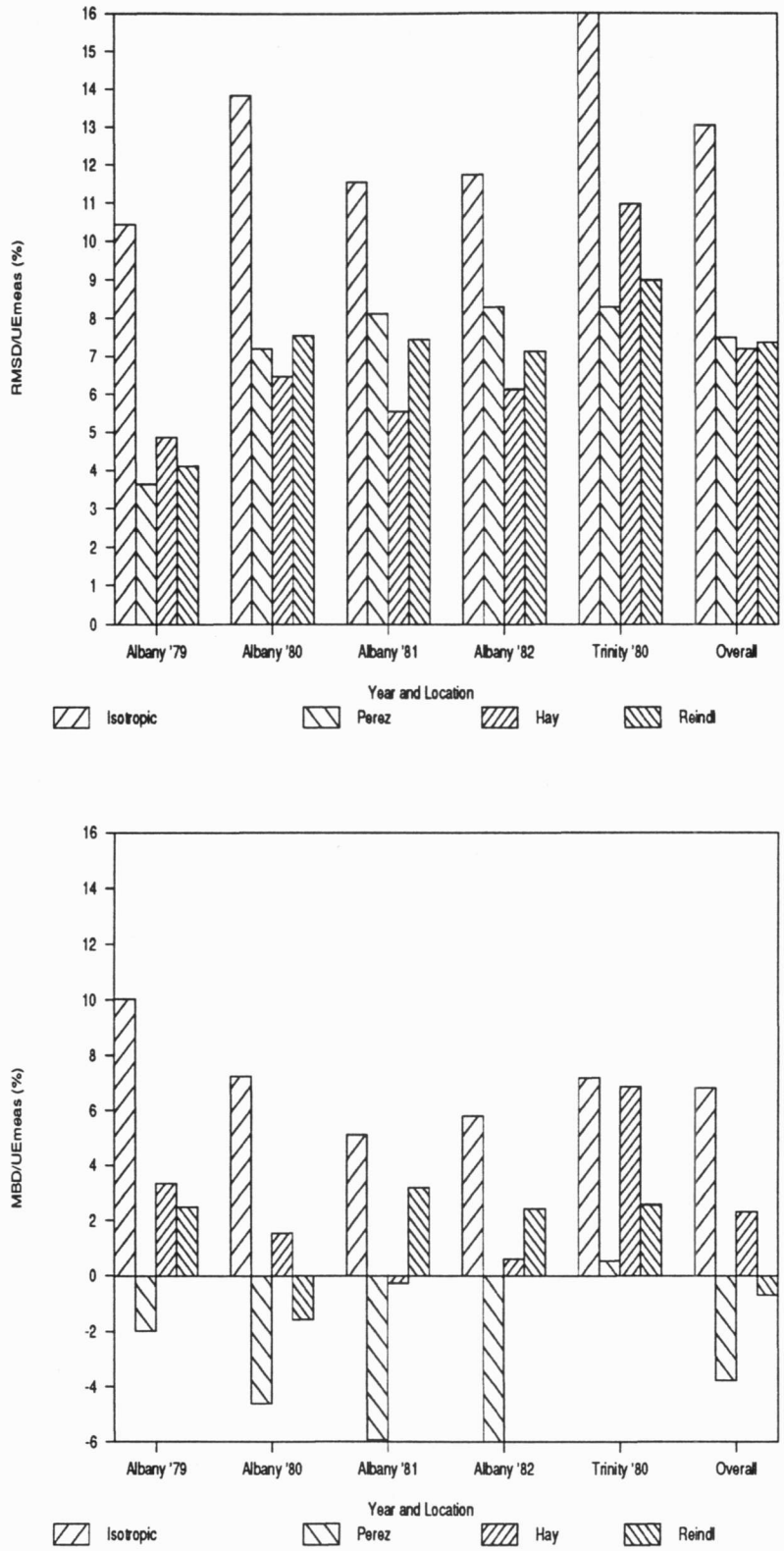

Figure 4.13: Normalized root mean square difference and normalized mean bias difference for all surface orientations using Orgill and Hollands correlation to estimate horizontal diffuse, 10-11:00 am

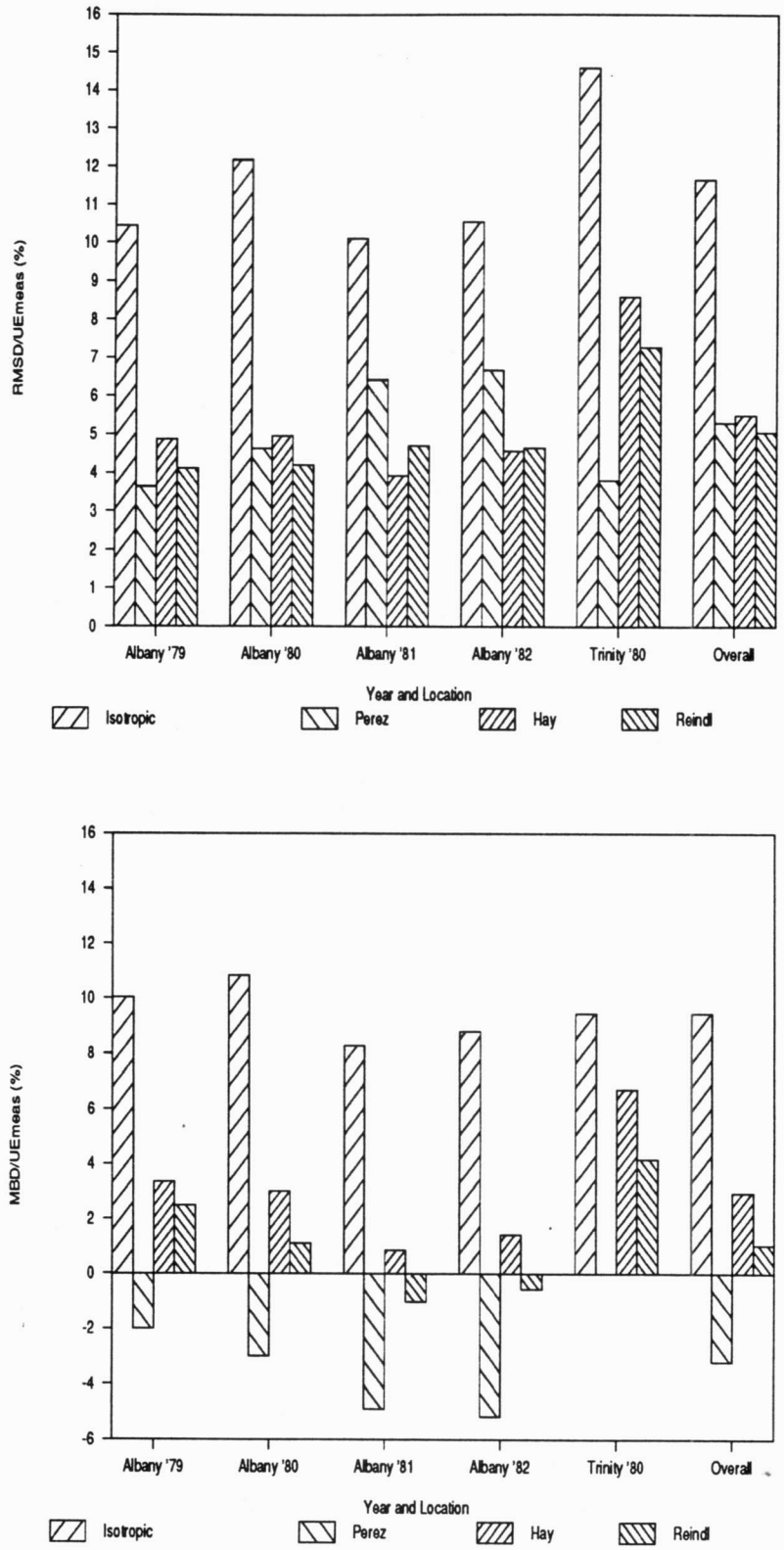

Figure 4.14: Normalized root mean square difference and normalized mean bias difference for south facing surfaces using Orgill and Hollands correlation to estimate horizontal diffuse, 10-11:00 am

4.5 Conclusions

Three existing models for estimating the diffuse radiation on a tilted surface were presented and evaluated in this Chapter. The models include: isotropic, Hay, and Perez. A fourth model was developed by modifying the Hay model to include horizon brightening. Utilizable energy is used as a metric for model performance evaluation. Each model used the same methods for projecting beam and ground reflected radiation onto a tilted surface. Thus, the only difference in the estimated total radiation on a tilted surface is due to the method used to project the diffuse radiation onto a tilted surface.

Two statistics were defined to quantify each model's short term and long term prediction performance. The statistics are normalized root mean square difference and normalized mean bias difference. On a model by model basis, the NRMSD and NMBD statistics were formed for five surface orientations and a range of critical levels.

Each tilted surface model requires hourly input of global horizontal radiation and horizontal diffuse radiation. Measured values of global horizontal and horizontal diffuse radiation were used as inputs to evaluate each model's ability to predict the measured utilizable energy on a tilted surface. To investigate the influence of diffuse radiation on the performance of each tilted surface model, three different correlations (equations 3.19-3.21, 3.22-3.24, and Orgill and Hollands) were used to estimate the horizontal diffuse radiation for input to the tilted surface models.

On an overall basis, the isotropic model showed the poorest performance and should not be used for estimating the hourly diffuse radiation on a tilted surface. The three anisotropic models: Perez, Hay and new model all have comparable performance. Plots presented suggest that the Perez model underpredicts the utilizable energy in the summer and overpredicts the utilizable energy in the winter months with the highest NRMSD present in the winter months for south facing non-vertical surface. The Hay and new model are more accurate in the winter months but tend to underpredict year round. The choice of the "best" model is influenced by the model's relative complexity. The Hay and new model are much simpler to use when compared to the Perez model. The new model is recommended because of its good NRMSD performance and its better NMBD performance when compared to the Hay model.

From a utilizable energy standpoint, the tilted surface models evaluated showed little sensitivity to the method for determining horizontal diffuse radiation. There was no significant degradation of tilted surface model performance when using any of the three diffuse fraction correlations mentioned above to estimate the horizontal diffuse for tilted surface model input.

Chapter 5 Conclusions and Recommendations

5.1 Conclusions

Diffuse Fraction Correlations

Chapter 3 of this thesis dealt with investigating the influence of climatic and geometric predictors on the hourly diffuse fraction. The goal was to determine if addition of these predictor variables will significantly reduce the standard error of existing Liu and Jordan type diffuse fraction correlations. This investigation used data from five locations (yielding 21,923 hours of measurements) to develop a new diffuse fraction correlation.

Stepwise regression is used to reduce the set of 28 potential predictor variables down to four significant variables. A piecewise correlation is developed to predict the diffuse fraction as a function of the clearness index, solar altitude, ambient temperature, and relative humidity. The method of least squares is used to fit the diffuse fraction in three intervals of k_t. In cases when ambient temperature is not available, a reduced form of the above correlation is included which predicts the diffuse fraction as a function of the clearness index and solar altitude.

The two correlations developed are compared to a Liu and Jordan type correlation ($\hat{I}_d/I = f(k_t)$) derived from the same data set. This provides a direct measure of the value of the added predictor variables. The full diffuse fraction

correlation reduced the residual sum squares by 14.4% when compared to the diffuse fraction correlation as a function of k_t only (derived from the same data set). The reduced form of the developed correlation diminished the residual sum squares by 9%.

Care should be taken when using empirically derived correlations due to their potential for being location dependent. In this research, the derived correlations exhibited some degree of location dependence. This is expected due to the fact that the climate types of each location in the data set differ. The derived correlations also showed slight seasonal variations. The prediction errors were higher in the spring and summer months.

Tilted Surface Models

Chapter 4 dealt with assessing the performance of various tilted surface radiation models. Three existing models (isotropic, Hay, and Perez) and a new model developed in section 4.2.4 are included in this investigation. The new model adds a horizon brightening term to the existing Hay model. Utilizable energy is used as a metric for model performance comparisons. The utilizable energy measured is compared with the utilizable energy predicted by each model for five surface orientations (43°s, 90°n, 90°s, 90°e, and 90°w) and a range of critical radiation levels at each surface orientation. Normalized root mean square difference and normalized mean bias difference difference statistics are formed for each model to quantify their individual performance.

All tilted surface models studied required inputs of global horizontal radiation and horizontal diffuse radiation. Measured values of global horizontal and horizontal diffuse radiation were provided as inputs to evaluate each model's ability to predict the utilizable energy on a tilted surface. Diffuse fraction correlations were also used to estimate horizontal diffuse radiation for model input.

The isotropic model showed the poorest performance and is not recommended for predicting the hourly radiation on a tilted surface. The remaining three anisotropic models: Hay, Perez, and new model all showed comparable performance. The Perez model tends to underpredict the utilizable energy in the summer and overpredict in the winter. The Hay and the new model are more accurate in the winter but tend to underpredict the utilizable energy year round.

Interestingly, the models showed little sensitivity to the method used for determining the horizontal diffuse radiation. No significant degradation of the tilted surface model performance is observed when correlations are used to estimate the horizontal diffuse radiation in lieu of measured horizontal diffuse radiation.

5.2 Recommendations

Although addition of climatic and geometric predictors to the Liu and Jordan type correlation yielded some reduction in the error of predicting the diffuse fraction, unexplained deviations in the diffuse fraction still remain. The unex-

plained error could be due to latent factors such as site pollution or cloud types. Study of diffuse radiation behavior in short time intervals i.e. one minute intervals may provide further insight regarding unexplained diffuse fraction errors. Also, additional data at intervals of high k_t values (> 0.75) may help explain the unusual behavior of the diffuse fraction in that interval.

The improvement to Liu and Jordan type correlations had little impact on a model's ability to predict the utilizable energy on a tilted surface. It would be interesting to observe the effect of diffuse faction correlations on the utilizable energy of systems using concentrating collectors.

All tilted surface models performed poorly on off south facing surfaces. Although this does not greatly affect simulation of energy systems, it is important for accurate studies of daylighting and building load analysis. Detailed data are needed to refine existing tilted surface models. Measurements of radiant intensities throughout the sky dome would be required to effectively build more accurate tilted surface models.

The weakness of the Hay and new model discussed in sections 4.2.2 and 4.2.4 regarding incidence angles greater than 90° and non-zero anisotropy index may be rectified by constraining the models. The constraint would require that the anisotropy index be set equal to zero when the angle of incidence is greater than 90°. This causes the models to revert to the isotropic (horizon enhanced for the new model) assumption when the circumsolar region is out of the collector's view.

Although not specifically investigated here, modified methods for determining the transmittance-absorptance ($\tau\alpha$) product are required when using anisotropic models. For the new model, the author recommends treating the circumsolar diffuse and isotropic/horizon diffuse separately. The ($\tau\alpha$) product for circumsolar radiation should be calculated as beam radiation i.e. effective angle of incidence is the angle of incidence of beam radiation. The effective angle of incidence for isotropic sky diffuse, as reported in Duffie and Beckman [5], varies as a function of surface slope from approximately 57-60°. The author recommends lumping the isotropic and horizon diffuse at an effective angle of 58° for purposes of calculating ($\tau\alpha$). The same procedure is recommended for the Hay model. These recommendations do not apply to the Perez model. The Perez model would require further investigation to determine the ($\tau\alpha$) product due to the large size of the circumsolar region.

The final recommendations are summarized below.

1. For estimating horizontal diffuse:
   full correlation - eq. 3.19-3.21

   if ambient temperature and/or relative humidity data are not available,
   reduced correlation - eq. 3.22-3.24
2. For estimating diffuse radiation on tilted surface,
   new model - eq. 4.15
3. Effective angle for transmittance-absorptance product,
   circumsolar diffuse - $\theta_e = \theta$
   isotropic/horizon - $\theta_e = 58$

Appendix A . Solar Radiation Principles

Unless specifically cited, the definitions and formulas presented have been taken from Duffie and Beckman [5]. They are included here for completeness.

A.1 Definitions and Formulas

Chapter 3 introduced diffuse fraction correlations. The hourly clearness index, k_t along with other variables were correlated with the hourly diffuse fraction. The hourly clearness index is given by,

$$k_t = \frac{I}{I_o}$$

where: I is the hourly total radiation on a horizontal surface and I_o is the hourly extraterrestrial radiation on a horizontal surface. The integrated hourly extraterrestrial radiation on a horizontal surface is calculated by the following relationship,

$$I_o = \frac{12 \times 3600}{\pi} G_{sc} \left[1 + 0.033 \cos\left(\frac{360n}{365}\right)\right] \times$$
$$\left[\cos(\phi)\cos(\delta)(\sin(\omega_2) - \sin(\omega_1)) + \frac{2\pi(\omega_2 - \omega_1)}{360}\sin(\phi)\sin(\delta)\right]$$

where: G_{sc} is the solar constant (a value of 1353 W/m² was used in this research), n is the day of the year, ϕ is the site latitude, δ is the declination, and ω_1, ω_2 are hour angles (ω_2 is larger, 15°/hr, mornings negative, afternoon postive). The declination is the angular position (at solar noon) with respect to the equator plane.

$$\delta = 23.45 \sin\left(360 \frac{284 + n}{365}\right)$$

The angle of incidence, θ, is required for tilted surface calculations and is given by,

$$\begin{aligned}\cos(\theta) = {} & \sin(\delta)\sin(\phi)\cos(\beta) - \sin(\delta)\cos(\phi)\sin(\beta)\cos(\gamma) \\ & + \cos(\delta)\cos(\phi)\cos(\beta)\cos(\omega) \\ & + \cos(\delta)\sin(\phi)\sin(\beta)\cos(\gamma)\cos(\omega) \\ & + \cos(\delta)\sin(\beta)\sin(\gamma)\sin(\omega)\end{aligned}$$

where: β is the surface slope, γ is the surface azimuth (=0 for south facing, east negative, west positive), ω is the hour angle. For this study, the angle of incidence was calculated at the midpoint of the hour by using the hour angle, ω, evaluated at the midpoint of the hour. When the surface slope is zero, the angle of incidence is the zenith angle. The zenith angle is given by,

$$\cos(\theta_z) = \cos(\delta)\cos(\phi)\cos(\omega) + \sin(\delta)\sin(\phi)$$

The zenith angle is related to the solar altitude angle, α, by the following,

$$\alpha = 90 - \theta_z$$

A.2 Utilizable Energy

Utilizable energy (as used in this research) is a statistic that represents the monthly average hourly amount that the critical radiation level is exceeded. For a given hour or hour pair, the monthly average utilizable energy is given by,

$$UE = \frac{1}{n} \sum_{n} (I_T - I_{T,c})^+$$

where: I_T is the hourly tilted surface radiation, $I_{T,c}$ is the critical radiation level, n is the number of hours over the month that the quantity is summed, and the + indicates only positive quantities of the difference are summed.

The utilizable energy on a tilted surface is a function of several variables including: month, location, hour pair, surface orientation, and critical radiation level. However in this research, the quantity of interest is the difference in the utilizable energy measured and the utilizable energy predicted.

$$\Delta UE = (UE_{meas} - UE_{pred})$$

where: UE_{meas} is calculated by using the measured tilted surface radiation in the equation for monthly average hourly utilizable energy and UE_{pred} is calculated by using the model predicted tilted surface radiation in the equation for monthly average hourly utilizable energy. Since ΔUE is the basis for forming the root mean square difference and mean bias difference statistics used for model comparison, it is of interest to determine the variables that affect ΔUE. One variable that did not significantly affect ΔUE is hour or hour pair used to calculate the utilizable energy. This was verfied by means of a fractional factorial data analysis using both hour and hour pair as variables and ΔUE as the response. The hour and hour pair (not including hours near sunrise and sunset) variables did not significantly affect the response; thus, they were not included as variables in the tilted surface model analysis. The tilted

surface model analysis used the hour 10-11:00 am for all calculations. The factors that are varied to observe the effects of ΔUE for each tilted surface model include: month, location, surface orientation, and critical radiation level.

Appendix B. Statistical Procedures / Techniques

The purpose of this section is to inform the reader of the statistical procedures and techniques used throughout the course of this research. Much of the information presented here is from Draper and Smith [40] and from class notes [46].

B.1 Regression Analysis by The Method of Least Squares

An empirical (regression) model is usually fitted to approximate a true but unknown function or relationship. A model typically takes the following general form.

$$Y = \text{Model Function} + \text{error}$$

where: Y is the response (dependent variable), the model function consists of predictor variables and model parameters used to describe the response. A simple example is the straight line model.

$$Y = \beta_o + \beta_1 X_1 + \varepsilon$$

where: the β's represent the model parameters, X is a predictor variable, and ε is the model error.

In this research, only linear models are considered. A *linear* model means linear in the model parameters. An example of linear and nonlinear models are given below,

$$Y = \beta_o + \beta_1 X_1 + \beta_{11} X_1^2 + \varepsilon \qquad \text{(linear)}$$

$$Y = e^{\beta_o} + e^{\beta_1} X_1 + \varepsilon \qquad \text{(nonlinear)}$$

The models proposed in this thesis were fit using the method of least squares. The method of least squares minimizes the error (residual) sum of squares. For example, the straight line case,

$$Y_i = \beta_o + \beta_1 X_1 + \varepsilon$$

$$P = \sum_{i=1}^{n} (\varepsilon_i)^2 = \sum_{i=1}^{n} (Y_i - \beta_o - \beta_1 X_1)^2$$

Estimates (b_o, b_1) of the true parameters (β_o, β_1) are chosen such that P is a minimum. This is accomplished by differentiating P with respect to each of the parameters and setting the result equal to zero producing a system of equations with unknown parameter values. In matrix form, this system of equations is given by the normal equations,

$$\underline{X'X}\,\underline{b} = \underline{X'Y}$$

where: $\underline{X}$ is an n x p matrix (p=# of parameters) that contains the value of each predictor, $\underline{X'}$ is the transpose matrix, $\underline{b}$ is a p x 1 vector containing the unknown model parameters, and $\underline{Y}$ is the n x 1 vector of response values. Estimates of the model parameters are found by solving the above system of normal equations.

B.2 Analysis of Variance

With estimates of the model parameters, the next step involves assessing the model fit. Analysis of variance (ANOVA) table is constructed to summarize the information crucial to judging the model fit. A typical ANOVA is presented below.

Source	d.f.	Sum Sq.	Mean Sq.
Regression | b_o	p-1	$\underline{b}'\underline{X}'\underline{Y} - \Sigma(Y_i)^2/n$	Sum Sq. / d.f.
Residual	n-p-2	$\underline{Y}'\underline{Y} - \underline{b}'\underline{X}'\underline{Y}$	Sum Sq. / d.f.
Total, corrected	n-1	$\underline{Y}'\underline{Y} - \Sigma(Y_i)^2/n$	

The entry Regression | b_o represents the regression sum squares (SS) corrected for the constant term b_o. The residual sum squares represents the response variation unexplained by regression. The sum of regression and residual sum squares comprise the total sum squares. An important entry in the ANOVA is the residual mean square. This quantity is an estimate of the overall variance of the fitted equation. A measure of the amount or percent variation explained by regression is given by R^2 (multiple correlation coefficient).

$$R^2 = \frac{\text{Regression| bo SS}}{\text{Total, Corrected SS}}$$

At this point, we are primarily interested in determining if the regression (more specifically each parameter) is statistically significant. Two tests that are helpful in assessing the statistical significance of the estimated model parameters include: t-test and F-test. Each test is performed by computing a t-statistic or F-statistic and comparing this value with the respective t- or F-distribution (at the desired confidence level and degrees of freedom). In its most general form, the t-statistic is given by the following,

$$t = \frac{\text{(estimate of parameter)} - \text{(postulated value of parameter)}}{\text{(std. error of the estimate of parameter)}}$$

For example in the straight line case if we are testing to determine if the parameter estimate b_o is significant, the following null hypothesis is assumed and t-statistic is computed,

$$H_o: \quad \beta_o = 0$$

$$t = \frac{b_o - 0}{se(b_o)}$$

The calculated t-statistic is compared to a t-distribution (at the desired confidence level) with degrees of freedom equal to the degrees of freedom in the standard error of b_o. If the calculated t-statistic is greater than the t-distribution value, the null hypothesis is rejected. That is, the estimate of b_o is not equal to zero. If the t-statistic is not significant (the calculated t-statistic is less than the t-distribution value), the null

hypothesis is not rejected.

When testing more than one parameter at once, the t-test cannot be used. The F-test is used to test multiple parameters. For example, the F-test for overall regression in a multiple parameter model is given by,

$$H_o: \quad \beta_o = \beta_1 = \beta_2 = \ldots = \beta_n = 0$$

$$F_{\nu_1,\nu_2} = \frac{MS_{reg}}{s^2} = \frac{MS_{reg}}{MS_{resid}}$$

where: MS_{reg} is the regression mean square and MS_{resid} is the residual mean square, ν_1 is the degrees of freedom in MS_{reg}, and ν_2 is the degrees of freedom in MS_{resid}. The F-statistic is compared with an F-distribution (at the desired confidence level) with ν_1, ν_2 degrees of freedom. If the calculated F-statistic exceeds the F-distribution value, the null hypothesis is rejected. This indicates that the null hypothesis is not true i.e. all parameters are not zero. If the calculated F-statistic is less than the F-distribution value, the null hypothesis is not rejected. Large F-statistics are desired because it removes the doubt of significance.

The test for overall significance does not discern if particular parameters are zero. Testing individual parameters (or groups of parameters) for significance is accomplished by performing a partial F-test. The partial F-test is presented by way of an example.

Assume the following model:

$$Y = \beta_o + \beta_1 X_1 + \beta_{11} X_1^2 + \varepsilon \qquad \text{(full model)}$$

Suppose we want to test if the parameter, β_{11} is significant. To test this parameter, a partial F-statistic is formed. The first step is to generate a reduced model which omits the parameter being tested.

$$Y = \beta_o + \beta_1 X_1 + \varepsilon \qquad \text{(reduced model)}$$

The null hypothesis and partial F-statistic are given by,

H_o: $\beta_{11} = 0$

$$F_{v_1,v_2} = \frac{(S_1 - S_2)/d.f.}{s^2} = \frac{(S_1 - S_2)/d.f.}{MS_{resid}}$$

where: S_1 is the regression sum square from the full model, S_2 is the regression sum square from the reduced model, d.f. is the degrees of freedom in the null hypothesis (d.f. = 1 in this case), and s^2 is the residual mean square from the full model. The difference (S_1 - S_2) is commonly referred to as the extra sum squares (ESS). Similar to the tests previously described, the computed F-statistic is compared to the F-distribution to determine significance. If the tested variable is important, the F-statistic will be large and the null hypothesis would be rejected.

When testing a single parameter, the following relationship can be used,

$$t_{\nu_2}^2 = F_{\nu_1,\nu_2}$$

For the t- and F-tests to be valid, the errors (residuals) are required to be independent and normally distributed with zero mean and constant variance, σ^2

$$\underline{\varepsilon} \sim \underline{N}(\underline{0},\underline{I}\sigma^2)$$

These assumptions are either confirmed or denied by performing the appropriate residual analysis. Various residual plots can be constructed to determine if the above assumption applies to the given data set and fitted equation. However, the following procedures are valid or unaffected by the above distributional assumptions.

Without Distributional Assumptions:

1. Estimates of parameters are the estimates that minimize the error sum of squares.

2. Variance of each parameter can be calculated by,

$$V(\underline{b}) = (\underline{X}'\underline{X})^{-1}\sigma^2$$

3. ANOVA can be constructed.

4. The multiple correlation coefficient, R^2, can be calculated.

5. Fitted values can be obtained by,

$$\underline{\hat{Y}} = \underline{X}\,\underline{b}$$

With Distributional Assumptions:

1. All distribution related tests (t-test and F-tests) can be performed and are valid.

B.3 Selection Procedure

A useful tool in regression model building is a selection procedure. When several possible variables are proposed to predict a response, a procedure is helpful to select the best set of predictor variables to "explain" the deviations of the response. The goal is to obtain a fitted equation with a minimum number of variables but that provides reliable estimates of the response. The specific goal in this research is to minimize the overall standard error while maintaining a reasonable number of predictors in the final regression equation.

The selection procedure used in this research is stepwise regression. The stepwise procedure is introduced by an example.

Given a set of three predictor variables, Z_1, Z_2, Z_3, the goal is to find the model which minimizes the overall standard error using the least number of predictor variables. The stepwise procedure begins with the following base model,

$$Y = \beta_o + \varepsilon \qquad \text{(base model)}$$

To determine the best variable to add to the base model, partial F-statistics are computed for each by the following,

$$F_{Z_1} = \frac{(S_1 - S_2)/d.f.}{s^2} = \frac{(ESS)/d.f.}{MS_{resid}}$$

$$F_{Z_2} = \frac{(S_1 - S_2)/d.f.}{s^2} = \frac{(ESS)/d.f.}{MS_{resid}}$$

$$F_{Z_3} = \frac{(S_1 - S_2)/d.f.}{s^2} = \frac{(ESS)/d.f.}{MS_{resid}}$$

In each case, the extra sum squares is computed by the difference in regression sum squares from a proposed model which includes the respective Z_1, Z_2, and Z_3 predictors and the base model regression sum square. The MS_{resid} is the residual mean square from the larger model (proposed model). The variable with the highest F-statistic will be considered for addition to the base model. Assume the variable Z_2 produced the highest F-statistic. The Z_2 F-statistic is compared with the F-distribution. If the F-statistic is not significant, the variable is not added to the base model and the stepwise procedure stops (no variables are significant) and the base model is adopted. If the Z_2 F-statistic is significant, the variable is added to the base model to produce a

new base model for the next step in the regression procedure. Assuming Z_2 (actually β_2 parameter) is significant, the second step in the stepwise procedure begins with the following base model,

$$Y = \beta_o + \beta_2 Z_2 + \varepsilon \qquad \text{(base model)}$$

The next best variable to enter into the model is determined by computing the following partial F-statistics,

$$F_{Z_1|Z_2} = \frac{(ESS)/d.f.}{MS_{resid}}$$

$$F_{Z_3|Z_2} = \frac{(ESS)/d.f.}{MS_{resid}}$$

where: $F_{Z_1|Z_2}$ is the partial F for Z_1 given Z_2 is already in the equation similarly, $F_{Z_3|Z_2}$ is the partial F for Z_3 given Z_2. The largest partial F-statistic is compared with the F-distribution for significance. If it is not significant, stepwise regression is halted and the base model which includes Z_2 is adopted. If it is significant, the variable is added to the model. Assume Z_3 has the highest F-statistic and is significant. At this point, the initial variable entered in the first step, Z_2, is also tested to assure it is still significant since the new variable, Z_3, has entered the model. This procedure is continued until no variables can enter or all predictors are exhausted. The best equation (based on the criteria used in this thesis) will have the smallest overall

standard error with a reasonable number of predictor variables.

Although slight variations in the described stepwise regression procedure exist, the underlying principle is the same.

B.4 Residual Analysis

After the selection procedure ends and a fitted regression equation is obtained, the appropriate residual analysis must be performed to assure the distributional assumptions are satisfied and no obvious errors or model deficiencies exist. The following residual plots are typically used in the course of model diagnostics:

1. Histogram or overall plot of residuals.
2. Normal probability plot.
3. Time sequence plot (if time order is known).
4. Plot against predictor variables.
5. Plot against predicted values.

The histogram and normal probability plots help to determine if the assumption of normality in the residuals is valid. The overall plot of the residuals should look like a normal distribution centered at zero. When the residuals are plotted in a normal probability plot, they should form a straight line.

The remaining plots should produce residuals centered at zero and appear as a band of noise, Figure B.1. Three common faults uncovered in residual plots are

shown in Figures B.2-B.4. The first plot shows the behavior of residuals that have non-constant variance. The second plot shows that a linear effect has not been removed or an error has been made in analysis (such as omitting the constant term b_o). The last plot identifies that a quadratic term may be missing. For further information on residuals and their use in diagnostic analysis see Draper and Smith [40] and Belsely et al. [41].

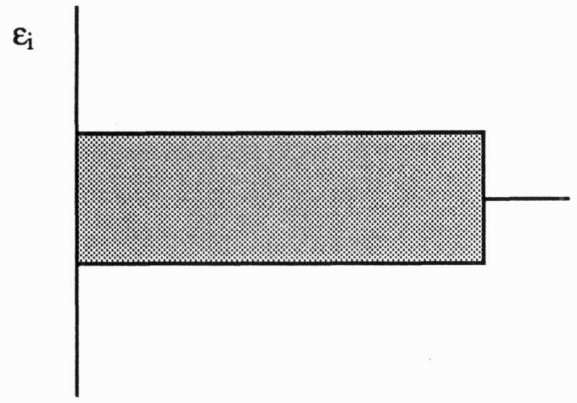

Figure B.1: Acceptable residual plot

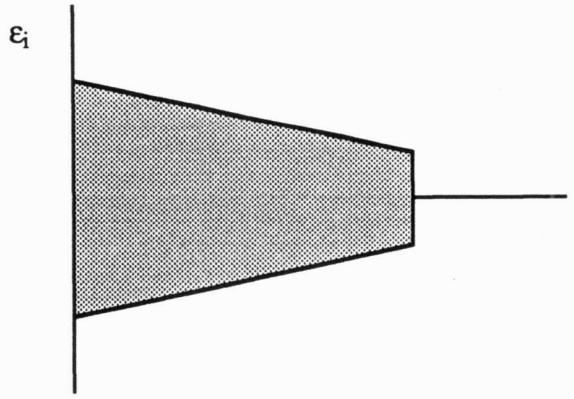

Figure B.2: Residuals with non-constant variance

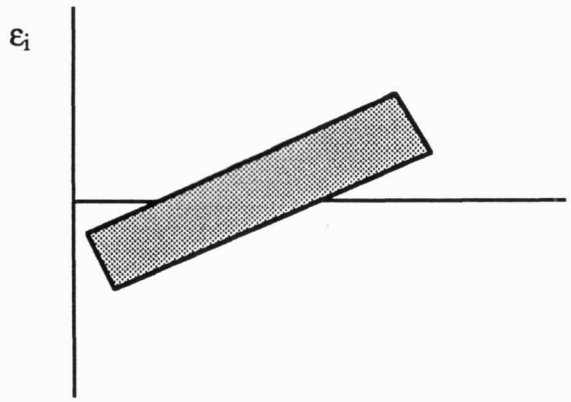

Figure B.3: Residuals with linear effect not removed

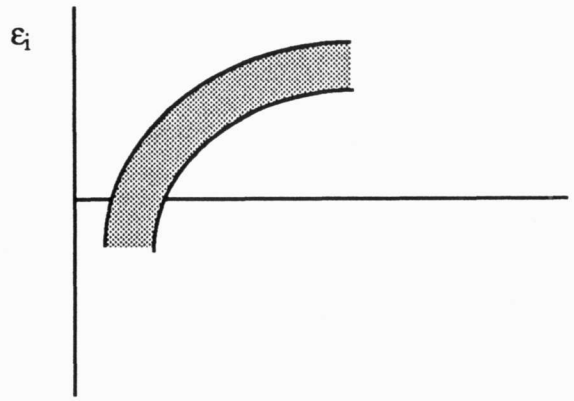

Figure B.4: Residuals with quadratic effect not removed

Appendix C: Plots

Time Series Plot of Hourly Residual vs. Day of Year

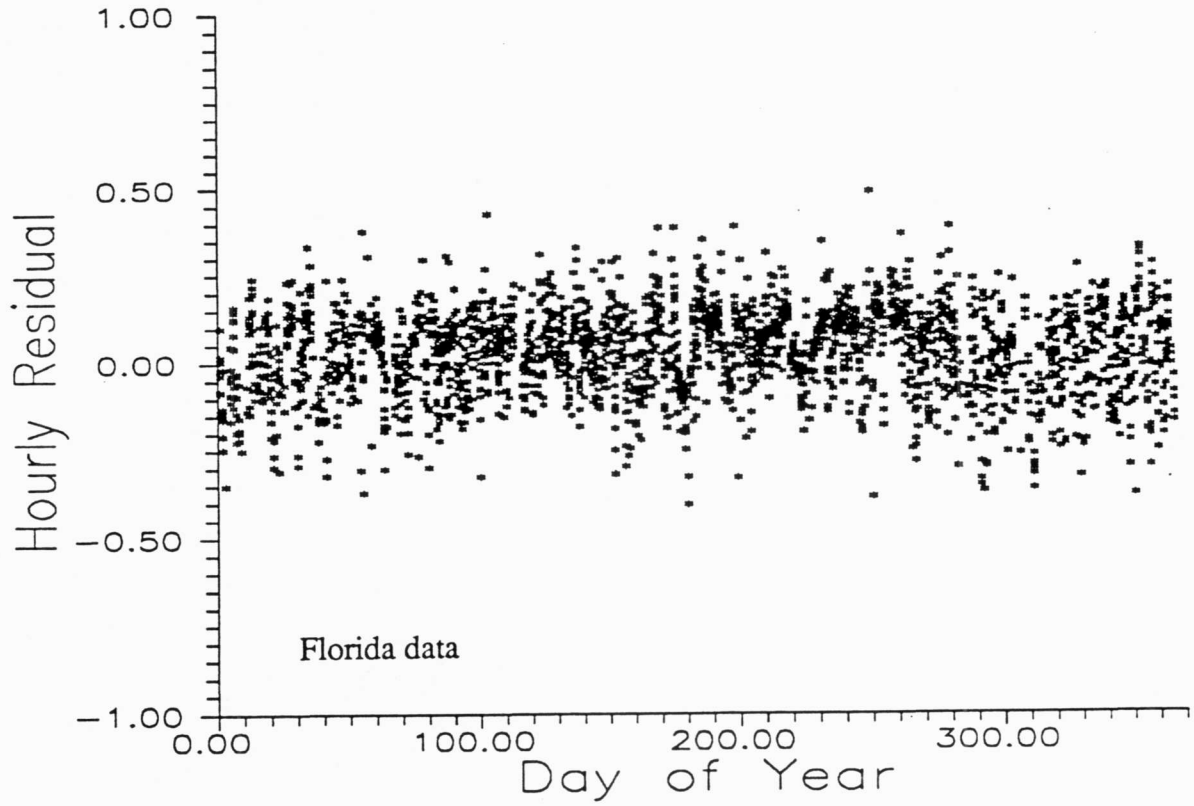

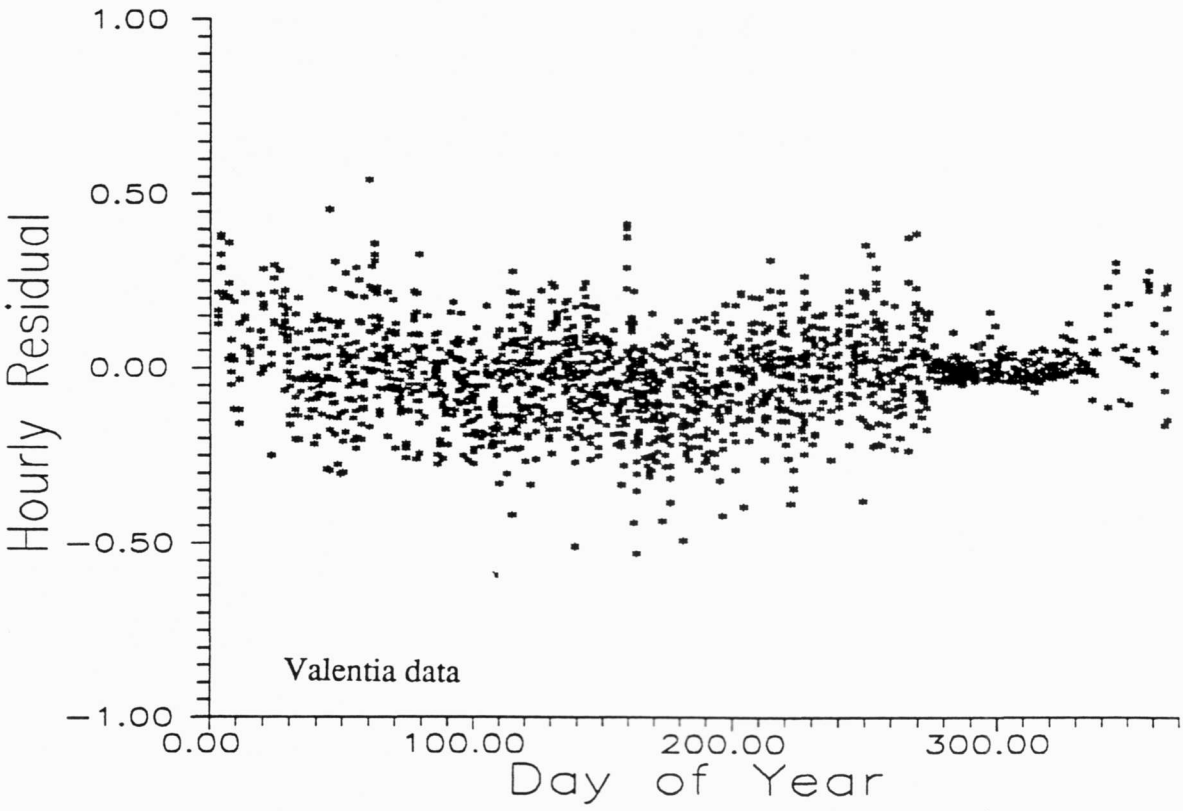

Time Series Plot of Hourly Residual vs. Day of Year

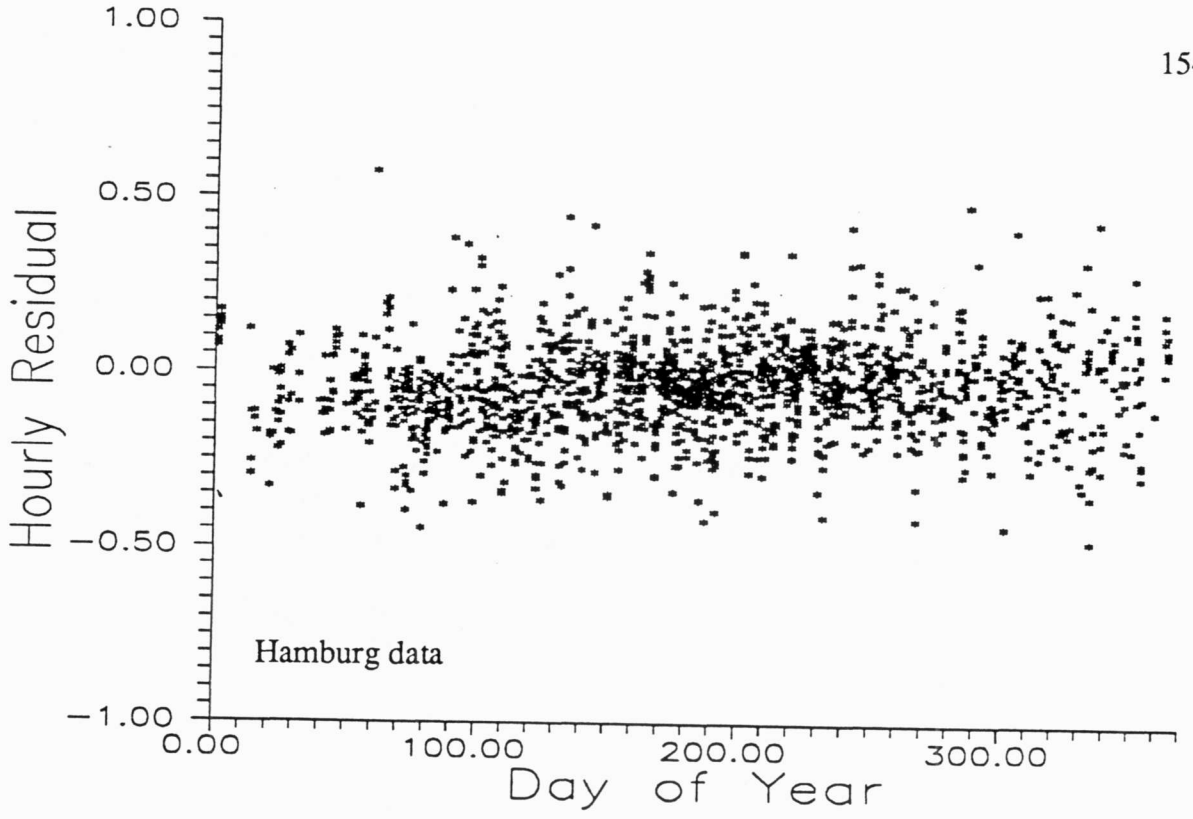

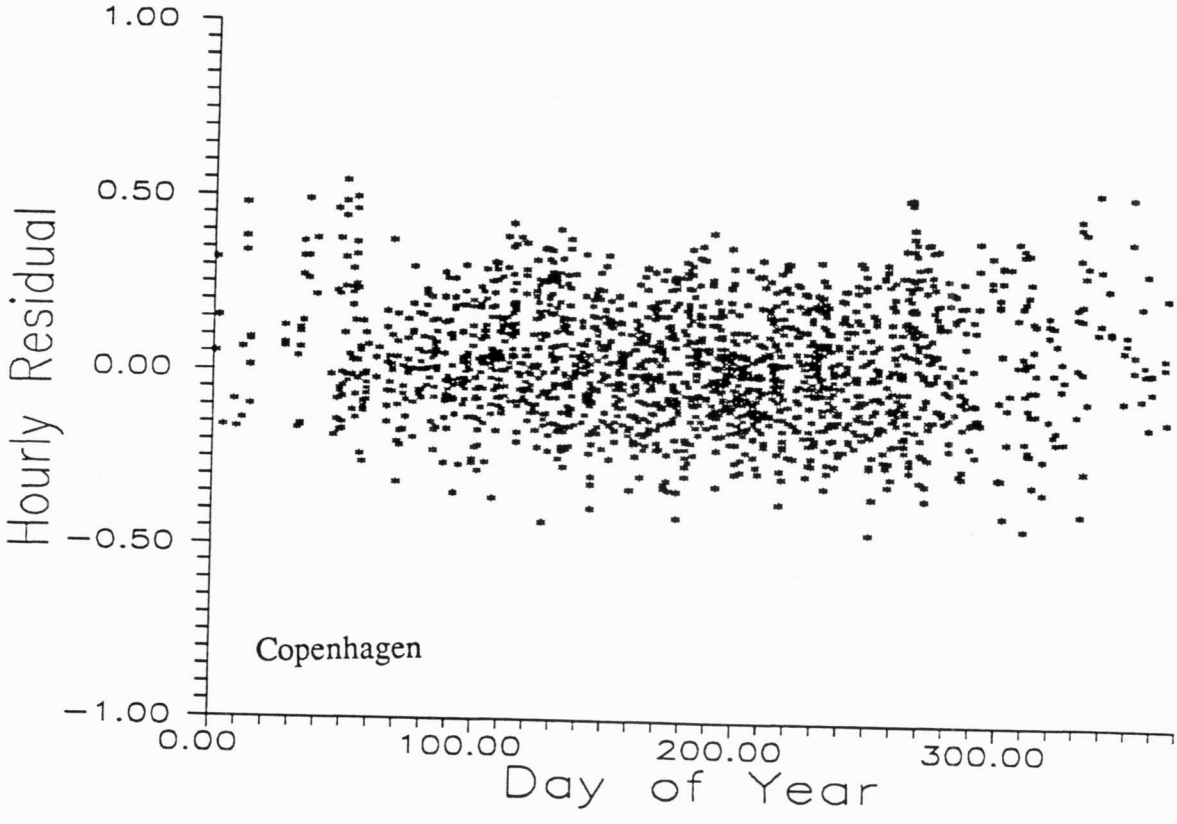

Time Series Plot of Hourly Residual vs. Hour of Day

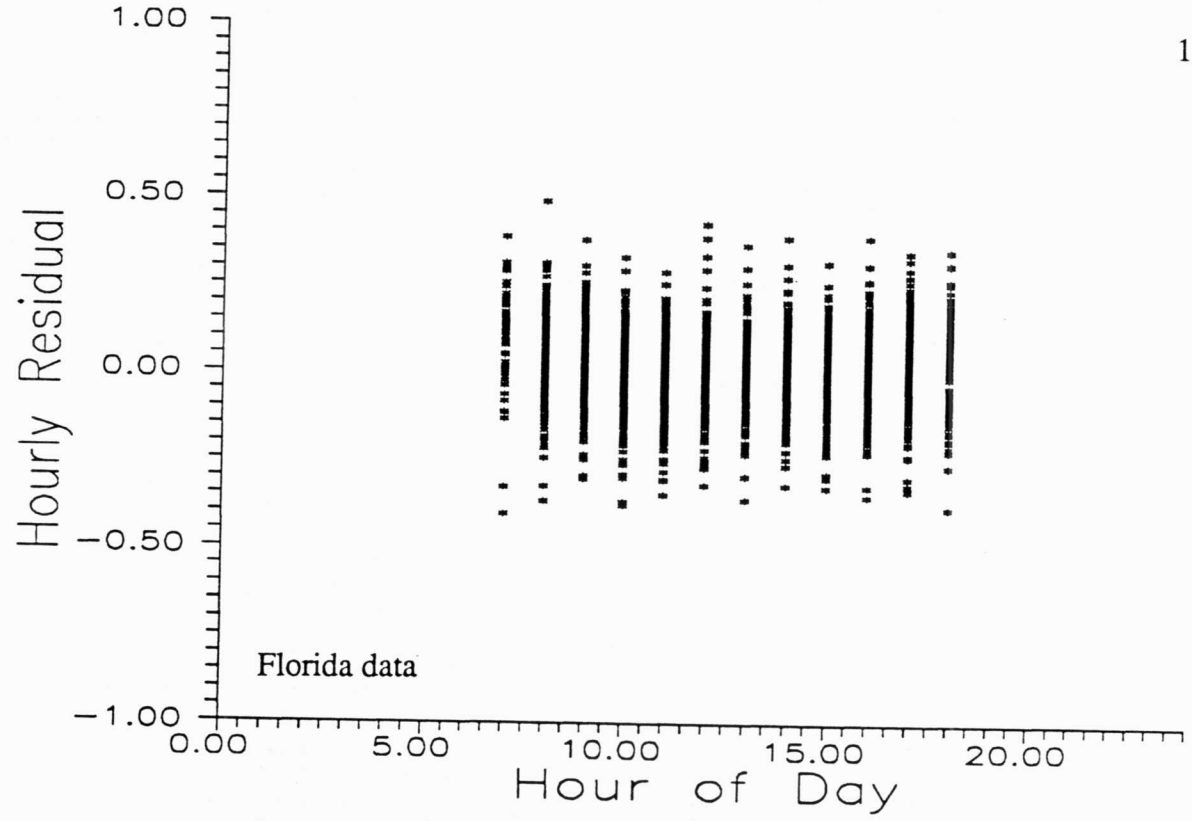

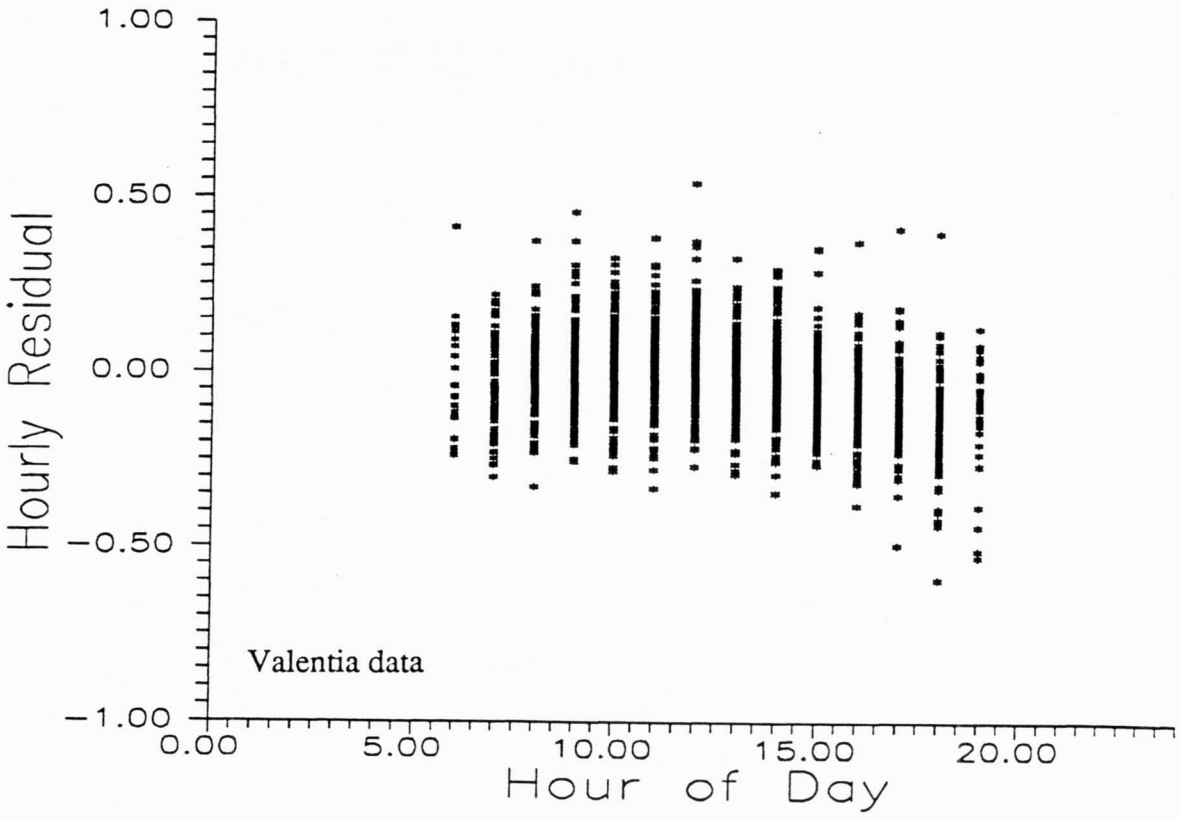

Time Series Plot of Hourly Residual vs. Hour of Day

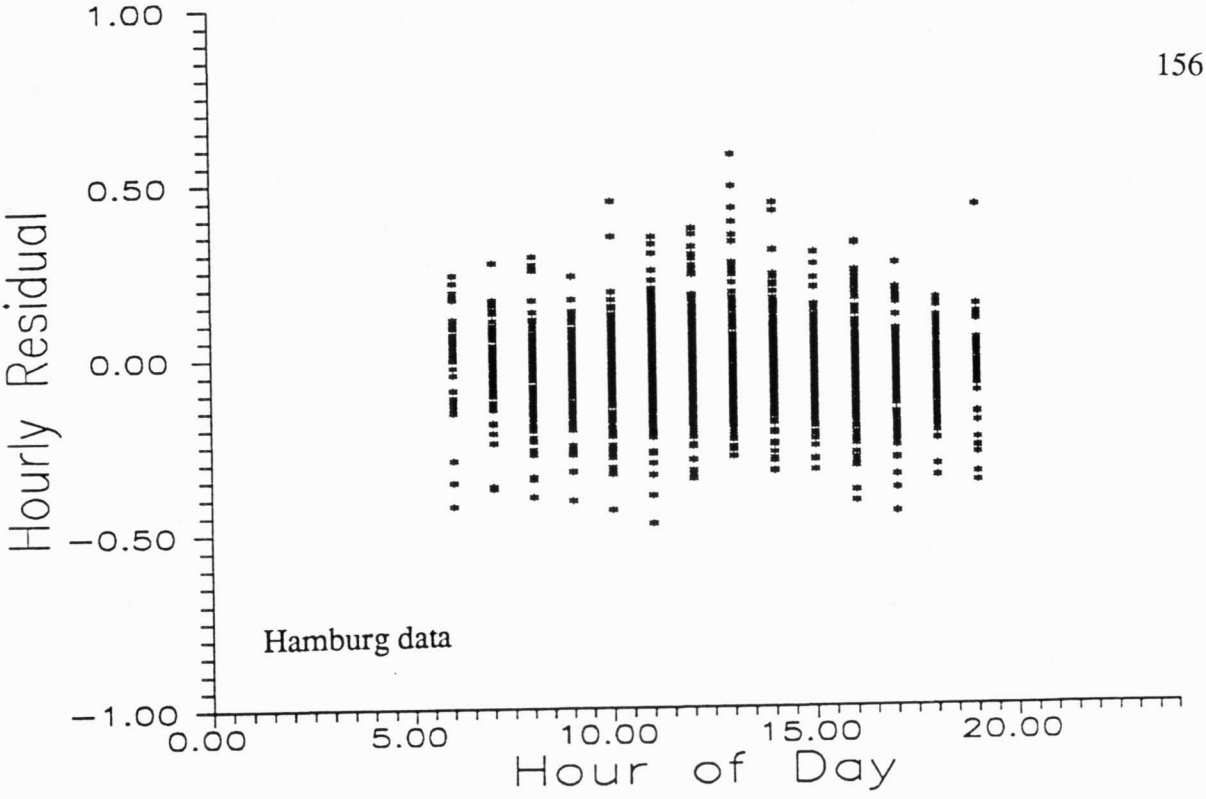

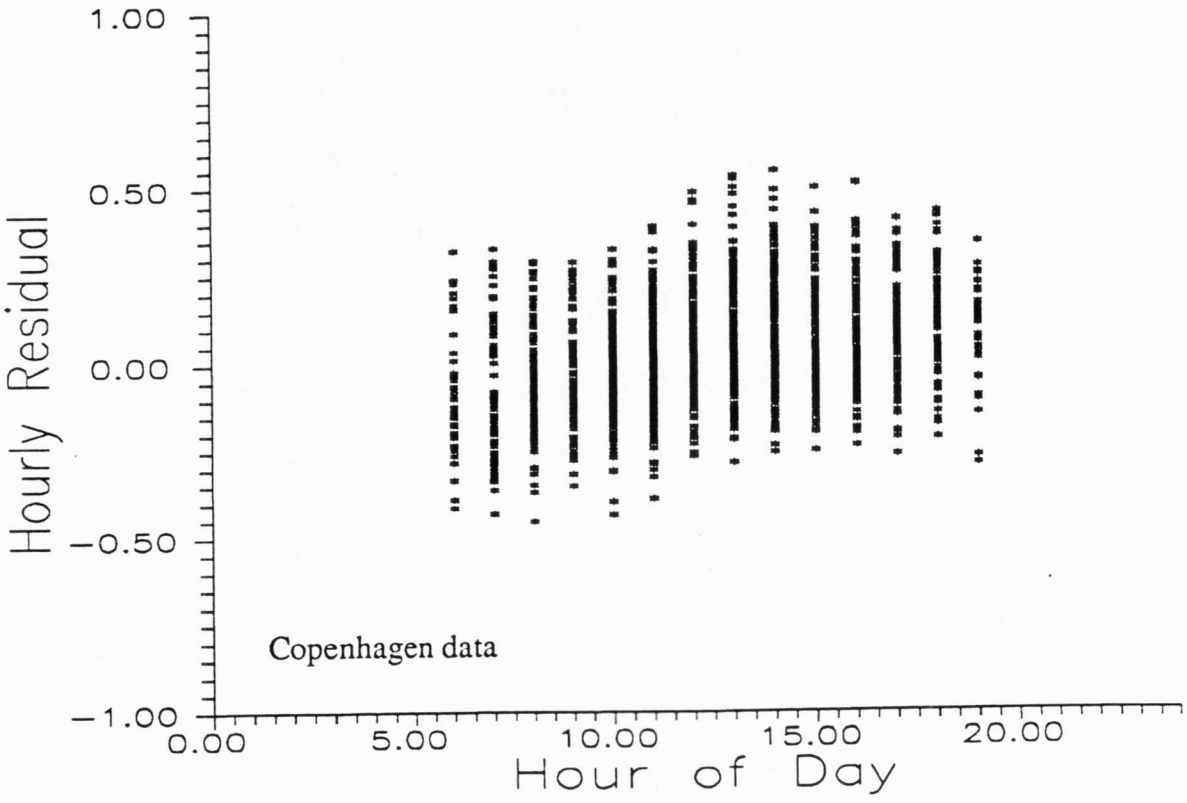

Residual vs. kt

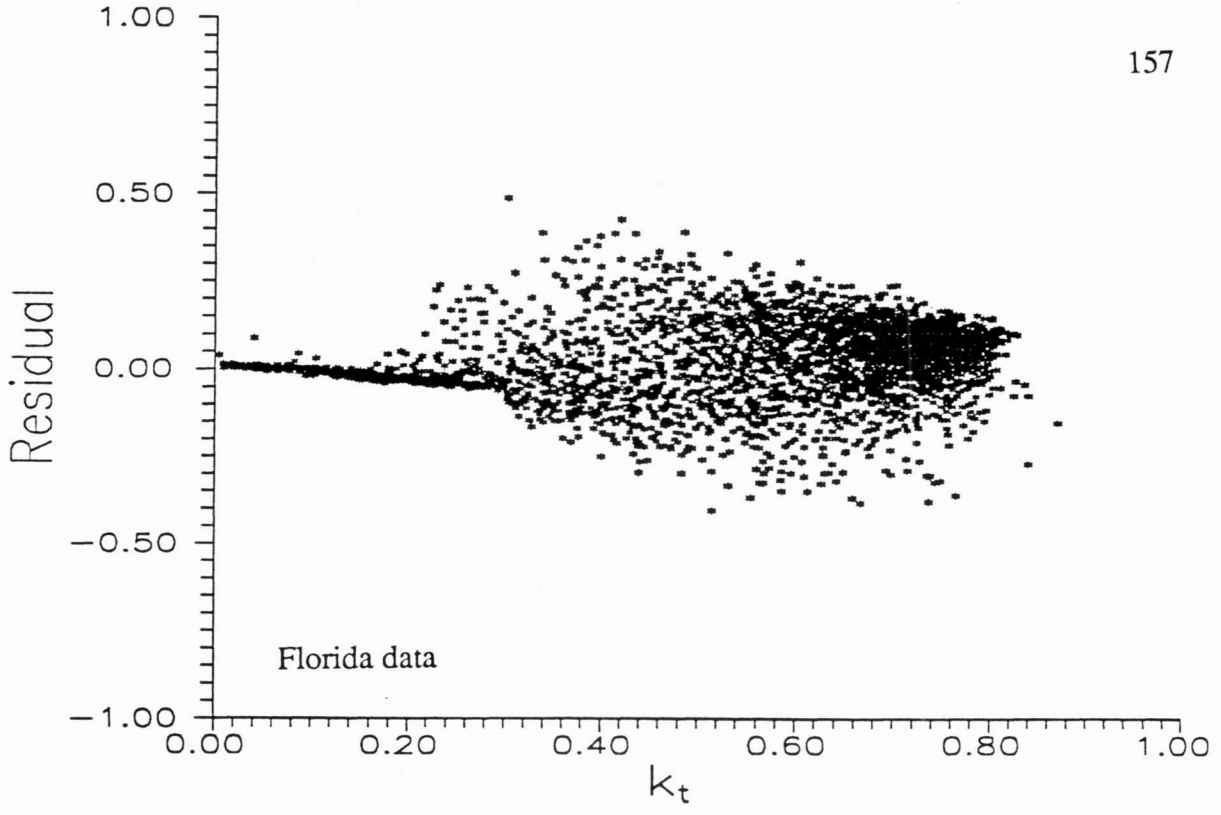

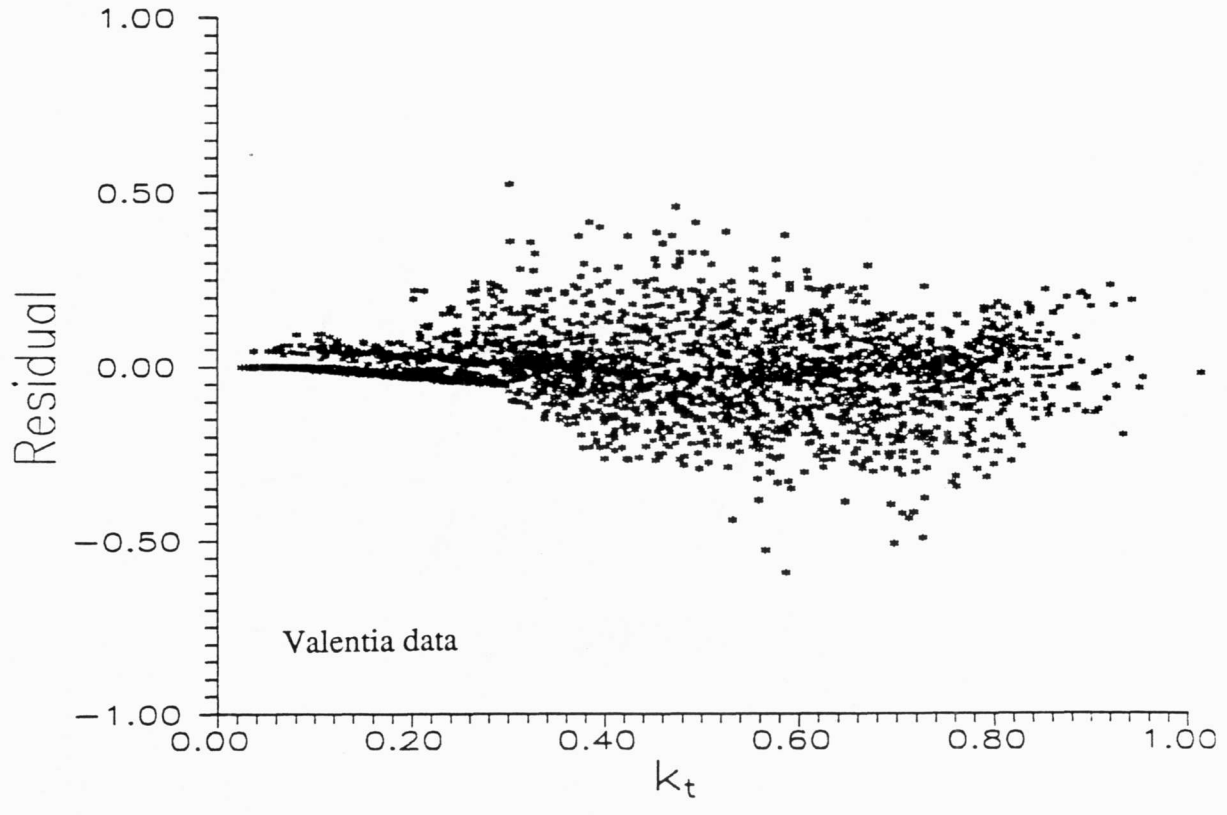

Residual vs. kt

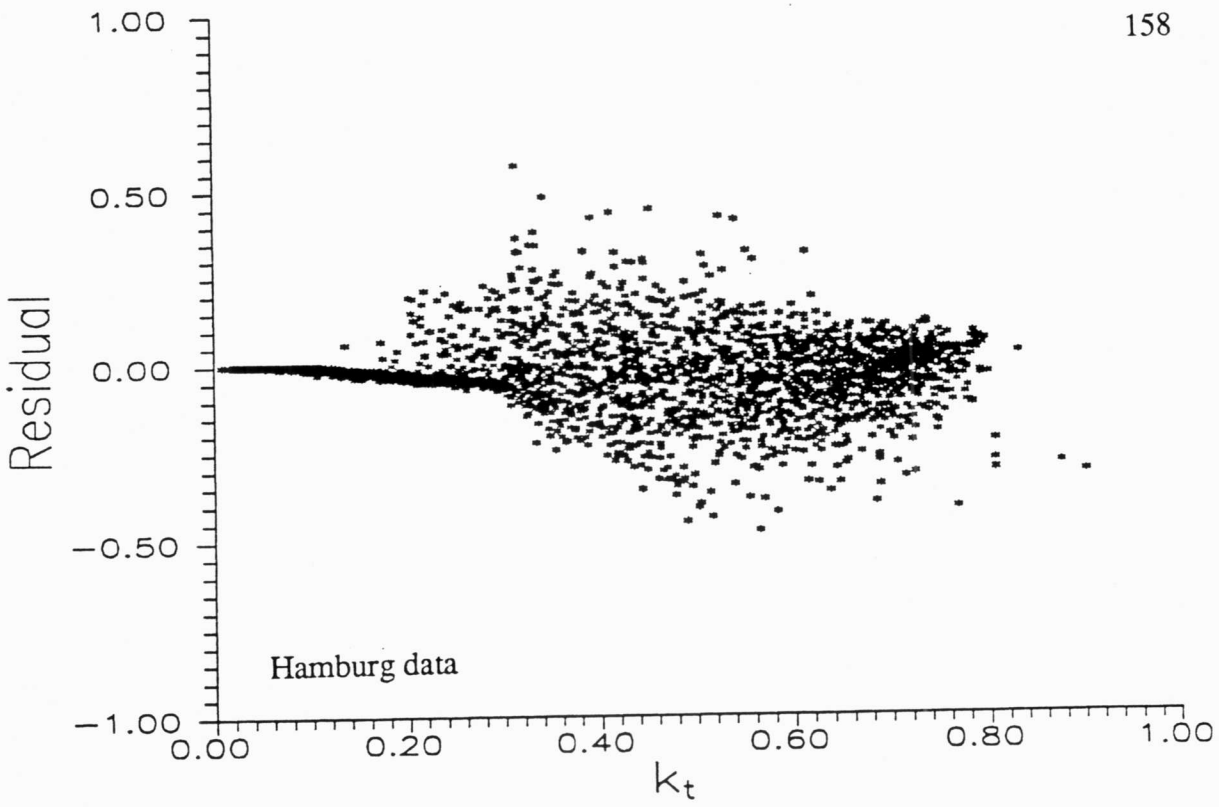

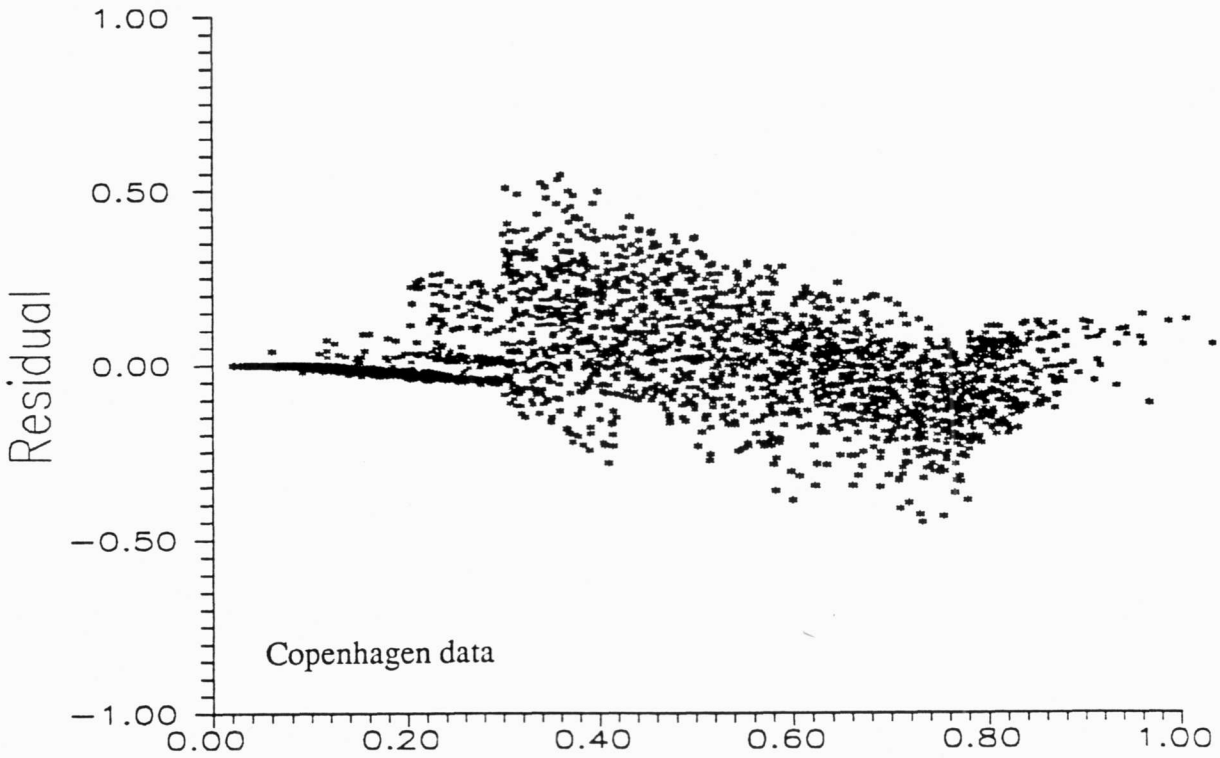

Residual vs. Sin(alt)

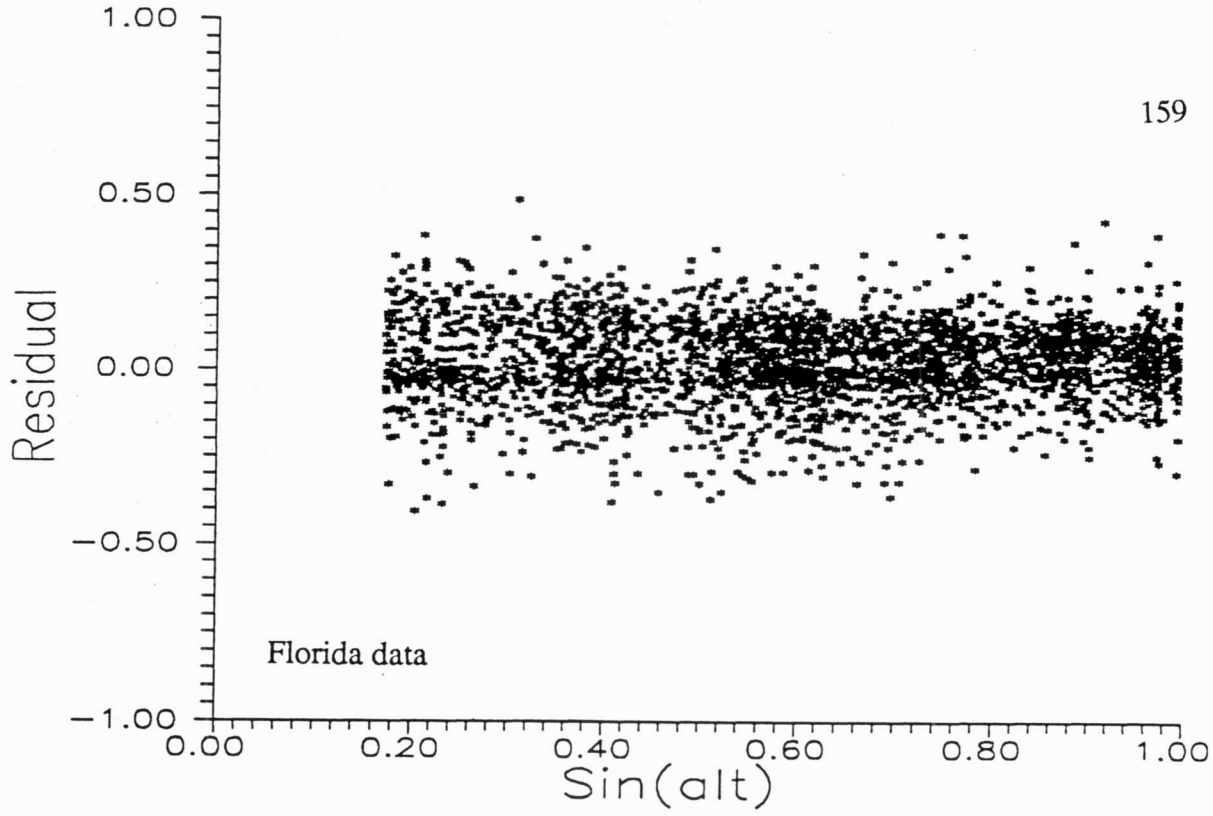

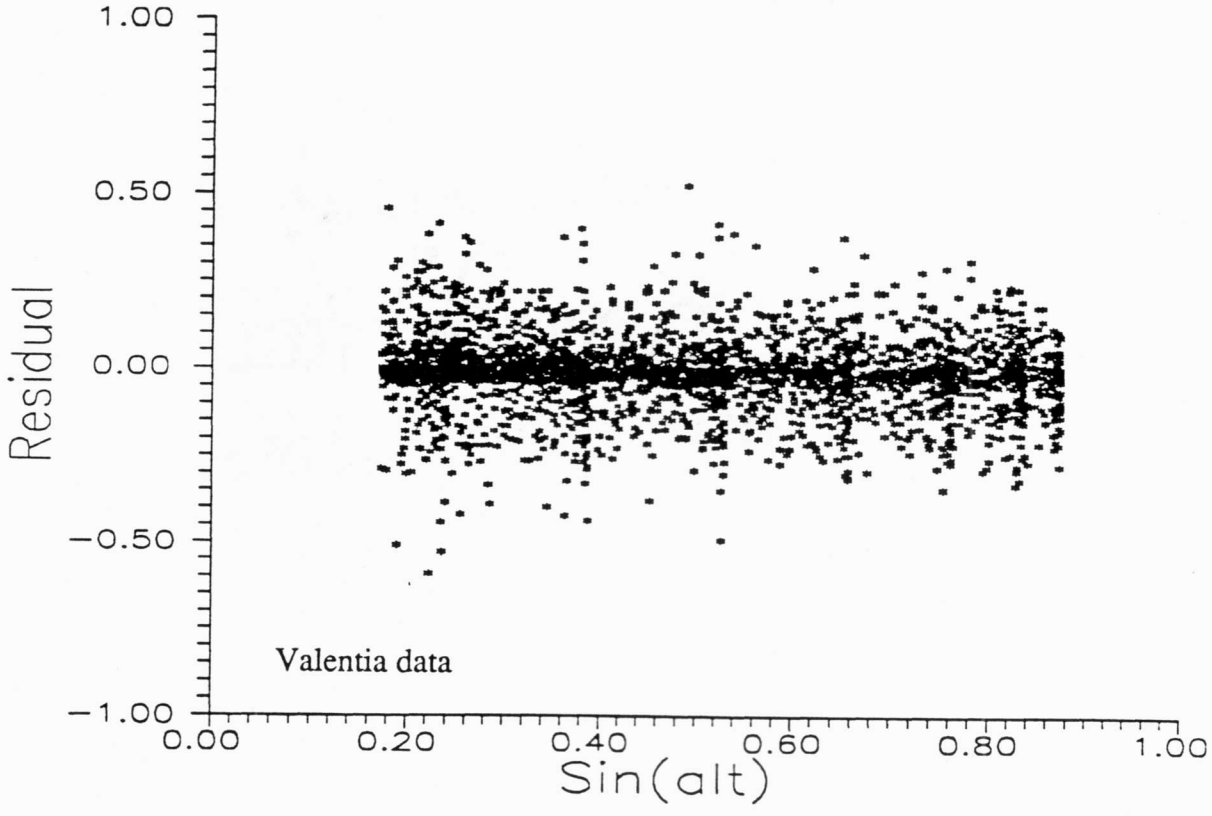

Residual vs. Sin(alt)

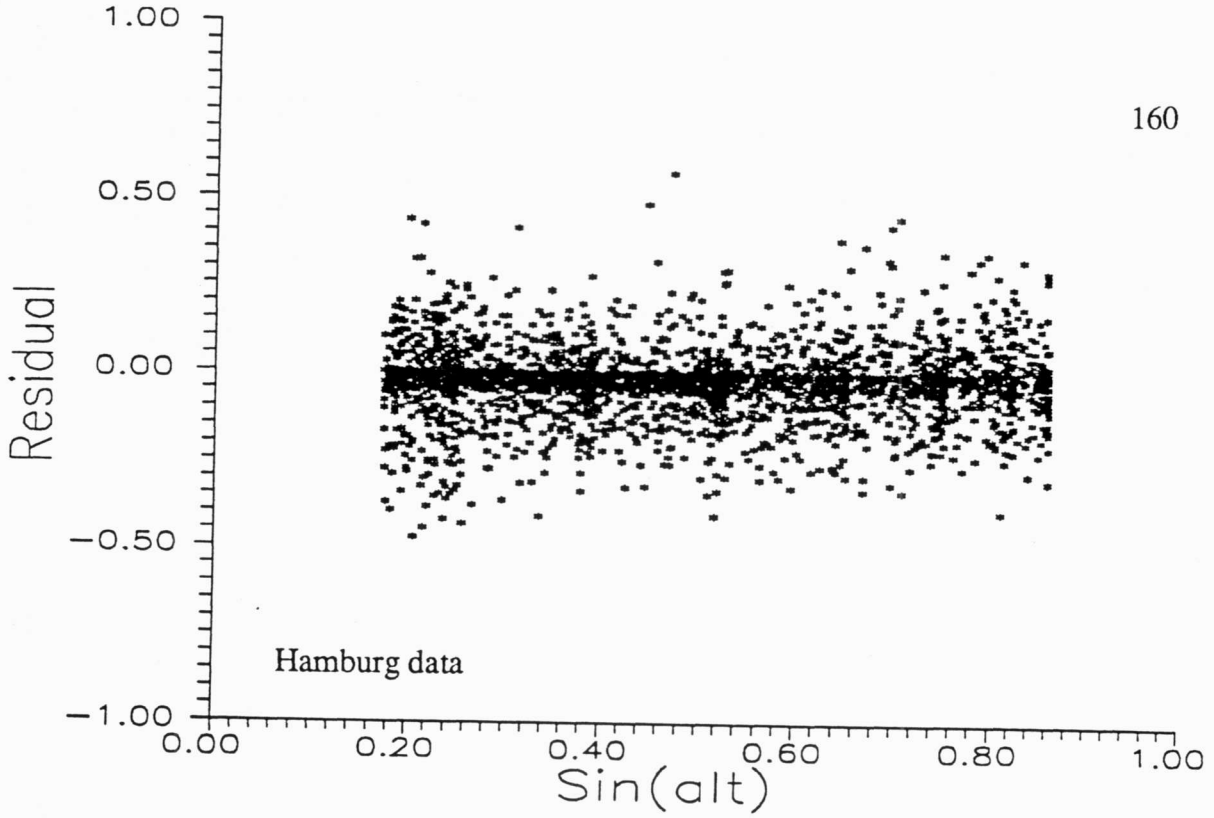

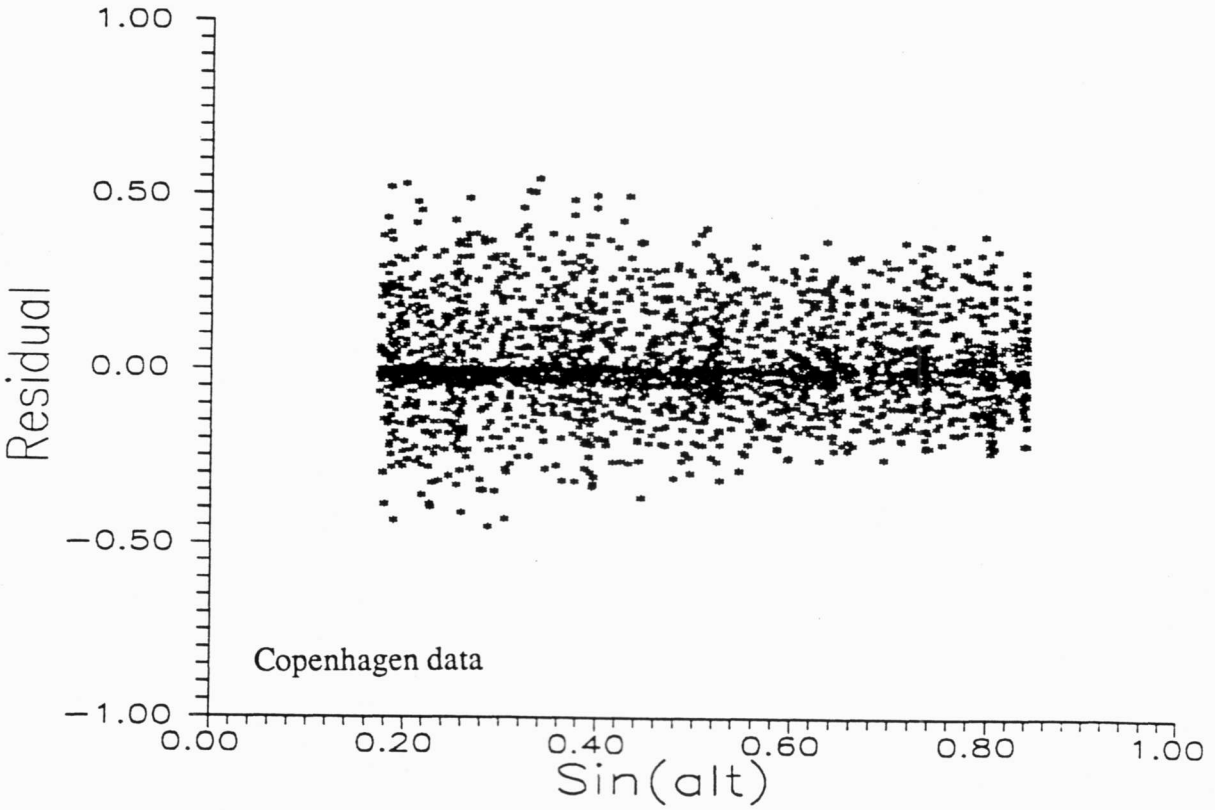

Residual vs. Ta

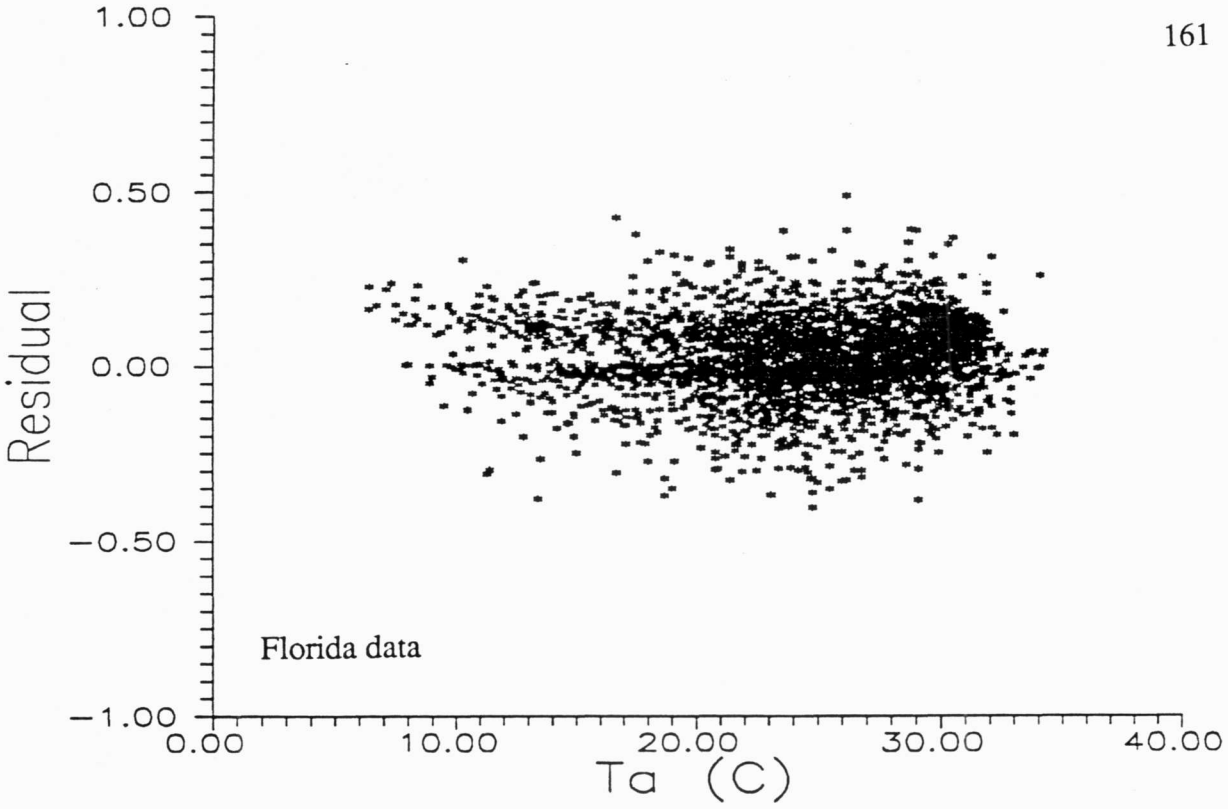

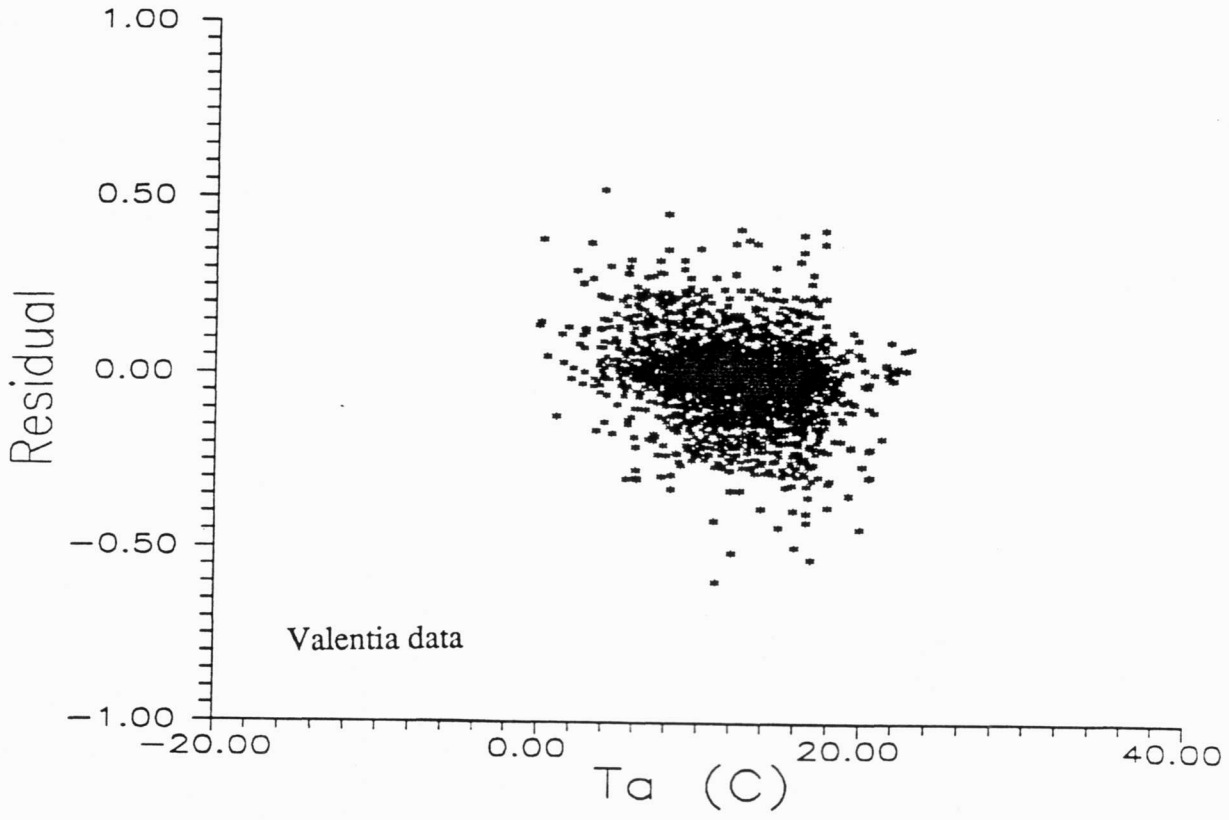

Residual vs. Ta

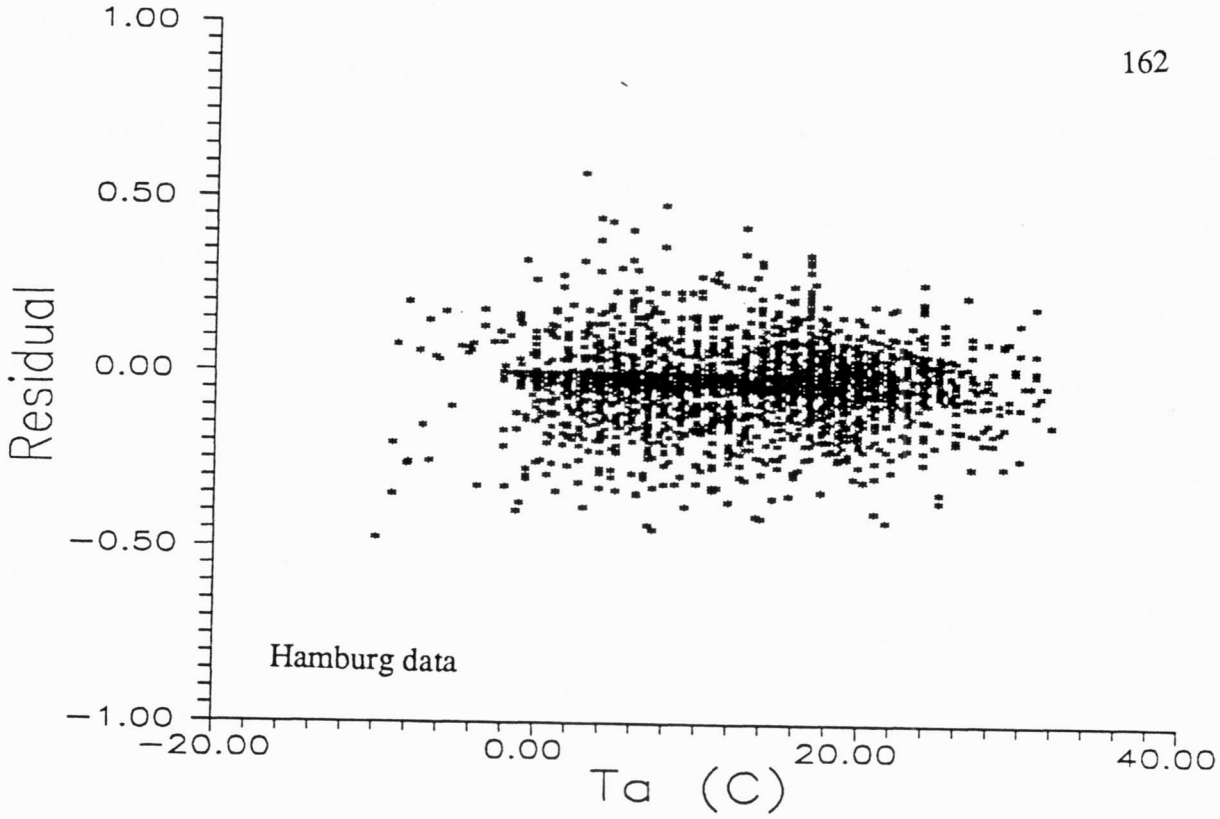

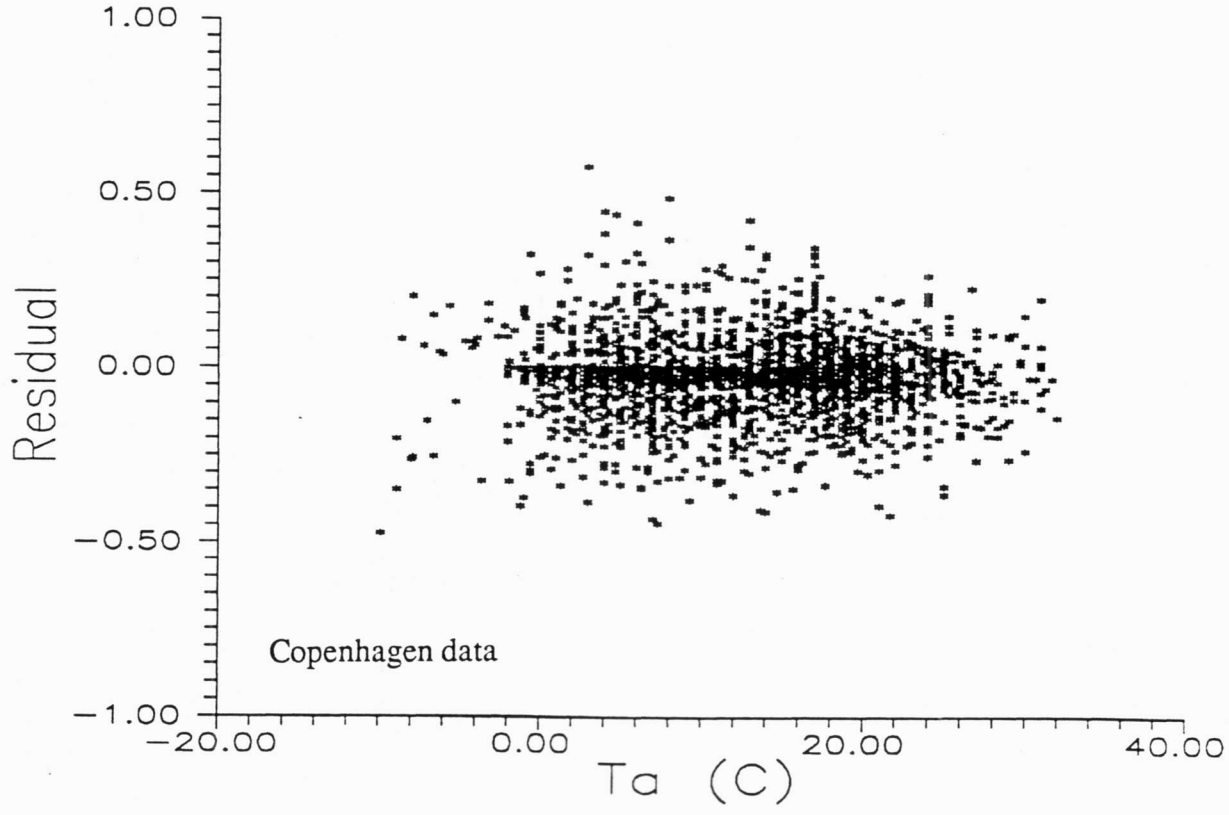

Residual vs. Relative Humidity

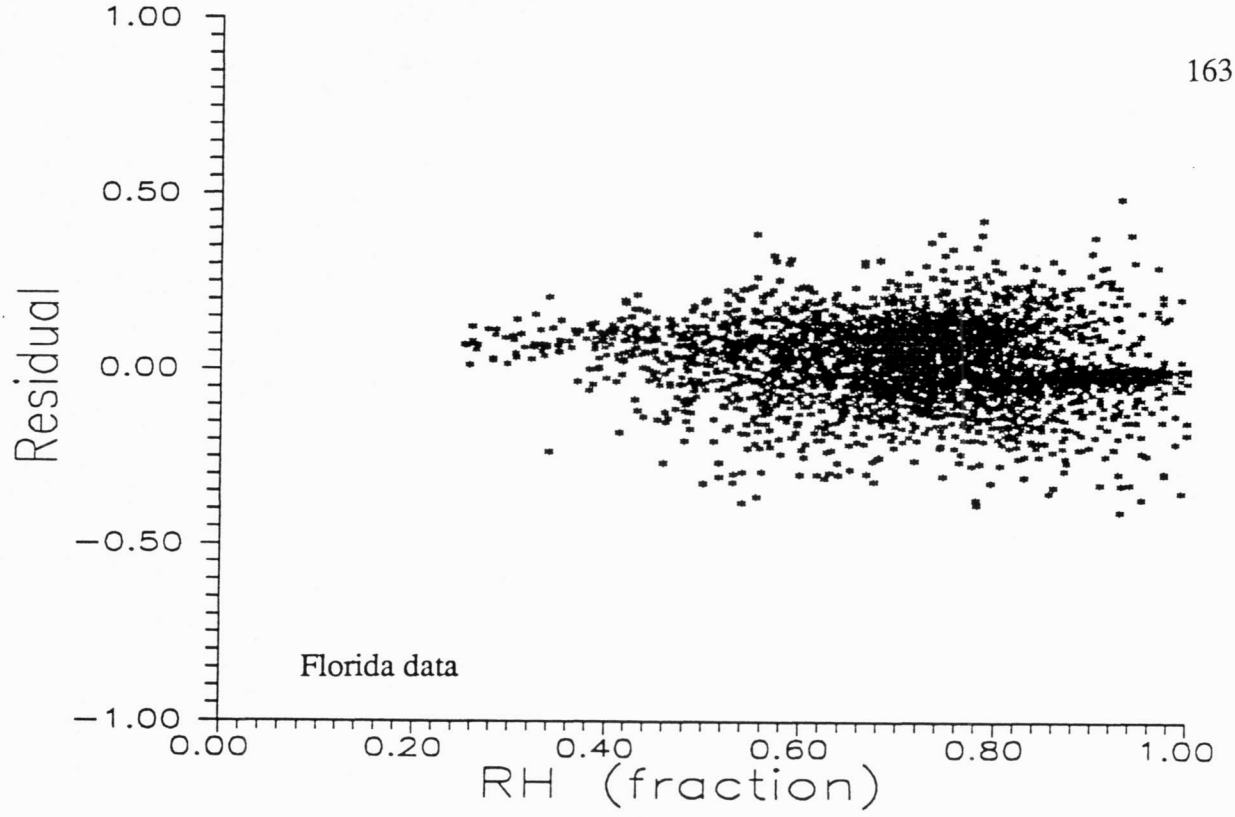

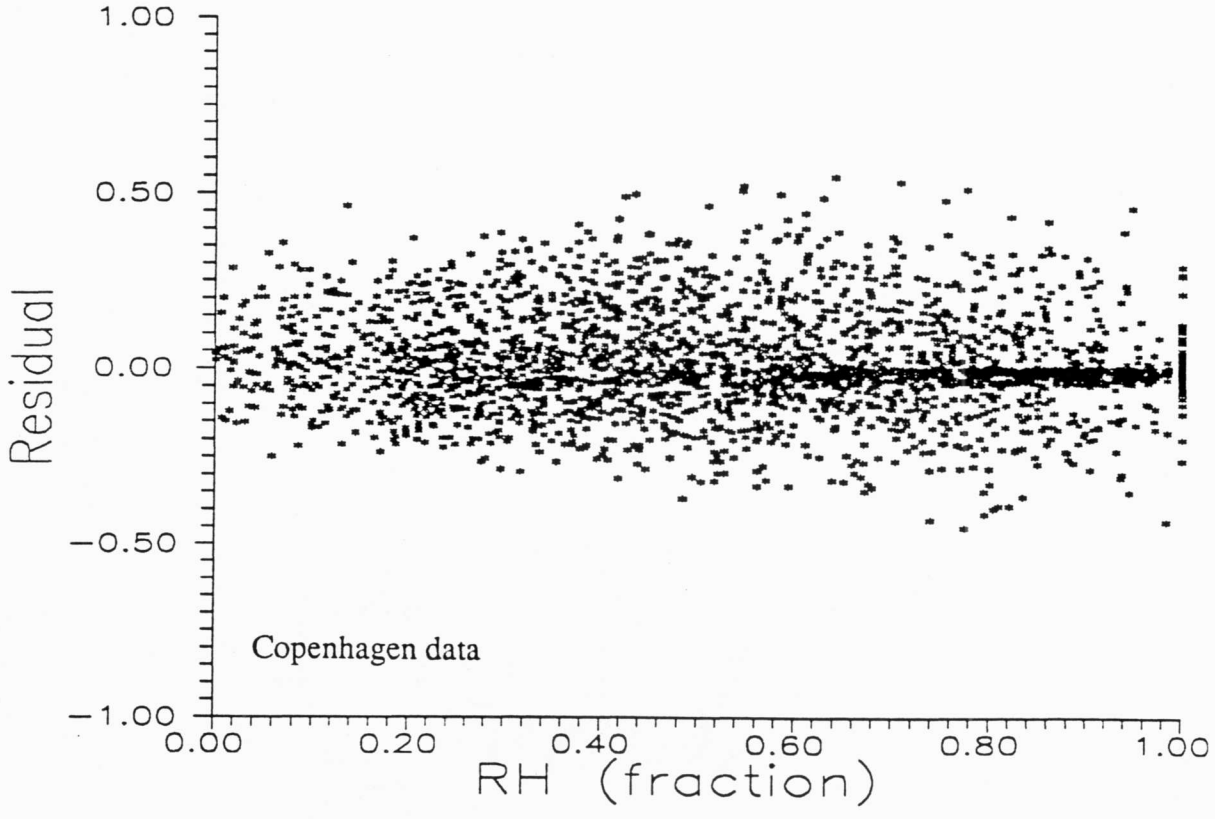

Residual vs. Predicted Diffuse Fraction

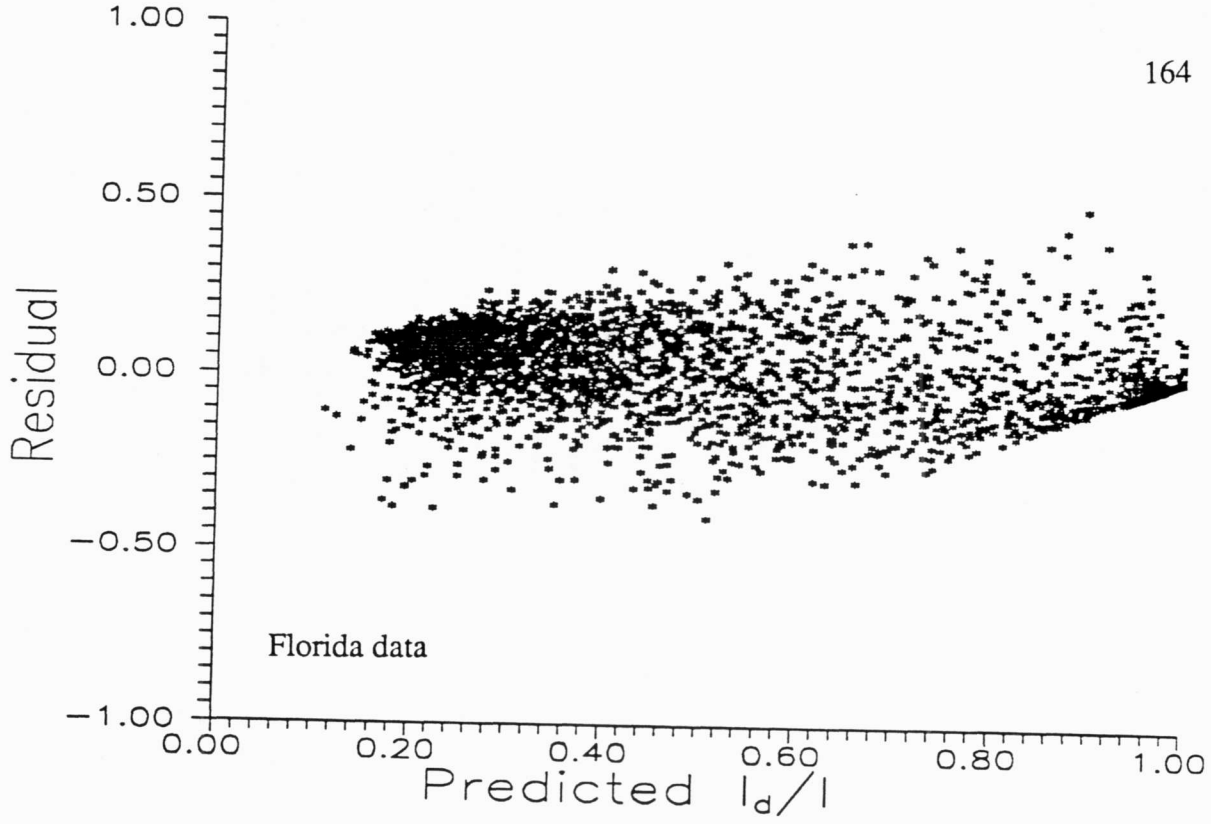

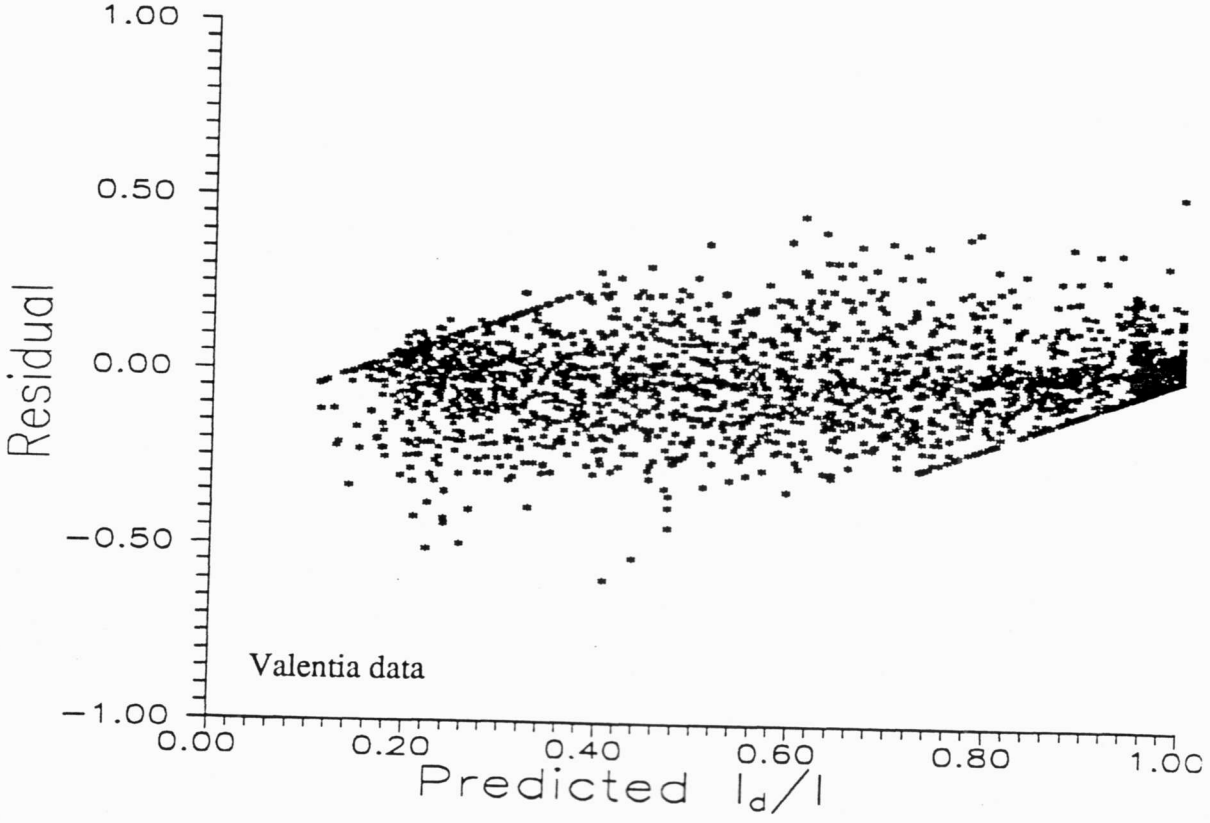

Residual vs. Predicted Diffuse Fraction

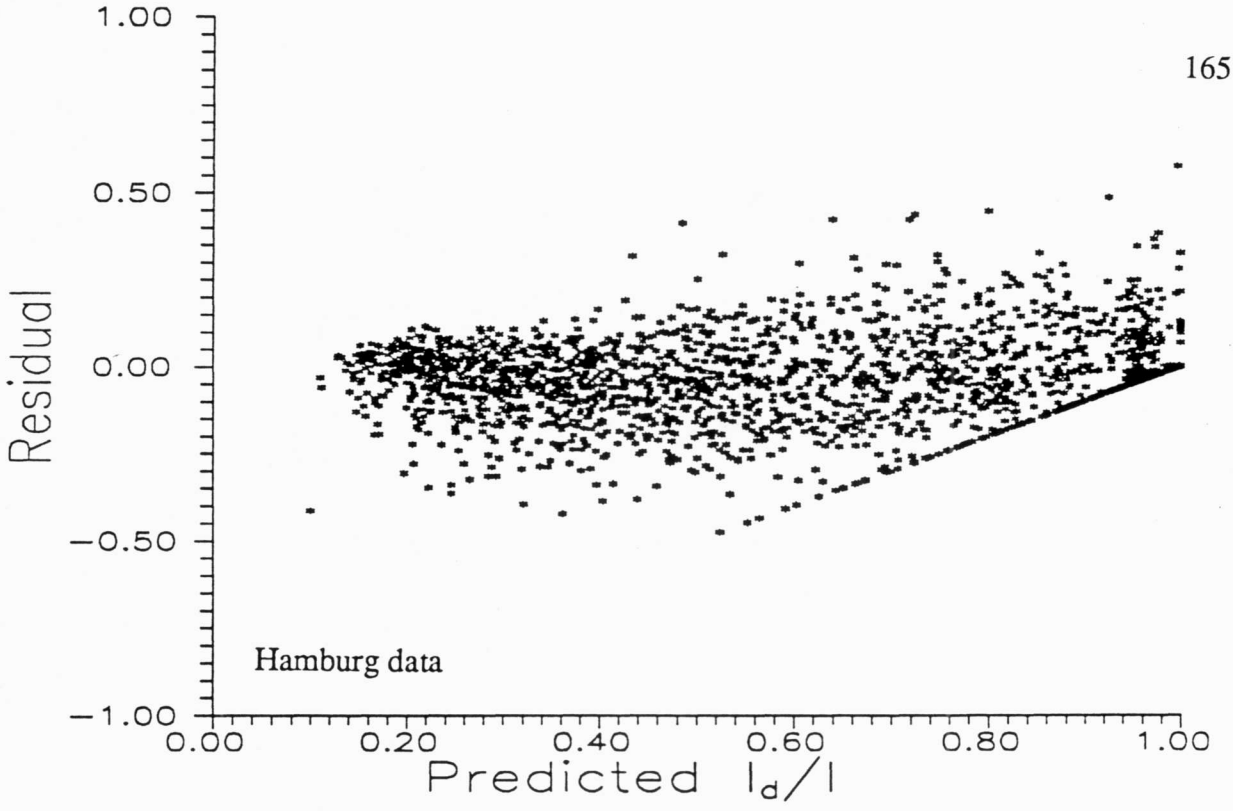

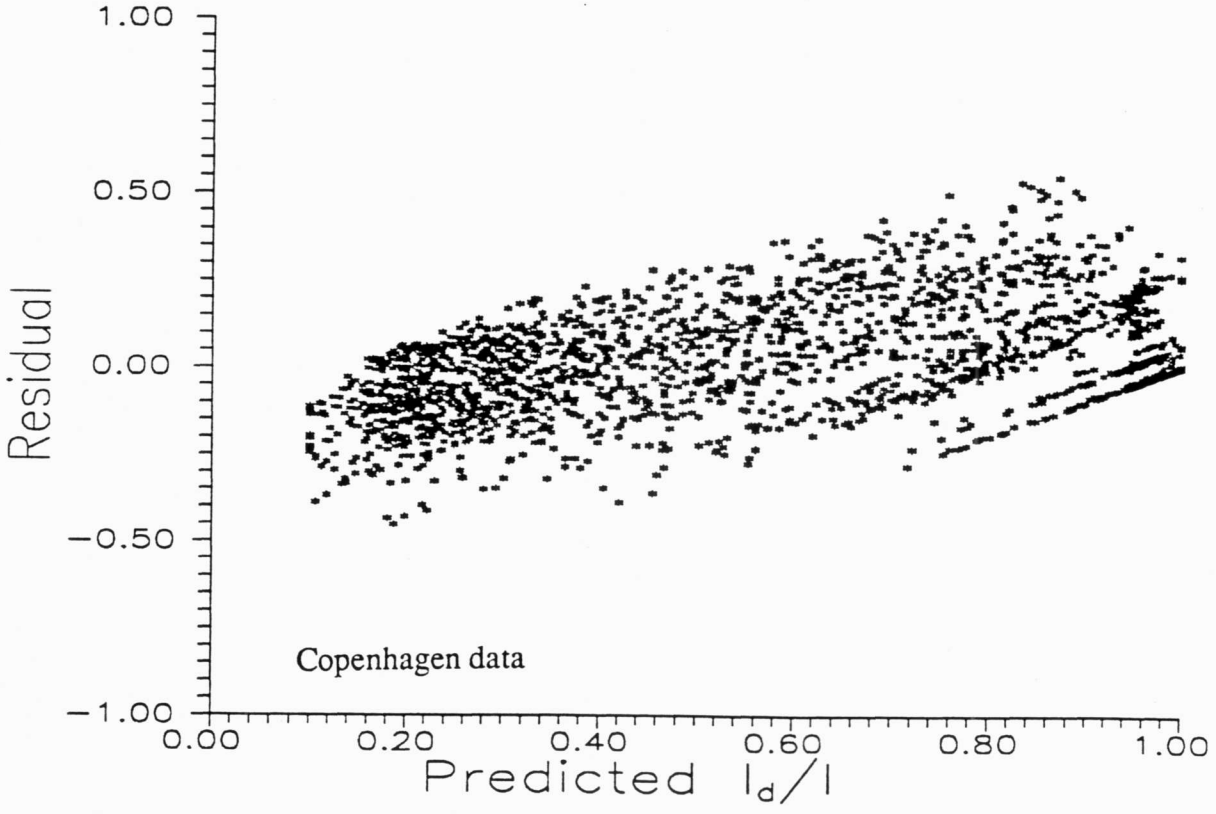

Predicted Diffuse Fraction vs. kt

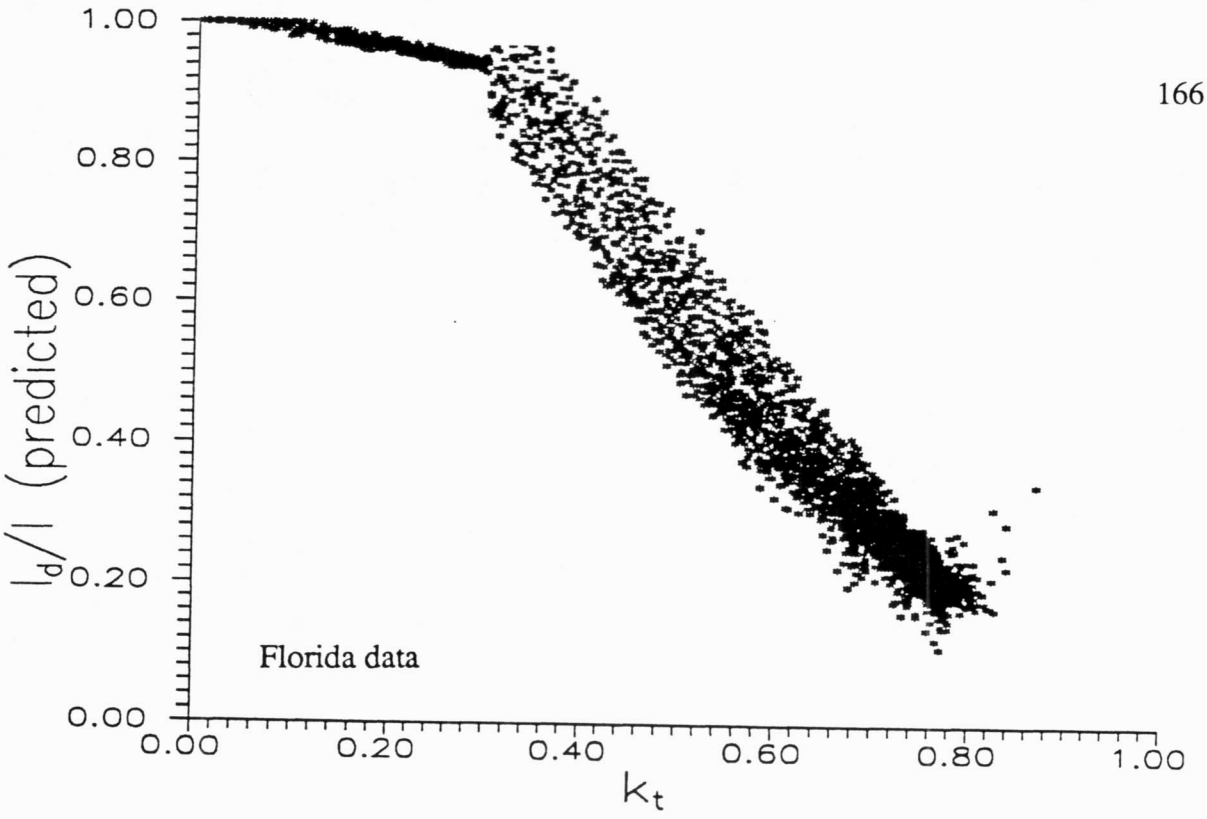

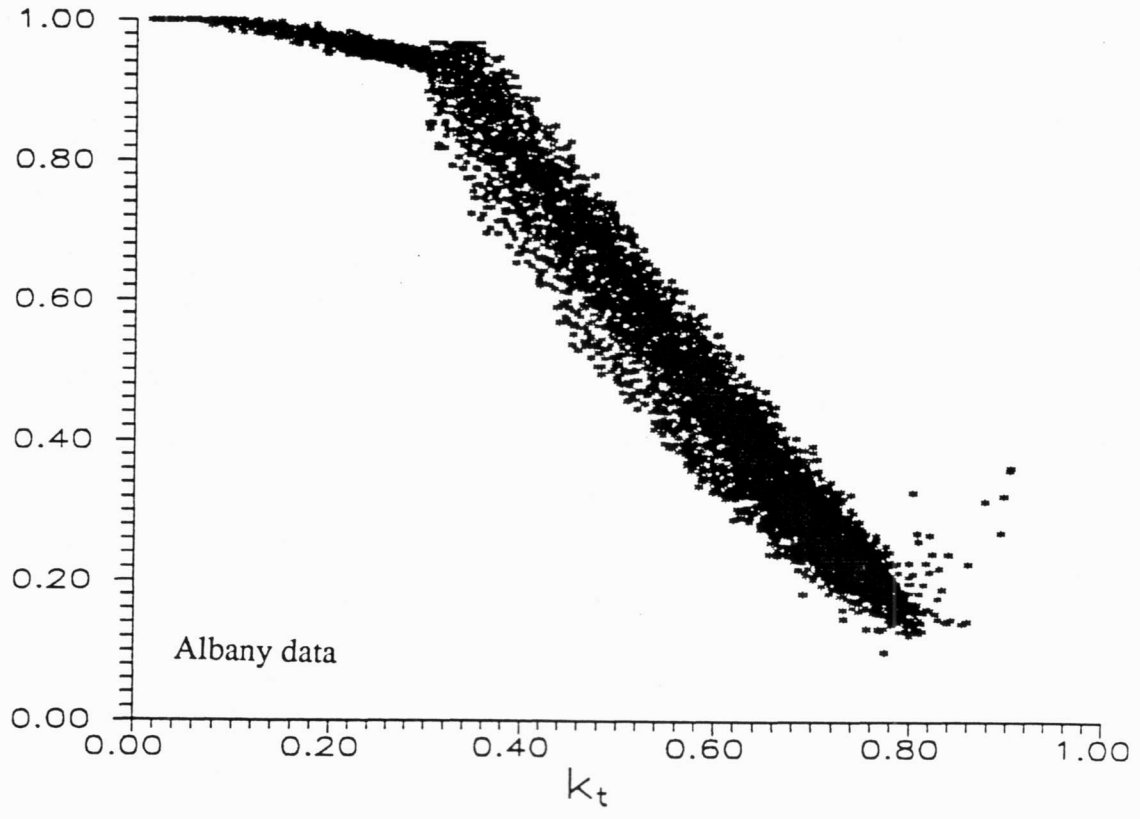

Predicted Diffuse Fraction vs. kt

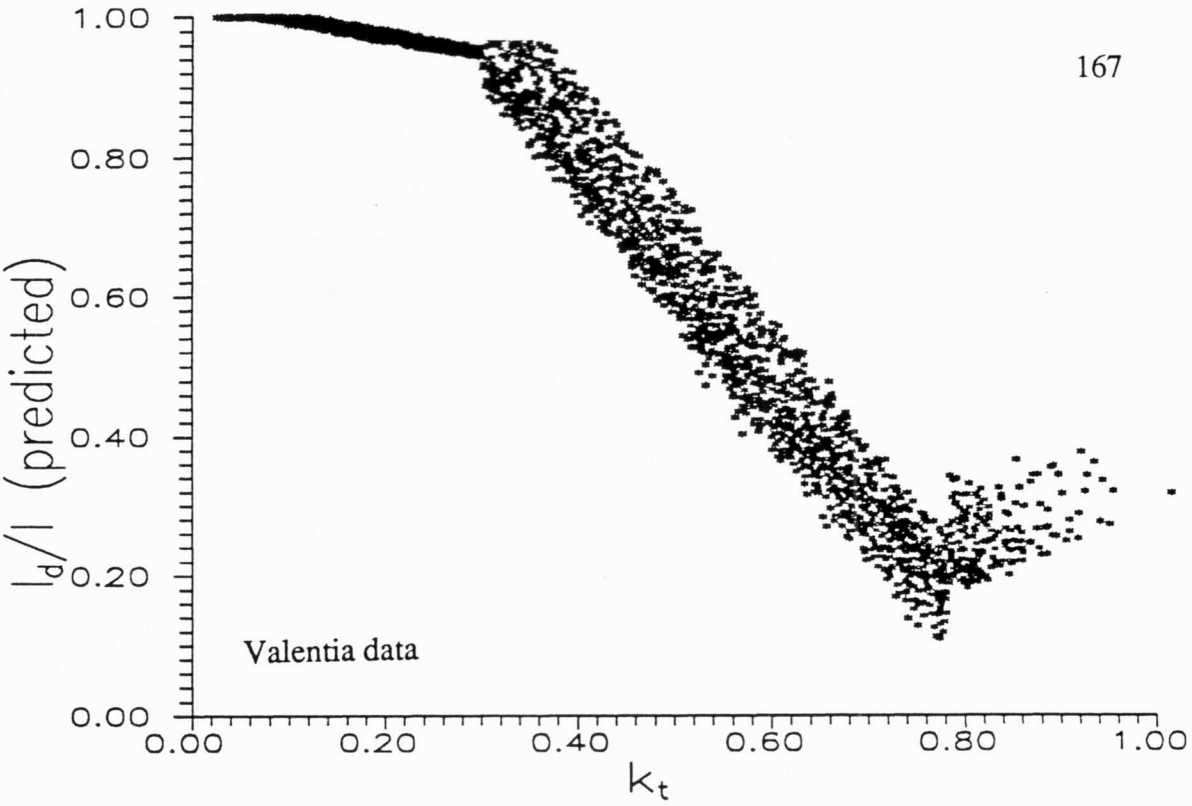

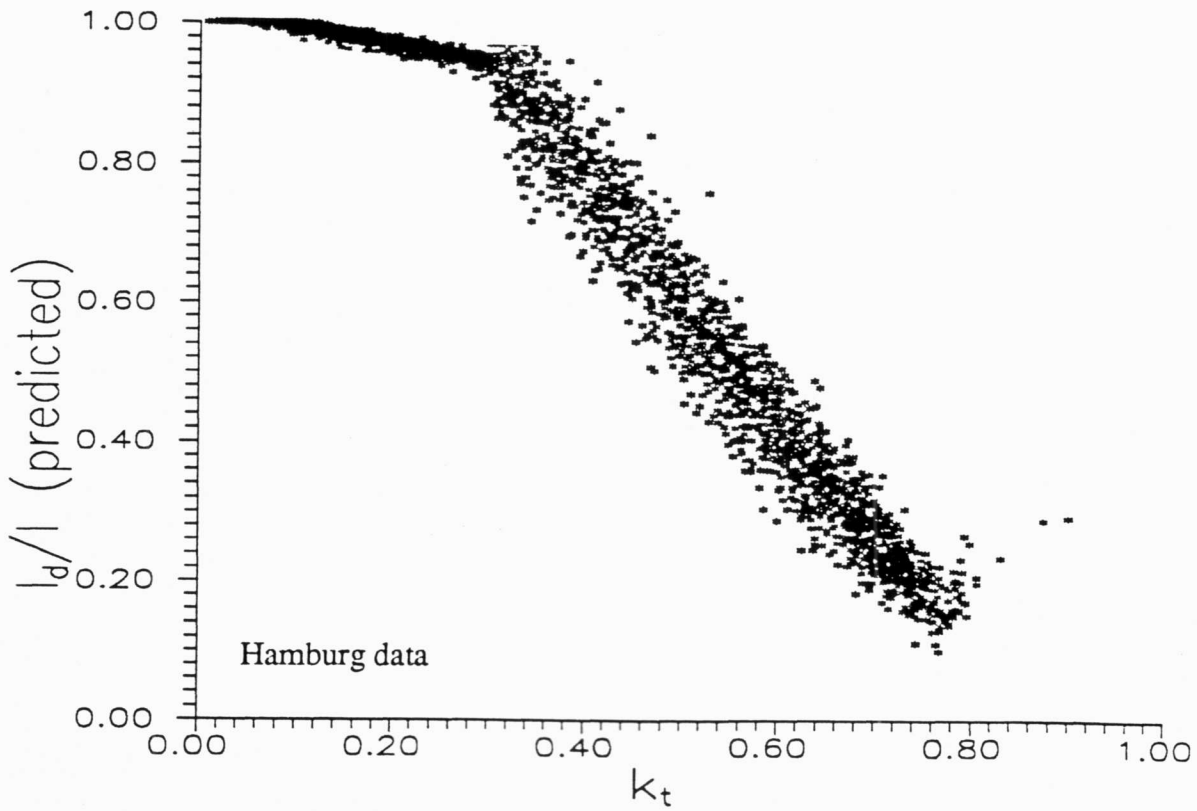

Predicted Diffuse Fraction vs. kt

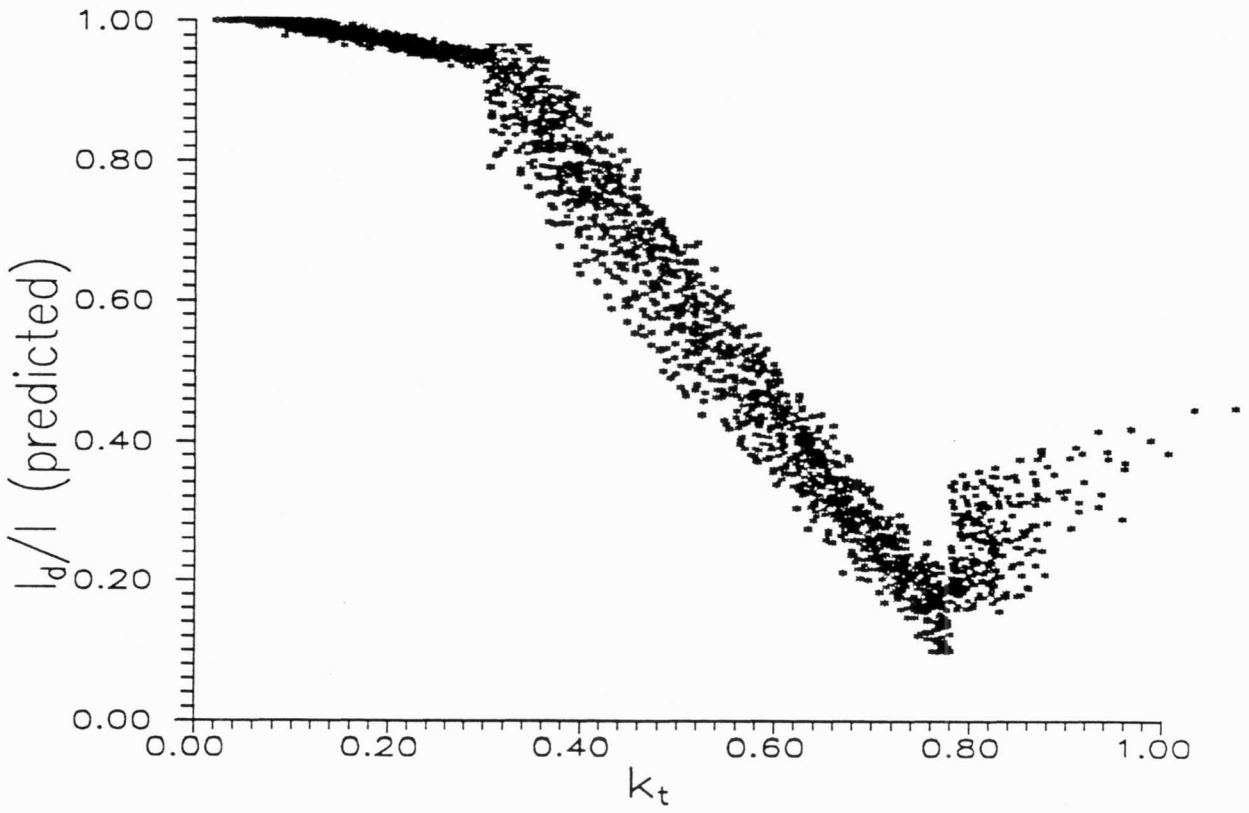

Copenhagen data

Appendix D. Ad Hoc Location Results

Four additional sites with less than one year of data from each location comprise the "ad hoc" dataset. Table C.1 indicates the locations and site information available and Table C.2 details the radiation and climatic information monitored at the ad hoc sites. All the data measurement information is common to the four sites.

Table C.1: Ad Hoc Site Information

Location: Osage City, Kansas	Latitude: 38.6° north
Data Period: 12/1/86 - 6/30/87	Longitude: 95.8° west
Interval: Integrated hourly	Standard Meridian: 90.0° west
Location: Albuquerque, New Mexico	Latitude: 35.05° north
Data Period: 11/1/86 - 6/30/87	Longitude: 106.5° west
Interval: Integrated hourly	Standard Meridian: 105.0° west
Location: El Monte, California	Latitude: 34.05° north
Data Period: 12/1/86 - 6/30/87	Longitude: 118.0° west
Interval: Integrated hourly	Standard Meridian: 120.0° west
Location: Phoenix, Arizona	Latitude: 33.43° north
Data Period: 12/1/86 - 6/30/87	Longitude: 112.0° west
Interval: Integrated hourly	Standard Meridian: 105.0° west

Table C.2: Ad Hoc Site Measurements

Instrument	Description	Inst. Type	Interval	Units
1	Ambient Temp.	unknown	hourly	°K
2	Wet bulb	unknown	"	"
3	Global, horizontal	"	"	W/m^2
4	Direct normal	"	"	"
5	45 south	"	"	"
6	90 north	"	"	"
7	90 south	"	"	"
8	90 east	"	"	"
9	90 west	"	"	"

The NRMSD and NMBD statistics were calculated for the above locations for each measured surface orientation and a range of critical levels. Table C.3 shows the surface slopes and range of critical levels used to generate the above statistics.

Table C.3: Tilted Surface Model Parameters (Ad Hoc locations)

Location/Year	Slope/Azimuth	I_{tc} (increment), kJ/m²
Osage, KS	43°s	0 - 2500 (500)
	90°s	0 - 1000 (500)
	90°w	0
	90°e	0 - 500 (500)
	90°n	0
Phoenix, AZ	43°s	0 - 2500 (500)
	90°s	0 - 1000 (500)
	90°w	0
	90°e	0
	90°n	0
Albuq., NM	43°s	0 - 2500 (500)
	90°s	0 - 1000 (500)
	90°w	0
	90°e	0
	90°n	0
El Monte, CA	43°s	0 - 2500 (500)
	90°s	0 - 1000 (500)
	90°w	0
	90°e	0
	90°n	0

Figure C.1 provides the NRMSD and NMBD results for each location, all surface orientations, and critical radiation levels. Figure C.2 provides the results for south facing surfaces. On an overall basis, the results from the ad hoc data set support the conclusions regarding tilted surface models.

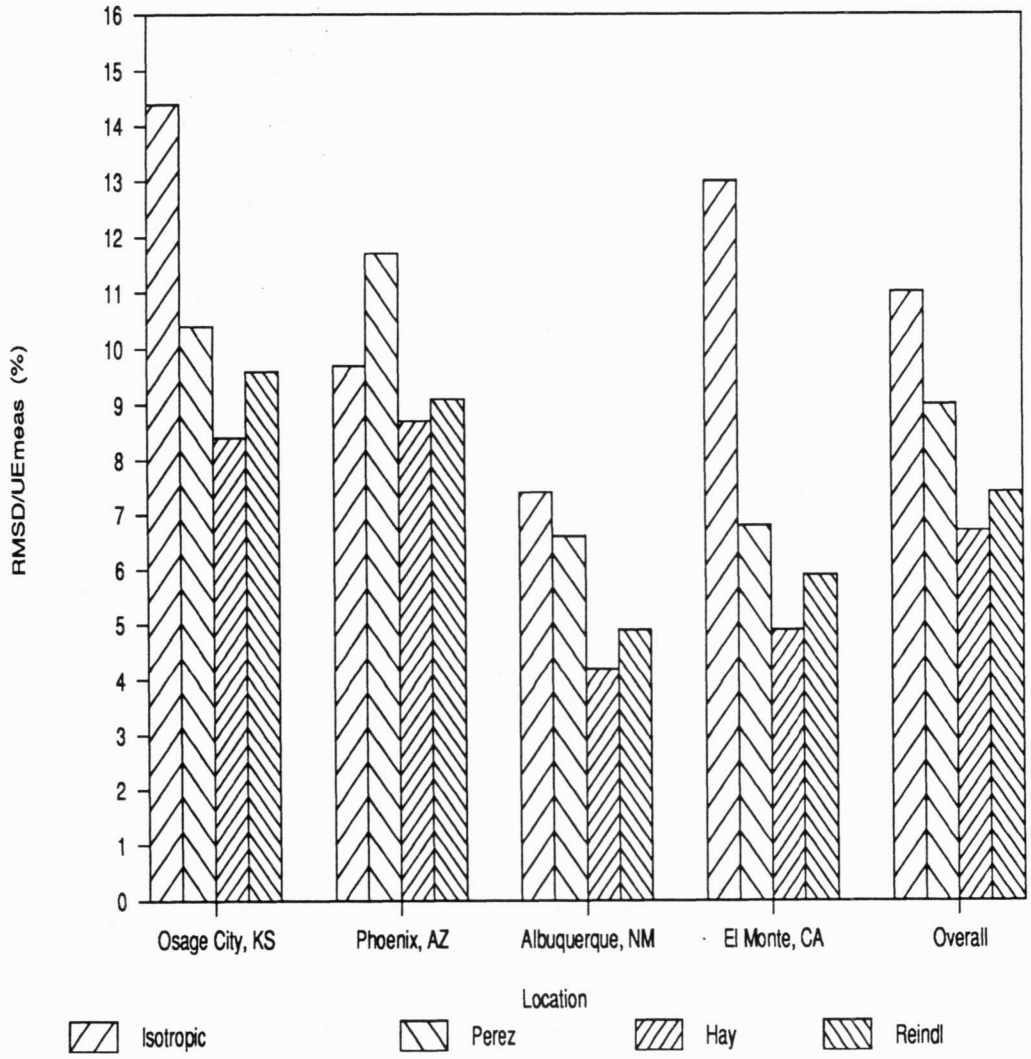

Figure D.1: NRMSD for all surface orientations, 10-11:00

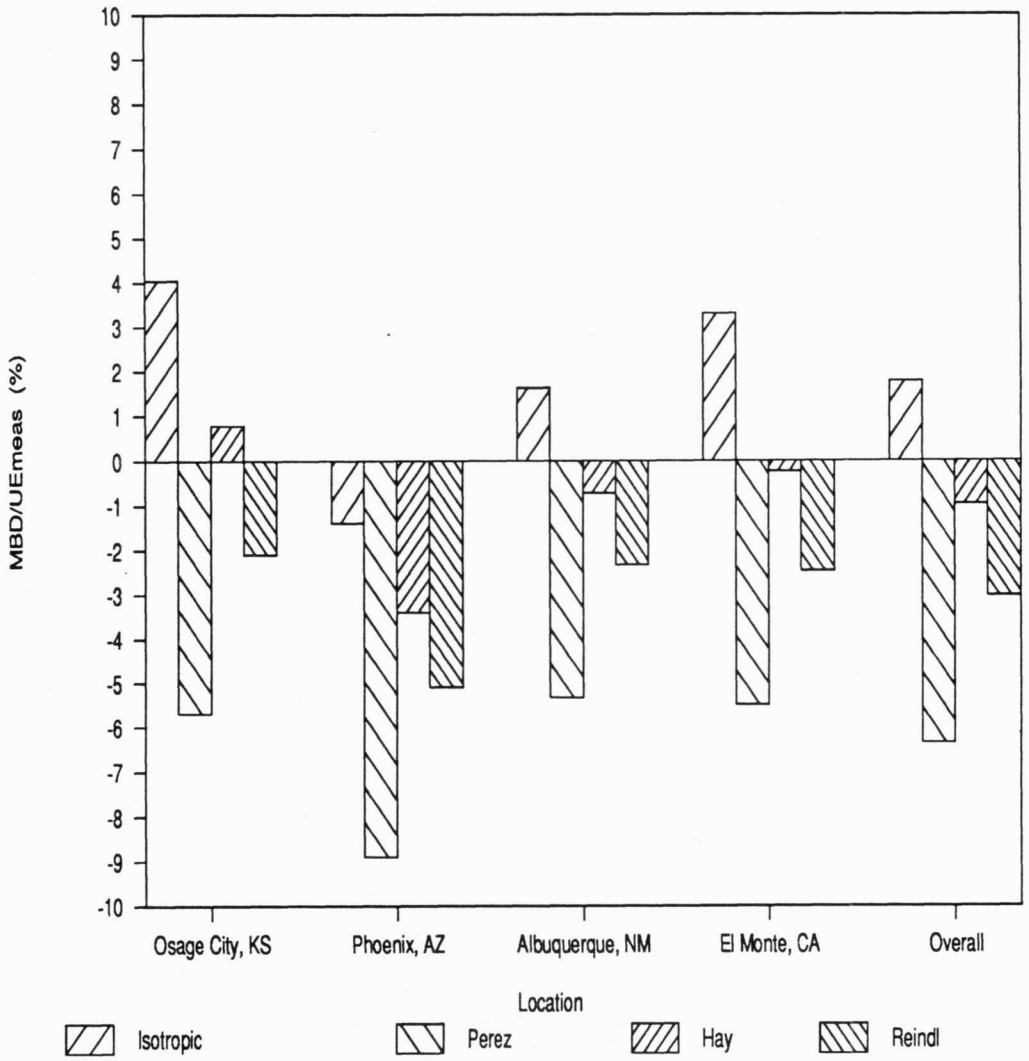

Figure D.1: NMBD for all surface orientations, 10-11:00

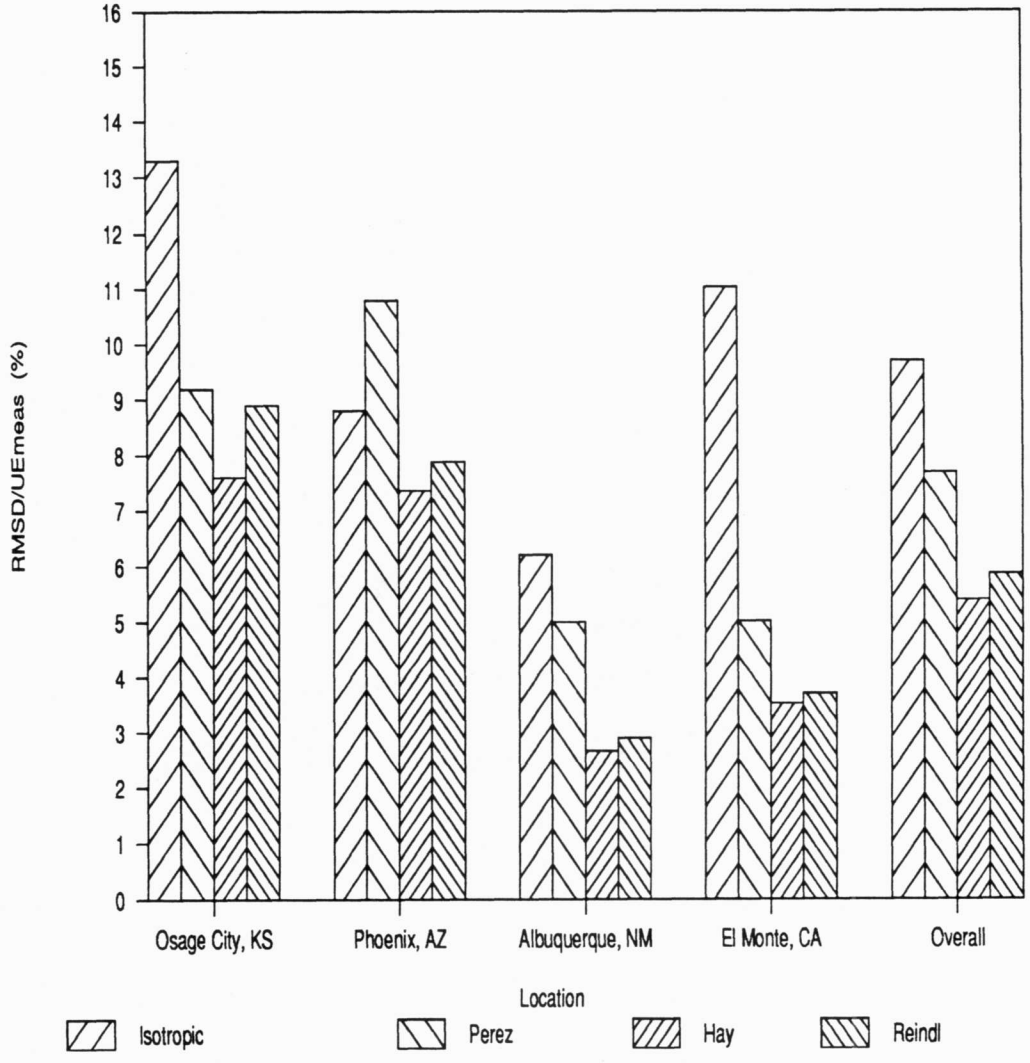

Figure D.2: NRMSD for south facing surfaces, 10-11:00

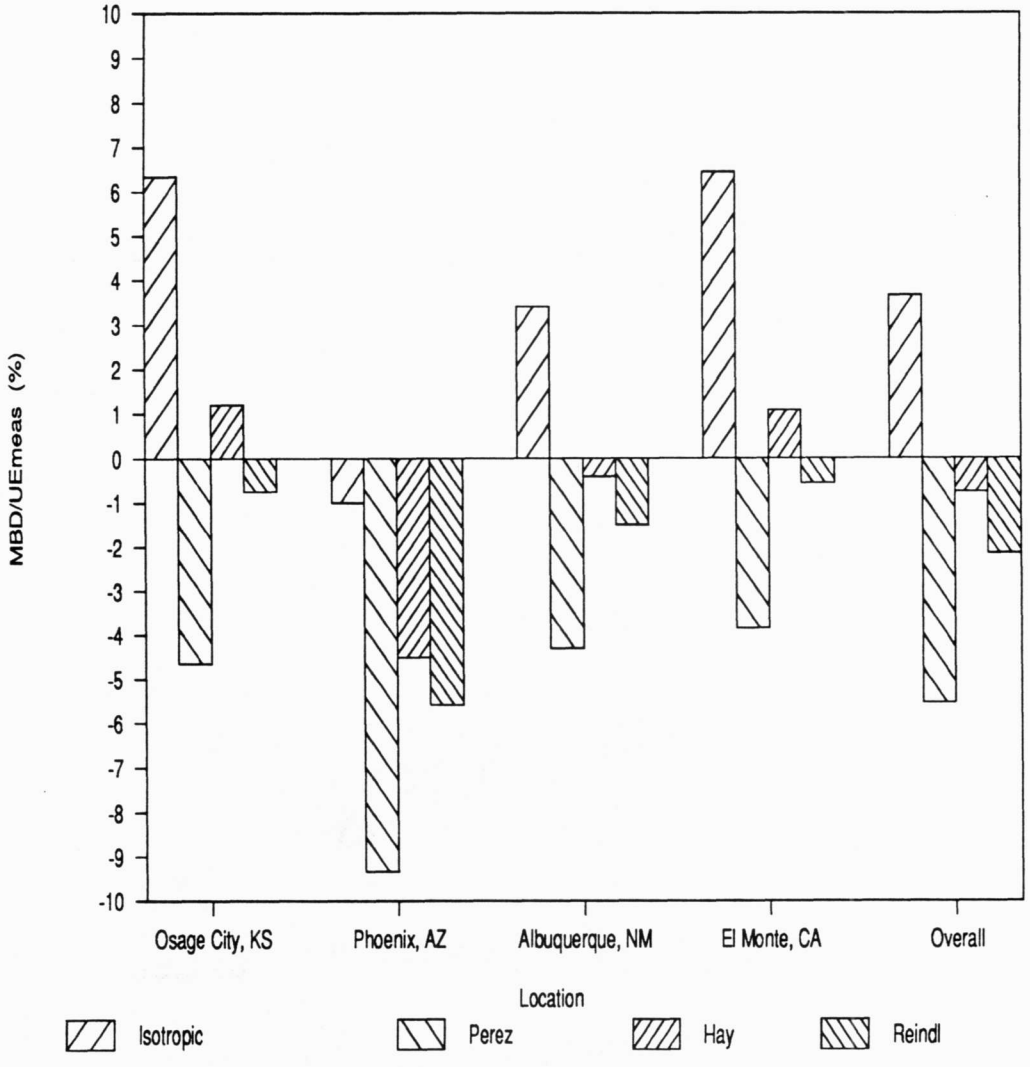

Figure D.2: NMBD for south facing surfaces, 10-11:00

Appendix E. Computer Programs

This subroutine will calculate the basic radiation components and angles associated with the sun's position.

```
      subroutine radiat (in, out, info, mode)
      implicit none
      integer j, n, dferr, IbgtIo, throw, ss
      integer highkt, kterr1, kterr2, kterr3,info(10)
      real dfract, in(10), out(11), beta, gamma, DTR, phi
      real I, Id, Idn, day, theta, thetaz, lat, kt, altit, erbs
      real  hr, hour, pi, G, w1, w2, ws, wm, declin, Ta, Tdp
      real Io, coef1, coef2, coef3, coef4, coef5, p1, p2
      real a1, a2, a3, a4, psydat(9)
      character*4 mode
      parameter (pi= 3.141529, G = 1353.)
c
c  this subroutine performs basic radiation and geometric calculations
c
c  ------------------------------------------------------------
c  radiation calculations                          -
c  ------------------------------------------------------------
c   day    = day of the year
c   hour = hour of the day
c
      lat   = in(1)
      day   = in(2)
      hour  = in(3)
      I     = in(4)
      Idn   = in(5)
      Id    = in(6)
      beta  = in(7)
      gamma = in(8)
      Ta    = in(9)
      Tdp   = in(10)
c  initialize error or info array
      do 90 j=1,10
        info(j) = 0
 90   continue
```

```
c  calculating declination  (all angles in degees)
     declin = 23.45 * sind( 360. * (284. + day) / 365.)
c  sunset hr angle
     ws = acosd(-tand(lat) * tand(declin))
c  find hour angles for start and end of timestep
c   if sunrise or sunset is inclusive, skip calcs
     if (hour - 12.) 94, 95, 96
 94   w2 = (hour - 12.) * 15.
 95   w2 = 0.0
 96   w2 = (hour - 12.) * 15.
     w1 = w2 - 15.
     if (w2.le.-ws.or.w1.ge.ws) then
      info(9) = 1
      go to 100   ! end if hr includes sr or ss
     else
      info(9) = 0
     endif
     wm = (w1 + w2) * 0.5
     p1 = cosd(declin) * cosd(lat) * cosd(wm)
     p2 = sind(declin) * sind(lat)
     thetaz = acosd(p1 + p2)
     altit = 90. - thetaz                ! solar altitude angle
     a1 = sind(declin) * sind(lat) * cosd(beta) - sind(declin) *
    &     cosd(lat) * sind(beta) * cosd(gamma)
     a2 = cosd(declin) * cosd(lat) * cosd(beta) * cosd(wm)
     a3 = cosd(declin)*sind(lat)*sind(beta)*cosd(gamma)*cosd(wm)
     a4 = cosd(declin) * sind(beta) * sind(gamma) * sind(wm)
     theta = acosd(a1 + a2 + a3 + a4)
c  calc extraterrestrial radiation.
c   finding largest hr angle
     if (w1.ge.w2) then
       coef3 = sind(w1)-sind(w2)
       coef4 = w1 - w2
     else
       coef3 = sind(w2)-sind(w1)
       coef4 = w2 - w1
     endif
```

```
      coef1 = 12.*3600./pi * 1353.*(1.+ 0.033 * cosd(360.*day/365.))
      coef2 = cosd(lat) * cosd(declin)
      coef5 = 2.* pi * coef4/360. * sind(lat) * sind(declin)
      Io = ( coef1 * (coef2 * coef3 + coef5) ) * 0.001   ! kJ/m^2
      if (Io.le.0.0) then
        info(9) = 1
        go to 100
      else
        info(9) = 0
      endif
c  computing kt
      kt = I / Io
c
c  checking what mode is for calculating diffuse fraction
      if (mode.eq.'meas') then    ! using measured data
         if (Id.le.0)  Id = I - Idn * cosd(thetaz)
         if (Idn.le.0) Idn = (I - Id) / cosd(thetaz)
         dfract = Id / I                ! measured diffuse fraction
      endif
c
c  if Orgill and Hollands is to be used to estimate Id
c
       if (mode.eq.'OH') then
          if(kt.ge.0.0.and.kt.le.0.35)
     &        dfract = 1.0 - 0.249 * kt
          if(kt.gt.0.35.and.kt.lt.0.75)
     &        dfract = 1.557 - 1.84 * kt
          if(kt.ge.0.75)
     &        dfract = 0.177
        Id = dfract * I
        Idn = (I - Id) / cosd(thetaz)
       endif
c
c  DTR reduced correlation
      if (mode.eq.'dtr1') then
       if(kt.le.0.3) then
         dfract = 1.02 - 0.254 * kt - 0.0123 * sind(altit)
```

```
          if (dfract.gt.1.0) dfract = 1.0
        endif
        if(kt.gt.0.3.and.kt.lt.0.78) then
          dfract = 1.3995 - 1.7489 * kt + 0.1772 * sind(altit)
          if (dfract.gt.0.97) dfract = 0.97
          if (dfract.lt.0.1) dfract = 0.1
        endif
        if(kt.ge.0.78) then
          dfract = 0.486 * kt - 0.182 * sind(altit)
          if (dfract.lt.0.1) dfract = 0.1
        endif
        Id = dfract * I
        Idn = (I - Id) / cosd(thetaz)
      endif
c  using full dtr correlation
c     if (mode.eq.'dtr') then
        if(Ta.ge.99990.and.Tdp.ge.99990) go to 100  ! if Temps bad
          psydat(1) = 1.0       ! ambient temp. (atm)   assume cons
          psydat(2) = Ta        ! dry bulb temp (deg C)
          psydat(5) = Tdp       ! dew point temp (deg C)
          call psych(1, 3, 1, psydat)
          phi = psydat(4)
          Ta = psydat(2)
          Tdp = psydat(5)
c compute dfract  by  DTR correlation
        if(kt.ge.0.0.and.kt.le.0.3) then
          dfract = 1.0 - 0.232 * kt + 0.0239 * sind(altit) - 0.000682
     &         * Ta + 0.0195 * phi
          if(dfract.gt.1.0) dfract = 1.0
        endif
        if(kt.gt.0.3.and.kt.lt.0.78) then
          dfract = 1.329 - 1.716 * kt + 0.267 * sind(altit) - 0.00357
     &           * Ta + 0.106 * phi
          if(dfract.gt.0.97) dfract = 0.97
          if(dfract.lt.0.1) dfract = 0.1
        endif
        if(kt.ge.0.78) then
```

```
        dfract = -0.0312 + 0.426 * kt - 0.256 * sind(altit) - 0.00349
     &          * Ta + 0.0734 * phi
        if(dfract.lt.0.1) dfract = 0.1
       endif
       Id = dfract * I
       Idn = (I - Id) / cosd(thetaz)
c
c  checking if beam is greater than extraterrestrial
c   if beam is greater, use extraterrestrial
      if (Idn*cosd(thetaz).gt.Io) then
        info(2) =  1
        Idn = Io
      else
        info(2) = 0
      endif
c  checking if kt > 1.1 if so reject data
      if (kt.gt.1.1) then
         info(3) = 1
         go to 100
      else
         info(3) = 0
      endif
c  checking for reasonable diffuse fraction for a given kt
      if (dfract.gt.0.80.and.kt.gt.0.60) then
         info(4) = 1
         go to 100
      else
         info(4) = 0
      endif
      if (dfract.lt.0.90.and.kt.lt.0.20) then
         info(5) = 1
         go to 100
      else
         info(5) = 0
      endif
      if (thetaz.gt.80.0) then
         info(6) = 1
```

```
        go to 100
      else
        info(6) = 0
      endif
c
c ============================
c output data          =
c ============================
      out(1)  = hour
      out(2)  = I
      out(3)  = Idn
      out(4)  = Id
      out(5)  = altit
      out(6)  = kt
      out(7)  = dfract
      out(8)  = DTR
      out(9)  = theta
      out(10) = thetaz
      out(11) = Io
c
      info(1) = dferr
      info(2) = IbgtIo
      info(3) = highkt
      info(4) = kterr1
      info(5) = kterr2
      info(6) = kterr3
      info(7) = throw
      info(9) = ss
c  return if all values are ok
      return
 100  continue
c  report back all 0's if value(s) are bad
      do 110 j=1, 10
        out(j) = 0.0
 110  continue
      return
      end
```

This subroutine calculates the tilted surface radiation by isotropic, Hay, Perez, and new model methods. The only difference in the tilted surface radiation calculated is the diffuse radiation on a tilted surface.

```
      Subroutine TYPE16(TIME,XIN,OUT,T,DTDT,PAR,INFO)
c
c  This subroutine will calculate the radiation on a tilted surface
c  using the isotropic, Hay, Perez, and new models.
      integer bin, j, n, s
      real I, Ib, Id, Idn, Io, Ion, IdtH, ItH, IdtP, ItP
      real Ibt, Igt, Inmax, It1,It3, IdtH1, IdtH3, ItH3
      real theta, thetaz, alpha, beta, AI, cir, iso
      real delta, epsilon, m, pi, rho, Idtiso, Itiso
      real alfl, alfh, psi, psiz, b, cf, Rb, hori, hori2, f
      real F11(8), F12(8), F13(8), F21(8), F22(8), F23(8), F1, F2
      real TIME, XIN(11), OUT(33), T, DTDT, PAR, INFO(20)
      parameter (pi=3.141529)
c
      data F11 /-0.011, -0.038,0.166,0.419,0.71,0.857,0.734,0.421/
      data F12 /0.748,1.115,0.909,0.646,0.025,-0.37,-0.073,-0.661/
      data F13 /-0.08,-0.109,-0.179,-0.262,-0.29,-0.279,-0.228,0.097/
      data F21 /-0.048,-0.023,0.062,0.14,0.243,0.267,0.231,0.119/
      data F22 /0.073,0.106,-0.021,-0.167,-0.511,-0.792,-1.18,-2.125/
      data F23 /-0.024,-0.037,-0.05,-0.042,-0.004,0.076,0.199,0.446 /
c
c  ***************************************************************
c  Nomenclature:                                                 *
c  -------------                                                 *
c  AI    = Anisotropy index for Hay model                        *
c  alpha = circumsolar solid half angle (degrees)                *
c  b     = a/c ratio coefficient in Perez correlation            *
c  beta  = surface slope angle (degrees)                         *
c  bin   = epsilon bin # for determining F1, F2 coefficients     *
c  delta = sky brightness parameter                              *
c  epsilon = sky clearness parameter                             *
```

```
c  F##  = corr. coeff's for calculating tilted surface diffuse          *
c  I    = global radiation on a horizontal surface                     *
c  Ib   = beam radiation on a horizontal surface                       *
c  Id   = diffuse radiation on a horizontal surface                    *
c  In   = direct normal radiation                                      *
c  Ibt  = beam radiation on a tilted surface                           *
c  IdtH = diffuse radiation on a tilted surface by Hay corr.           *
c  Idtp = diffuse radiation on a tilted surface by PEREZ               *
c  Igt  = ground reflected radiation on a tilted surface               *
c  ItH  = total radiation on a tilted surface by Hay correlation       *
c  Itp  = total radiation on a tilted surface by PEREZ                 *
c  Io   = extraterresterial radiation on a horizontal surface          *
c  Ion  = direct component of extra-terr. radiation                    *
c  m    = air mass                                                     *
c  n    = case number used to calculate "b"                            *
c  Rb   = ratio of beam rad on tilt to that on horizontal              *
c  Rd   = ratio of diffuse radiation on a tilt to that on hor.         *
c  theta = radiation angle of incidence (degrees)                      *
c  thetaz= solar zenith angle (degrees)                                *
c  rho  = ground reflectance                                           *
c  ********************************************************************
c -------- identifying the appropriate inputs and outputs ----------
c
      Id = XIN(1)              ! diffuse on a horizontal
      I  = XIN(2)              ! global on a horizontal
      Io = XIN(3)              ! extraterrestrial radiation
      thetaz = XIN(4)          ! zenith angle  (degrees)
      theta  = XIN(5)          ! radiation angle of incidence
      beta   = XIN(6)          ! surface slope (degrees)
      alpha = XIN(7)           ! circumsolar half angle (Perez)
      rho   = XIN(8)           ! surface ground reflectance
      Idn   = XIN(9)           ! measured direct normal radiation
c     checking if radiation exists and if it is valid.
c     if not skip all calculations and set the
c     outputs = 0.0 and end subroutine
      if (Io.le.0.or.I.le.0.or.thetaz.gt.80)
     &     go to 1000
```

```
      Ion = Io / cosd(thetaz)     ! direct component of extraterr.
c  Horizontal surface component relationships
c   (do not calculate if In is given as an input)
c   use the direct normal to calculate the diffuse
c   radiation on a horizontal surface
      if (Idn.eq.0.0) then
        Ib = I - Id
        Idn = (I - Id) / cosd(thetaz)
      else
        Ib = Idn * cosd(thetaz)
        Id = I - Ib
      endif
      if (Ib.le.0) go to 1000
c  calculating air mass
      if (thetaz.gt.10.and.thetaz.le.70.) m = 1. / cosd(thetaz)
      if (thetaz.lt.10.or.thetaz.gt.70.) m = 1./(cosd(thetaz)+0.15*
     1   (thetaz + 3.885)** -1.253)
c ***************************************************************
c   Tilted Surface Calculations                                  *
c ***************************************************************
c ---------------------------
c -        PEREZ MODEL.        -
c ---------------------------
c  Let the coefficient ratio a/c = b.  alfl and alfh represent the
c  limits (in degrees) for determining the ratio a/c.
c
      alfl = 90. - alpha                ! degrees
      alfh = 90. + alpha                 ! degrees
      psi = 90. - theta + alpha
      psiz = 90. - thetaz + alpha
c
c  5 cases for calculating a/c = b
c  case i
      if (theta.lt.alfl.and.thetaz.lt.alfl) then
      b = cosd(theta) / cosd(thetaz)
      n = 1
      endif
```

```
c  case ii
      if (theta.gt.alfl.and.theta.lt.alfh.and.thetaz.lt.alfl)
     -  then
      b = (psi * sind(psi/2.) / (2.* alpha * cosd(thetaz)) )
      n = 2
      endif
c case iii
      if (theta.gt.alfh) then
        b = 0.0
        n = 3
      endif
c  case vi
      if (theta.lt.alfl.and.thetaz.gt.alfl) then
         b = cosd(theta) / sind(psiz/2.)
         n = 4
      endif
c  case v
      if (theta.gt.alfl.and.theta.lt.alfh.and.thetaz.gt.alfl) then
         b = ( psi * sind(psi/2.) ) / (2.* alpha * sind(psiz/2.) )
         n = 5
      endif
c  calculating epsilon and delta parameters
      if (Id.lt.00001) then
        epsilon = 99999.
      else
        epsilon = (Id + Idn) / Id
      endif
      delta = Id / Io
c  finding the appropriate bin number to determine the brightness
c  coefficients, F1 and F2.
      if (epsilon.gt.0.0.and.epsilon.le.1.056) bin = 1
      if (epsilon.gt.1.056.and.epsilon.le.1.253) bin = 2
      if (epsilon.gt.1.253.and.epsilon.le.1.586) bin = 3
      if (epsilon.gt.1.586.and.epsilon.le.2.134) bin = 4
      if (epsilon.gt.2.134.and.epsilon.le.3.230) bin = 5
      if (epsilon.gt.3.230.and.epsilon.le.5.980) bin = 6
      if (epsilon.gt.5.980.and.epsilon.le.10.08) bin = 7
```

```
      if (epsilon.gt.10.08) bin = 8
c  Calculating the brightness coefficients
      F1 = F11(bin) + F12(bin)*delta + F13(bin)*thetaz *pi/180.
      F2 = F21(bin) + F22(bin)*delta + F23(bin)*thetaz *pi/180.
c  Calculating the components on the tilted surface
      Ibt = Idn * cosd(theta)
      if (Ibt.lt.0.0)  Ibt = 0.0
c  Diffuse component
      IdtP = Id * ( 0.5 * (1. + cosd(beta)) * (1. - F1) + F1 * b
     &      + F2 * sind(beta) )
      if (IdtP.lt.0.0)   IdtP = 0.0
c  Ground reflected component
      Igt = I * rho * 0.5 * ( 1. - cosd(beta) )
c  Total on a tilted surface
      ItP = Ibt + IdtP + Igt
c
c ---------------------------
c -         Hay Model              -
c ---------------------------
      AI = Ib / Io
c  to avoid numerical problems with rb at sunrise and sunset hours
c  the zenith angle is limited to 80 degrees
      if(theta.lt.80.0) then
         cir = (AI * cosd(theta)) / cosd(thetaz)
      else
         cir = 0.0
      endif
      iso   = (1. - AI) * 0.5 * (1. + cosd(beta))
      hori  = 1. + f * (sind(beta/2.)**3)
      IdtH  = Id * ( cir + iso )
c
c addition of horizon term to hay model representing new model
c
      hori2 = 1. + sqrt(Ib/I) * sind(beta/2.)**3   !horizon term
      IdtH3 = Id * ( cir + hori2 * iso )          !new model
c
c  total on a tilted surface due to Hay and new models
```

```
c
      ItH  = Ibt + IdtH  + Igt   ! hay
      ItH3 = Ibt + IdtH3 + Igt   ! new model
c
c ------------------------
c  Isotropic Model      -
c ------------------------
      Idtiso = Id * 0.5 * (1. + cosd(beta))
      Itiso = Ibt + Idtiso + Igt
c  --------------------------
c  -    OUTPUT OF DATA      -
c  --------------------------
      OUT(1) = Io
      OUT(2) = I
      OUT(3) = Id
      OUT(4) = Idn
      OUT(5) = Ibt
      OUT(6) = Igt
      OUT(7) = Idtiso
      OUT(8) = IdtP              ! diffuse on tilt surface by Perez
      OUT(9) = IdtH              ! diffuse on tilt surface by Hay
      OUT(10) = Itiso            ! total rad on a tilt by isotropic
      OUT(11) = ItP              ! total rad on a tilt by Perez
      OUT(12) = ItH              ! total rad on a tilt by Hay
      OUT(19) = ItH3             ! total rad on tilt by new model
      return
 1000 continue
c  if calcs are in error or no radiation exists set outputs
c  equal to 0
        do 20 j=1, 33
          out(j) = 0.0
 20     continue
      Return
      End
```

This TRNSYS subroutine was used to calculate the pschrometric properties for input to the diffuse fraction correlation.

```
      SUBROUTINE PSYCH(IUNITS,MODE,WBMD,PSYDAT)
      INTEGER WBMD,WBMODE
      DIMENSION PSYDAT(9)
      DATA RA/287.055/, LIMIT/100/, IWARNS/0/,PATMOLD/0./
C
C MODES 1-5:
C THESE MODES TAKE AS INPUT PATM (IN ATMOSPHERES), A DRY BULB
C TEMP., AND ONE OTHER PROPERTY: WET BULB TEMP., REL.HUMIDI-
TY(FRACTION),
C DEW PT.TEMP.,HUMIDITY RATIO, OR ENTHALPY, DEPENDING ON
MODE.
C OUTPUTS ARE HUMIDITY RATIO (OR REL.HUMIDITY IN MODE 4), WET
BULB TEMP.,
C ENTHALPY (OR REL.HUMIDITY IN MODE 5), MIXTURE DENSITY, AND
DRY
C AIR DENSITY.
C
C MODE 6:
C MODE 6 TAKES AS AN INPUT PATM, HUMIDITY RATIO AND EN-
THALPY, AND
C RETURNS ALL OF THE OTHER PROPERTIES.
C
C THE WET BULB TEMPERATURE IS ONLY CALCULATED IF WBMODE
EQUALS ONE.
C
C TEMPERATURES ARE IN CELSIUS (IUNITS=1) OR FAHRENHEIT (IU-
NITS=2).
C ENTHALPY IS IN KJ/KG (IUNITS=1) OR BTU/LBM (IUNITS=2), AND
C DENSITY IS IN KG/M**3 (IUNITS=1) OR LBM/FT**3 (IUNITS=2).
C THE REFERENCE STATES FOR ENTHALPIES ARE:
C       HAIR=0.0 AT 0. DEG C AND 0. DEG F
C       HW(LIQUID)=0.0 AT 0. DEG C AND 32. DEG F
C THE PSYDAT ARRAY CONTAINS THE MOIST AIR PROPERTIES.
C ASSIGN LOCAL VARIABLES:
```

```
      WBMODE = WBMD
      PATM = PSYDAT(1)
      TDB =  PSYDAT(2)
      TWB =  PSYDAT(3)
      TWBOLD=-9.999E20
      RH =   PSYDAT(4)
      TDP =  PSYDAT(5)
      W =    PSYDAT(6)
      H =    PSYDAT(7)
C  UNIT CONVERSIONS
      IF(IUNITS .EQ. 2) THEN
       TDB = (TDB - 32.)/1.8
       TWB = (TWB - 32.)/1.8
       TDP = (TDP - 32.)/1.8
       H   = (H - 7.687)/0.43002
      ENDIF
C-- CHECK THAT THE TOTAL PRESSURE IS WITHIN THE IDEAL GAS
RANGE.
      IF (PATM .GT. 5.0) THEN
        WRITE(*,500)
        IWARNS = IWARNS + 1
      END IF
      IF (PATM .LE. 0.0) THEN
        WRITE(*,250)
        STOP
      END IF
C  FOR MODE 6, CHECK THAT THE ENTHALPY IS GREATER THAN THE
C  SATURATION ENTHALPY (MINIMUM) FOR THE GIVEN HUMIDITY
RATIO
C  AND THAT THE HUMIDITY RATIO IS GREATER THAN 0.
      IF (MODE .EQ. 6) THEN
          IF (W .LT. 0.) THEN
            WRITE(*,1500)
            IWARNS = IWARNS + 1
            W = 0.
            GO TO 99
          ELSE IF (W .EQ. 0.) THEN
```

```
          GO TO 99
         END IF
        CALL DEWPT(PATM,W,TDP,IWARNS)
        HDP = TDP + W*(2501. + 1.805*TDP)
        HMIN = HDP
         IF (H .LT. HMIN) THEN
           WRITE(*,1000)
           IWARNS = IWARNS + 1
           H = HMIN
         END IF
99       TDB = (H - 2501.*W)/(1. + 1.805*W)
      END IF
C
C FIND SATURATION PRESSURE OF WATER AT WET BULB, DRY BULB,
OR
C  DEW POINT TEMPERATURE.
C
      CALL SAT(TDB,PSATDB,IWARNS)
      GOTO (1,2,3,2,2,2) ,MODE
C-- CHECK FOR IMPOSSIBLE WET BULB TEMPERATURES AND CORRECT
THEM
C   IF POSSIBLE.
1     IF (TWB .GT. TDB .AND. PSATDB .GE. PATM) THEN
        WRITE(*,1750)
        STOP
      ELSE IF (TWB .GT. TDB) THEN
        WRITE(*,2000)
        IWARNS = IWARNS + 1
        TWB = TDB
        PSAT = PSATDB
        GOTO 5
      END IF
      CALL SAT (TWB,PSAT,IWARNS)
C-- ERROR: IF PSATWB IS GREATER THAN PATM.
       IF (PSAT .GE. PATM) THEN
         WRITE(*,1750)
         STOP
```

```
      END IF
     GOTO 5
2    PSAT = PSATDB
     GOTO 5
C-- CHECK FOR IMPOSSIBLE DEW POINT TEMPERATURES AND
C   CORRECT THEM IF POSSIBLE.
3    IF (TDP .GT. TDB .AND. PSATDB .GE. PATM) THEN
       WRITE(*,2250)
       STOP
     ELSE IF (TDP .GT. TDB) THEN
       WRITE(*,2500)
       IWARNS = IWARNS + 1
       TDP=TDB
     END IF
     CALL SAT(TDP,PSAT,IWARNS)
C-- ERROR: IF PSATDP IS GREATER THAN PATM.
     IF (PSAT .GE. PATM) THEN
       WRITE(*,2250)
       STOP
     END IF
5    CONTINUE
C   CALCULATE HUMIDITY RATIO AND WET BULB TEMPERATURE
     GO TO (10,20,30,40,50,60), MODE
C   MODE 1 -- DRY BULB AND WET BULB SUPPLIED
10   IF (TWB .LE. 0.) THEN
       P = PSAT - 5.704E-4*(TDB-TWB)*PATM
       W = .62198 * P/(PATM-P)
     ELSE
       WSAT = .62198 * PSAT/(PATM-PSAT)
       W = WSAT - (TDB-TWB)*(0.24 + .441*WSAT)/(597.31
    .     + 0.441*TDB - TWB)
     ENDIF
     IF (W .LT. 0.0) THEN
       WRITE(*,3000)
       IWARNS = IWARNS + 1
       W = 0.0
       H = TDB
```

```
      TWBOLD = TWB
      WBMODE = 1
      PSAT = PSATDB
      GO TO 60
    END IF
    H = TDB + W*(2501. + 1.805*TDB)
    GO TO 100
C  MODE 2 -- DRY BULB AND RELATIVE HUMIDITY SUPPLIED
20   IF (RH .LT. 0.) THEN
       WRITE(*,3500)
       IWARNS = IWARNS + 1
       RH=0.0
    ELSE IF (PSAT .GE. PATM) THEN
       RHMAX = PATM/PSAT
       IF (RH .GE. (.99*RHMAX)) THEN
         WRITE(*,3750)
         STOP
       END IF
    ELSE IF (RH .GT. 1.) THEN
       WRITE(*,4000)
       IWARNS = IWARNS + 1
       RH=1.0
    END IF
    W = .62198 * PSAT*RH/(PATM-PSAT*RH)
    GO TO 40
C  MODE 3 -- DRY BULB AND DEW POINT SUPPLIED
30   W = .62198 * PSAT/(PATM-PSAT)
C  FIND ENTHALPY FOR MODES 2 - 4
40   IF (PSATDB .LT. PATM) THEN
       WMAX = .62198 * PSATDB/(PATM-PSATDB)
       IF (W .GT. WMAX) THEN
         WRITE(*,4500)
         IWARNS = IWARNS + 1
         W = WMAX
       END IF
    END IF
    IF (W .LT. 0.0) THEN
```

```
        WRITE(*,1500)
        IWARNS = IWARNS + 1
        W = 0.
      END IF
      H = TDB + W*(2501. + 1.805*TDB)
      GO TO 60
C  MODE 5 -- DRY BULB AND ENTHALPY SUPPLIED
50    IF (PSATDB .LT. PATM) THEN
        WMAX = .62198 * PSAT/(PATM-PSAT)
        HMAX = TDB + WMAX*(2501. + 1.805*TDB)
        IF (H .GT. HMAX) THEN
          WRITE(*,5000)
          IWARNS = IWARNS + 1
          H = HMAX
        END IF
      END IF
      HMIN = TDB
      IF (H .LT. HMIN) THEN
        WRITE(*,5500)
        IWARNS = IWARNS + 1
        H = HMIN
      END IF
       W = (H-TDB)/(2501.+1.805*TDB)
C  FIND WET BULB TEMPERATURE FOR MODES 2 - 6 IF WBMODE EQUALS
1.
60    IF (WBMODE .NE. 1) THEN
        TWB=TDB
        GO TO 100
      END IF
      DPRESS = ABS(1.-PATM)
C  THE FOLLOWING CORRELATION IS FOR 1 ATMOSPHERES TOTAL
PRESSURE.
C  IF OUTSIDE THE CORRELATION RANGE, THE CORRELATION IS USED
FOR
C  THE INITIAL GUESS IN THE ITERATIVE METHOD.
      IF (H .GT. 0. .AND. H .LT. 2000.) THEN
        Y = ALOG(H*.43002+7.687)
```

```
      IF (H .LE. 9.473) THEN
        TWB=-17.4422+1.9356*Y+.7556*Y**2+.5406*Y**3
      ELSE IF (H .GT. 9.473) THEN
        TWB=-.6008-22.04556*Y+11.4356*Y**2-.97667*Y**3
      END IF
    ELSE
      TWB = 9.99999E25
    END IF
C  USE A NEWTON'S ITERATIVE METHOD TO FIND THE WET BULB
C  TEMPERATURE.
    IF (DPRESS.GT..001 .OR. H.LE.0. .OR. H.GT.275.) THEN
      ITEST=0
      IF (ABS(PATM-PATMOLD) .GT. 1.0E-10) THEN
      CALL BOIL(PATM,TBOIL)
      PATMOLD = PATM
      END IF
C-- INITIAL GUESS
      TWBNEW=AMIN1(TWB,(TBOIL-0.1),TDB)
70     IF (TWBNEW .GE. (TBOIL-0.09)) TWBNEW=TBOIL-0.1
      CALL SAT(TWBNEW,PSAT,IWARNS)
      WSSTAR=.62198*PSAT/(PATM-PSAT)
      IF(MODE .EQ. 5) THEN
       W = (H-TDB)/(2501.+1.805*TDB)
      END IF
      WNEW=((2501.-2.381*TWBNEW)*WSSTAR-(TDB-TWBNEW))/
     .      (2501.+1.805*TDB-4.186*TWBNEW)
      ERR = W - WNEW
      IF (ABS(ERR) .LE. (.01*W)) GO TO 75
      IF (W .EQ. 0.) THEN
        IF (ABS(ERR) .LE. .0001) GO TO 75
      END IF
      ITEST = ITEST + 1
      IF (ITEST .GE. 25) GO TO 75
C--FIND THE SLOPE OF THE ERROR FUNCTION
      TSLOPE = 0.999*TWBNEW
      IF (TWBNEW .EQ. 0.) TSLOPE = -.005
      CALL SAT(TSLOPE,PSLOPE,IWARNS)
```

```
      WSSLP=.62198*PSLOPE/(PATM-PSLOPE)
      WSLOPE=((2501.-2.381*TSLOPE)*WSSLP-(TDB-TSLOPE))/
     .    (2501.+1.805*TDB-4.186*TSLOPE)
      ERRSLP = W - WSLOPE
      DERRDT = (ERRSLP - ERR)/(TSLOPE - TWBNEW)
      TWBNEW = TWBNEW - ERR/DERRDT
      GO TO 70
75     TWB = TWBNEW
    END IF
    IF (TWB .LT. TWBOLD) TWB = TWBOLD
100  CONTINUE
C  FIND RELATIVE HUMIDITY, DEW POINT, MIXTURE DENSITY,
C  AND DRY AIR DENSITY
    PV  = PATM*W/(.62198+W)
    IF(MODE .NE. 2) RH = PV/PSATDB
    IF(MODE .NE. 3 .AND. PV .GT. 0.) THEN
     CALL DEWPT(PATM,W,TDP,IWARNS)
    ELSE IF (MODE .NE. 3 .AND. PV .LE. 0) THEN
C  FOR DRY AIR, THERE IS NO DEW POINT TEMPERATURE
     TDP=-9.99999E25
    ENDIF
    SPCVOL = RA*(TDB+273.15)/(PATM*101325)*(1+1.6078*W)
    RHOWA = 1/SPCVOL
    RHOWM = RHOWA*(1+W)
C  CONVERT OUTPUTS TO APPROPRIATE UNITS
    IF(IUNITS .EQ. 2) THEN
     H   = H*0.43002+7.68
     TDB = 1.8*TDB + 32.
     TWB = 1.8*TWB + 32.
     IF (TDP .GT. -9.99999E24) THEN
      TDP = 1.8*TDP + 32.
     END IF
     RHOWM = RHOWM/16.02
     RHOWA = RHOWA/16.02
    ENDIF
C SET OUTPUTS
    IF(MODE .EQ. 6) PSYDAT(2) = TDB
```

```
      PSYDAT(3) = TWB
      PSYDAT(4) = RH
      PSYDAT(5) = TDP
      PSYDAT(6) = W
      PSYDAT(7) = H
      PSYDAT(8) = RHOWM
      PSYDAT(9) = RHOWA
      IF (IWARNS .GE. LIMIT) THEN
        WRITE(*,6000) IWARNS
        STOP
      END IF
      RETURN
  250 FORMAT(/20X,'*** ERROR ***',/6X,'THE PSYCHROMETRICS
     . SUBROUTINE WAS CALLED WITH AN ATMOSPHERIC PRESSURE',/6X,
     .'LESS THAN OR EQUAL TO 0.')
  500 FORMAT(/20X,'*** WARNING ***',/6X,'THE PSYCHROMETRICS
     . SUBROUTINE WAS CALLED
     . WITH A TOTAL PRESSURE',/6X,'GREATER THAN 5 ATMOSPHERES.
     . BEWARE THAT THE IDEAL GAS RELATIONS USED',/6X,'IN THE
     . PSYCHROMETRICS ARE NOT ACCURATE AT HIGHER PRESSURES.')
 1000 FORMAT(/20X,'*** WARNING ***',/6X,'THE PSYCHROMETRICS
     . SUBROUTINE WAS CALLED
     . WITH AN ENTHALPY LESS',/6X,'THAN POSSIBLE FOR THE GIVEN
     . HUMIDITY RATIO.  THE AIR WAS ASSUMED TO',/6X,'BE
     . SATURATED AT THE GIVEN HUMIDITY RATIO AND THE ENTHALPY
     . SET FOR',/6X,'THIS CONDITION.')
 1500 FORMAT(/20X,'*** WARNING ***',/6X,'THE PSYCHROMETRICS
     . SUBROUTINE WAS CALLED
     . WITH A HUMIDITY RATIO LESS',/6X,'THAN 0.0.  DRY AIR WAS
     . ASSUMED AND THE HUMIDITY RATIO SET TO 0.0.')
 1750 FORMAT(/20X,'*** ERROR ***',/6X,'THE PSYCHROMETRICS
     . SUBROUTINE WAS CALLED WITH A WET BULB TEMPERATURE',/6X,
     .'ABOVE THE MAXIMUM FOR THE GIVEN ATMOSPHERIC PRESSURE.')
 2000 FORMAT(/20X,'*** WARNING ***',/6X,'THE PSYCHROMETRICS
     . SUBROUTINE WAS CALLED WITH A WET BULB TEMPERATURE',/6X,
     .'GREATER THAN THE DRY BULB TEMPERATURE.  SATURATED AIR
     . WAS ASSUMED',/6X,'AND THE WET BULB TEMPERATURE SET TO THE
```

```
   . DRY BULB TEMPERATURE.')
2250  FORMAT(/20X,'*** ERROR ***',/6X,'THE PSYCHROMETRICS
   . SUBROUTINE WAS CALLED WITH A DEW POINT TEMPERATURE',/6X,
   .'ABOVE THE MAXIMUM FOR THE GIVEN ATMOSPHERIC PRESSURE.')
2500  FORMAT(/20X,'*** WARNING ***',/6X,'THE PSYCHROMETRICS
   . SUBROUTINE WAS CALLED
   . WITH A DEW POINT TEMPERATURE',/6X,
   .'GREATER THEN THE DRY BULB TEMPERATURE. THE DEW
   . POINT WAS SET EQUAL',/6X,'TO THE DRY BULB TEMPERATURE.')
3000  FORMAT(/20X,'*** WARNING ***',/6X,'THE PSYCHROMETRICS
   . SUBROUTINE WAS CALLED WITH A WET BULB TEMPERATURE',/6X,
   .'BELOW THAT FOR DRY AIR AT THE GIVEN DRY BULB TEMPERA-
TURE.
   . DRY AIR',/6X,'WAS ASSUMED AND A NEW WET BULB TEMPERATURE
   . FOUND.')
3500  FORMAT(/20X,'*** WARNING ***',/6X,'THE PSYCHROMETRICS
   . SUBROUTINE WAS CALLED WITH A RELATIVE HUMIDITY',/6X,
   .'LESS THAN 0. THE RELATIVE HUMIDITY WAS SET TO 0.0.')
3750  FORMAT(/20X,'*** ERROR ***',/6X,'THE PSYCHROMETRICS
   . SUBROUTINE WAS CALLED WITH A RELATIVE HUMIDITY',/6X,
   .'GREATER THAN POSSIBLE AT THE GIVEN DRY BULB TEMPERA-
TURE.')
4000  FORMAT(/20X,'*** WARNING ***',/6X,'THE PSYCHROMETRICS
   . SUBROUTINE WAS CALLED WITH A RELATIVE HUMIDITY',/6X,
   .'GREATER THEN 1.0. THE RELATIVE HUMIDITY WAS SET TO 1.0.')
4500  FORMAT(/20X,'*** WARNING ***',/6X,'THE PSYCHROMETRICS
   . SUBROUTINE WAS CALLED WITH A HUMIDITY RATIO ABOVE',/6X,
   .'THE SATURATION HUMIDITY RATIO FOR THE GIVEN DRY BULB
   . TEMPERATURE.',/6X,'THE AIR WAS ASSUMED SATURATED AT THE
   . GIVEN DRY BULB TEMPERATURE',/6X,' AND THE HUMIDITY RATIO
   . SET FOR THIS CONDITION.')
5000  FORMAT(/20X,'*** WARNING ***',/6X,'THE PSYCHROMETERICS
   . SUBROUTINE WAS CALLED
   . WITH AN ENTHALPY GREATER',/6X,'THEN THAT FOR SATURATED
   . AIR AT THE GIVEN DRY BULB TEMPERATURE. THE',/6X,'AIR
   . WAS ASSUMED SATURATED AND THE ENTHALPY SET FOR THIS
   . CONDITION.')
```

```
5500  FORMAT(/20X,'*** WARNING ***',/6X,'THE PSYCHROMETERICS
     . SUBROUTINE WAS CALLED
     . WITH AN ENTHALPY LESS',/6X,'THEN THAT FOR DRY
     . AIR AT THE GIVEN DRY BULB TEMPERATURE.  DRY',/6X,'AIR
     . WAS ASSUMED AND THE ENTHALPY SET FOR THIS CONDITION.')
6000  FORMAT(/30X,'*** ERROR ***',/6X,'THE SIMULATION WAS HALTED
     . BECAUSE THERE WERE',1X,I3,1X,'WARNINGS FROM THE',/6X,
     .'PSYCHROMETRICS SUBROUTINE.  CHECK FOR PROPER USE OF
     . THIS SUBROUTINE.')
      END
C*********************************************************************
C  SUBROUTINE FOR FINDING SATURATION PRESSURE OF WATER AT A
GIVEN
C  TEMPERATURE
      SUBROUTINE SAT(TIN,PSAT,IWARNS)
C  THE FOLLOWING CORRELATION FOR THE SATURATION PRESSURE OF
C  WATER VAPOR (IN PASCALS) AS A FUNCTION OF TEMPERATURE IS
C  TAKEN FROM THE 1985 ASHRAE FUNDAMENTALS HANDBOOK (SI).
      DATA C1/-5674.5359/,C2/6.3925247/,C3/-0.9677843E-2/
      DATA C4/0.62215701E-6/,C5/0.20747825E-8/,C6/-0.9484024E-12/
      DATA C7/4.1635019/,C8/-5800.2206/,C9/1.3914993/
      DATA C10/-0.048640239/,C11/0.41764768E-4/,C12/-0.14452093E-7/
      DATA C13/6.5459673/
      T = TIN + 273.15
      IF (T .LE. 0.) THEN
        WRITE(*,200)
        STOP
      END IF
C  SATURATION PRESSURE OVER ICE (-100 C TO 0 C)
      IF (T .LT. 273.15) THEN
        PSAT=EXP(C1/T+C2+C3*T+C4*T**2+C5*T**3+C6*T**4+C7*ALOG(T))
C  SATURATION PRESSURE OVER LIQUID WATER (0 C TO 200 C)
      ELSE IF (T .GE. 273.15) THEN
        PSAT=EXP(C8/T+C9+C10*T+C11*T**2+C12*T**3+C13*ALOG(T))
      END IF
C  TEMPERATURE OUT OF THE RANGE USED FOR THE CORRELATION
      IF (T .LT. 173.15 .OR. T .GT. 473.15) THEN
```

```
      WRITE(*,100)
      IWARNS = IWARNS + 1
    END IF
C  CONVERT PRESSURE FROM PASCALS TO ATMOSPHERES
    PSAT = PSAT/101325
    RETURN
100  FORMAT(/20X,'*** WARNING ***',/6X,'THE CORRELATION, FROM
THE
   . 1985 ASHRAE FUNDAMENTALS HANDBOOK, USED',/6X,'TO CALCU-
LATE
   . THE WATER VAPOR SATURATION PRESSURE WAS INTENDED FOR',
   ./6X,'THE TEMPERATURE RANGE OF -100 C TO 200 C.  THE
   . PSYCHROMETRICS',/6X,'SUBROUTINE WAS CALLED WITH CONDI-
TIONS
   . OUTSIDE THIS RANGE.')
200  FORMAT(/20X,'*** ERROR ***',/6X,'THE "SAT" SUBROUTINE OF THE
   . PSYCHROMETRICS
   . SUBROUTINE WAS CALLED',/6X,'WITH A TEMPERATURE BELOW -273
C.')
    END
C*****************************************************************
C  SUBROUTINE FOR FINDING THE DEW POINT TEMPERATURE GIVEN
C  THE HUMIDITY RATIO.  THE CORRELATION IS FROM THE 1981
C  ASHRAE FUNDAMETALS HANDBOOK.  THE DEW POINT TEMPERATURE
C  IS IN DEGREES C AND ATMOSPHERIC PRESSURE IN PASCALS.
C
    SUBROUTINE DEWPT(PATM,W,TDP,IWARNS)
    PV  = PATM*W/(.62198+W)
    Y = ALOG(1.013E05*PV)
    TDP = -35.957 - 1.8726*Y + 1.1689*Y*Y
    IF(TDP .LT. 0.) TDP = -60.45 + 7.0322*Y + 0.3700*Y*Y
    IF (TDP.GT.70. .OR. TDP.LT.-60.) THEN
      WRITE(*,100)
      IWARNS = IWARNS + 1
    END IF
    RETURN
100  FORMAT(/20X,'*** WARNING ***',/6X,'THE CORRELATION, FROM
```

```
THE
   . 1981 ASHRAE FUNDAMENTALS HANDBOOK, USED',/6X,'TO CALCU-
LATE
   . THE DEW POINT TEMPERATURE, IS INTENDED FOR THE',
   ./6X,'TEMPERATURE RANGE OF -60 C TO 70 C.  THE PSYCHROMETRICS
   . SUBROUTINE',/6X,'WAS CALLED WITH CONDITIONS OUTSIDE THIS
   . RANGE.')
    END
C**************************************************************
C SUBROUTINE FOR FINDING THE BOILING TEMPERATURE OF WATER
GIVEN
C THE TOTAL PRESSURE.  A NEWTON'S METHOD IS USED WITH THE
C SATURATED WATER VAPOR PRESSURE CORRELATION FROM THE 1985
ASHRAE
C FUNDAMENTALS HANDBOOK.
C
    SUBROUTINE BOIL(PATM,TBOIL)
    DATA C1/-5674.5359/,C2/6.3925247/,C3/-0.9677843E-2/
    DATA C4/0.62215701E-6/,C5/0.20747825E-8/,C6/-0.9484024E-12/
    DATA C7/4.1635019/,C8/-5800.2206/,C9/1.3914993/
    DATA C10/-0.048640239/,C11/0.41764768E-4/,C12/-0.14452093E-7/
    DATA C13/6.5459673/
C
    PBOIL = PATM*101325
    ITEST = 0
    IF (PBOIL .LT. 611.21) GO TO 100
C--USING AHRAE CORRELATION FOR 0 C TO 200 C.
C  FIRST GUESS TBOIL EQUALS 100 C.
    T1 = 100 + 273.15
10   ZZ=C8/T1+C9+C10*T1+C11*T1**2+C12*T1**3+C13*ALOG(T1)
    P1=EXP(ZZ)
    ERR = PBOIL - P1
    IF (ABS(ERR) .LE. (.01*PBOIL)) THEN
      TBOIL = T1 - 273.15
      RETURN
    END IF
    ITEST = ITEST +1
```

```
      IF (ITEST .GT. 100) STOP
      DERRDT=-(P1)*(-C8/T1**2+C10+2*C11*T1+3*C12*T1**2+C13/T1)
      TOLD = T1
      T1 = T1 - ERR/DERRDT
      GO TO 10
100   CONTINUE
C--USING AHRAE CORRELATION FOR -100 C TO 0 C.
C  FIRST GUESS TBOIL EQUALS 0 C.
      T1 = 273.15
110   ZZ=C1/T1+C2+C3*T1+C4*T1**2+C5*T1**3+C6*T1**4+C7*ALOG(T1)
      P1=EXP(ZZ)
      ERR = PBOIL - P1
      IF (ABS(ERR) .LE. (.01*PBOIL)) THEN
        TBOIL = T1 - 273.15
        RETURN
      END IF
      ITEST = ITEST +1
      DERRDT=-P1*(-C1/T1**2+C3+2*C4*T1+3*C5*T1**2+4*C6*T1**3+C7/T1)
      TOLD = T1
      T1 = T1 - ERR/DERRDT
      GO TO 110
      END
```

REFERENCES

[1] Klein, S. A., et al., "TRNSYS - A Transient Simulation Program", University of Wisconsin - Madison, Engineering Experiment Station Report 38-12, Version 12.2, (1988).

[2] SOLMET, Volume I - User's Manual, "Hourly Solar Radiation Surface Meteorological Observations", #TD-9724 (1978).

[3] Watt, A. D., "Circumsolar Radiation", Sandia National Laboratories, Report # SAND 80-7009, pp. 9, (1980).

[4] Temps, R. C., Coulson, K. L., "Solar Radiation Incident Upon Slopes of Different Orientations", *Solar Energy*, **19** pp. 179-184, (1977).

[5] Duffie, J. A., Beckman, W. A., Solar Engineering of Thermal Processes, New York, Wiley-Interscience Publication, pp.1, 72 (1980).

[6] Fritz, S., "Transmission of Solar Energy Through The Earth's Clear and Cloudy Atmosphere", Transactions of the 1955 *International Conference on the Use of Solar Energy-The Scientific Basis*, Volume I, pp. 18, (1958).

[7] McKay, D. C., et al., As Noted in Final Report IEA Task IX "Validations of Models For Estimating Solar Radiation On Horizontal Surfaces", Data requests referred to Dr. D. C. McKay, Canada Climate Centre, The Atmospheric Environment Service, 4905 Dufferin Street, Downsview, Ontario, M3H5T4, Canada.

[8] Hay, J. E., McKay, D. C., "Estimating Solar Irradiance on Inclined Surfaces: A Review and Assessment of Methodologies", *International Journal of Solar Energy*, Volume 3, pp. 204, (1985).

[9] Orgill, J. F., Hollands, K. G. T., "Correlation Equation for Hourly Diffuse Radiation on a Horizontal Surface", *Solar Energy*, **19**, pp. 357, (1977).

[10] Erbs, D. G., "Methods for Estimating The Diffuse Fraction of Hourly, Daily, and Monthly-Average Global Solar Radiation", Masters Thesis in Mechanical Engineering, University of Wisconsin-Madison, (1980).

[11] Iqbal, M., "Prediction of Hourly Diffuse Solar Radiation From Measured Hourly Global Radiation on a Horizontal Surface", *Solar Energy*, **24**, pp. 491-503, (1980).

[12] Bugler, J. M., "The Determination of Hourly Insolation on an Inclined Plane Using a Diffuse Irradiance Model Based on Hourly Measured Global Horizontal Insolation", *Solar Energy*, **19**, pp. 477-491, (1977).

[13] Davies, J. A., McKay, D. C., Luciani, G., Abdel-Wahab, M., **DRAFT** Final Report IEA Task IX, "Validation of Models For Estimating Solar Radiation on Horizontal Surfaces", pp.3, 26, (1987).

[14] Hottel, H. C., Woertz, B. B., "Performance of Flat-Plate Solar-Heat Collectors", *Transactions of American Society of Mechanical Engineers*, **64**, pp. 91, (1942).

[15] Dave, J. V., "Validity of The Isotropic-Distribution Approximation In Solar Energy Estimations", *Solar Energy*, **19**, pp.331-333, (1977).

[16] Klucher, T. M., "Evaluation of Models To Predict Insolation on Tilted Surfaces", *Solar Energy*, **23**, pp. 111-114, (1979).

[17] Ma, C. C. Y., Iqbal, M., "Statistical Comparison of Models For Estimating Solar Radiation On Inclined Surfaces", *Solar Energy*, 31, pp.313-317, (1983).

[18] van den Brink, G. J., "Validation of Solar Radiation Models and Recommendation of The Model For Dutch Climatological Circumstances", technisch physische dienst, #314.226-3, (1987).

[19] Hay, J. E., McKay, D. C., "Calculation of Solar Irradiances for Inclined Surfaces: Verification of Models Which Use Hourly and Daily Data", **DRAFT**, 1988.

[20] Perez, R., Seals, R., Ineichen, P., Stewart, R., Menicucci, D., "A New Simplified Version of The Perez Diffuse Irradiance Model For Tilted Surfaces", *Solar Energy*, **39**, pp. 221-231, (1987).

[21] Hay, J. E., Davies, J. A., "Calculation of The Solar Radiation Incident On An Inclined Surface", *Proceedings First Canadian Solar Radiation Data Workshop*, pp., 59-72, (1980).

[22] Mohr, A. J., Dahlberg, D. A., Dirmhirn, I., "Experiences With Tests and Calibration of Pyranometers For A Mesoscale Solar-Irradiance Network", *Solar Energy*, **22**, pp. 197-203, (1979).

[23] Nast, P. M., "Measurements on The Accuracy of Pyranometers", *Solar Energy*, **31**, pp. 279-282, (1983).

[24] World Meteorological Organization, Guide to Meteorological Instruments and Observing Practices, 5th Edition, WMO-No. 8, Geneva, Switzerland, (1983).

[25] Balaras, C. A., "An Investigation of The Relationship Between Beam and Global Irradiation With The Development of Numerical Solar Radiation Models", Ph.D. Thesis, School of Mechanical Engineering, Georgia Institute of Technology, pp. 49, June, 1988.

[26] Solar Energy Meteorological Research and Training Site Program (SEMERTS), operated for U.S. Department of Energy by Meteorological Research Institute under contract No. EG-77-C-01-4042.

[27] Research Cooperator Format, Solar Energy Research Institute, (1980).

[28] Anscombe, F. J., "Rejection of Outliers", *Technometrics*, Volume 2, pp. 123-125, (May, 1960).

[29] Goody, R. M., Atmospheric Radiation I: Theoretical Basis, pp. 18-65, 232-248, Oxford University Press, (1964).

[30] Paltridge, G. W., Platt, C.M.R., Radiative Process in Meteorology and Climatology, pp. 69-81, 97-127, Elsevier Scientific Publishing Company, (1976).

[31] Liu, B.Y.H., Jordan, R.C., "The Interrelationship and Characteristic Distribution of Direct, Diffuse, and Total Solar Radiation", *Solar Energy*, **4**, pp. 1-19, (1960).

[32] Hollands, K.G.T., Crha, S.J., "A Probability Density Function For The Diffuse Fraction, With Applications", *Solar Energy*, **38**, pp. 237-245, (1987).

[33] Garrison, J. D., "A Study of The Division of Global Irradiance Into Direct And Diffuse Irradiance at Thirty Three U.S. Sites", *Solar Energy*, **35**, pp.341-351, (1985).

[34] Skartveit, A., Olseth, J. A., "A Model For The Diffuse Fraction of Hourly Global Radiation", *Solar Energy*, **38**, pp. 271-274, (1987).

[35] Ineichen, P., Gremand, J.M., Guisan, O., Mermond, A., "Study of The Corrective Factor Involved When Measuring The Diffuse Solar Radiation By Use of The Ring Method", *Solar Energy*, **32**, pp.585-590, (1984).

[36] Hogan, W.D., Loxsom, F.M., "Preliminary Validation of Models Predicting Insolation on Tilted Surfaces", *Proceedings of the 1981 Annual Meeting of the American Solar Energy Society* in Philadelphia, Pennsylvania, Volume 42, pp. 1521-1525, (1981).

[37] Huang, S., "An Algorithm For The Estimation of Diffuse Insolation on A Tilted Surface", Masters Thesis in Engineering Science, Trinity University, San Antonio, Texas, (1984).

[38] Wetz, J.M., "Criteria For Judging Adequacy of Estimation by An Approximating Response Function", Ph.D. Thesis, University of Wisconsin, (1964).

[39] Minitab Release 5.1.3, Minitab, Inc. (1985).

[40] Draper, N. R., Smith, H., Applied Regression Analysis, John Wiley and Sons, (1981).

[41] Belsely, D.A., Kuh, E., Welsch, R.E., Regression Diagnostics: Identifying Influential Data And Sources of Collinearity, New York: Wiley, (1980).

[42] Gardner, C. L., Nadeau, C. A., "Estimating South Slope Irradiance In The Arctic - A Comparison of Experimental and Modeled Values", *Solar Energy*, **41**, pp. 227-240, (1988).

[43] Gueymard, C., "An Anisotropic Solar Irradiance Model for Tilted Surfaces and Its Comparison With Selected Engineering Algorithms", *Solar Energy*, **38**, pp. 367-386, (1987).

[44] Liu, B.Y.H., Jordan, R. C., "The Long Term Average Performance of Flat-Plate Solar Energy Collectors", *Solar Energy*, **7**, pp 53-74 (1963).

[45] Hunn, B. D., Calafell, D. O., "Determination of Average Ground Reflectivity for Solar Collectors", *Solar Energy*, **19**, pp. 87-89, (1977).

[46] Draper, N. R., Stat 333, Applied Regression Analysis, University of Wisconsin-Madison, Spring 1988.

Index